Systematic studies of Japanese toads

Kazumi FUKUTANI

Contents

Introduction

Species delimitation is essential to understanding biodiversity (Hillis, 2019). The primary focus of systematic biology is delimiting species boundaries, which leads to understanding the evolutionary processes that generate biodiversity (Mayr, 1968). The criteria often used for species delimitation are phenotypic or molecular data (Wiens & Penkrot, 2002; Queiroz, 2007; Tobias et al., 2010; Leliaert et al., 2014).

Especially for amphibians, the less phenotypic differences between closely related taxa make it challenging to clarify the species delimitation (Fouquet et al., 2007). Over the last two decades, the development of the technologies of mitochondrial DNA (mtDNA) and nuclear DNA sequence data analyses has contributed to accelerating the discussion of species delimitation in amphibians (Nishikawa, 2017). These molecular approaches have primarily been driven by the expansive use of molecular data and new methods for analyses of increasingly large data sets. These have enabled the clarifying of genetic structure at a greater geographical scale, depth, and resolution than before. The extensive genome-scale approaches have accelerated the fine-scale research for speciation processes in amphibians, such as the timing of divergence, degree of migration, population-size changes, selection, drift, and recombination (Burbrink & Ruane, 2021).

While the genomic approaches in amphibians were historically limited to Europe and North America, exhaustive phylogeographic studies are now performed for previously overlooked regions, shedding light on outstanding amounts of unsuspected diversity (Dufresnes & Litvinchuk, 2021). These advances have the potential to identify biogeographic barriers responsible for species diversification in other areas like Asia.

In Japan, the diversity was shaped by the combined actions of geological and climatic events. However, despite millions of years of independent evolution, the resulting lineages often remained cryptic, sharing similar ecologies and featuring no apparent phenotypic differentiation. Amphibian species having conservative external morphology have been separated into multiple distinct species with the development of molecular systematics (e.g., Okamiya et al., 2018; Matsui et al., 2019b; Eto, Matsui & Sugahara, 2022). Despite these taxonomic revisions on amphibian species, there still exist some species with the potential for cryptic diversity, and one such example is *Bufo japonicus* (Igawa et al., 2006; Nishizawa et al., 2011; Matsui & Maeda, 2018).

The genus *Bufo* Garsault, 1764 contains 24 species and is distributed from Eurasia and Japan's temperate regions, south to North Africa, the Middle East, northeastern and western Myanmar, and northern Vietnam through China (Frost, 2023). There are two endemic *Bufo* species on the Japanese mainland, *Bufo japonicus* Temminck and Schlegel, 1838 and *B. torrenticola* Matsui, 1976 (Matsui & Maeda, 2018). *Bufo japonicus* is widely distributed in Honshu, Shikoku, Kyushu, and some adjacent islands and is a lentic breeder, similar to most congeneric species. This species is divided into two subspecies, *B. j. japonicus* from western Japan and *B. j. formosus* Boulenger, 1883 from eastern Japan (Matsui & Maeda, 2018). Matsui (1984) concluded that *B. j. japonicus* and *B. j. formosus* should be divided as subspecies. They were considered appropriate to be subspecies since it was difficult to determine them as different species because the climatic clines were shown in their morphometric characters, and the fundamental patterns of their lifestyle were identical (Matsui, 1984). These two subspecies are distributed parapatrically, with a boundary in the Kinki region (Matsui & Maeda, 2018). In contrast to *B. japonicus*, the range of *B. torrenticola* is limited to the mountainous areas of central Honshu, with lotic breeding habits rarely found in *Bufo*. *Bufo torrenticola* is distributed overlaying with *B. j. formosus* and sympatrically in several areas of central Honshu (Matsui & Maeda, 2018). Although *B. torrenticola* and *B. japonicus* differ in morphology and breeding ecology, the two species' genetic relationships are complicated, and *B. torrenticola* is close to *B. j. japonicus* in the mitochondrial genealogy (Igawa et al., 2006). Additionally, some artificially introduced populations are reported from Hokkaido, Izu Islands, and the Kanto regions (e.g., Matsui, 1984; Hase, Shimada & Nikoh, 2012; Matsui & Maeda, 2018; Suzuki et al., 2020). Despite some previous studies on intra- and inter-specific variations of *B. japonicus* and *B. torrenticola*, no comprehensive research has been conducted, and details of their variation, taxonomic relationships, and evolutionary history are still unclear.

In this study, I conducted molecular phylogenetic and population genetic surveys and ecological niche modelings on *B. japonicus* and *B. torrenticola* to assess their diversity and evolutionary history toward systematic revision of the group. First, in Chapter 1, I performed fundamental molecular phylogenetic analysis using samples of two species from their entire distributional ranges and examined their genetic variations and phylogenetic patterns. Next, in Chapter 2, I focused on the demography and niche modeling of the two species using molecular, ecological, and distribution data. Finally, in Chapter 3, I performed the SNP analysis and discussed the taxonomic revisions of *B. japonicus*. Of these chapters, Chapters 1

and 2 have been published in PeeJ vol.10 in 2022. The remaining one, Chapter 3, has been published in PeerJ vol.11 in 2023.

Chapters 1 and 2:

Fukutani K, Matsui M, Tran DV, Nishikawa K. 2022. Genetic diversity and demography of *Bufo japonicus* and *B. torrenticola* (Amphibia: Anura: Bufonidae) influenced by the Quaternary climate. *PeerJ* 10:e13452. DOI: https://doi.org/10.7717/peerj.13452.

Chapter 3:

Fukutani K, Matsui M, Nishikawa K. 2023. Population genetic structure and hybrid zone analyses for species delimitation in the Japanese toad (*Bufo japonicus*). *PeerJ* 11:e16302. DOI: https://doi.org/10.7717/peerj.16302.

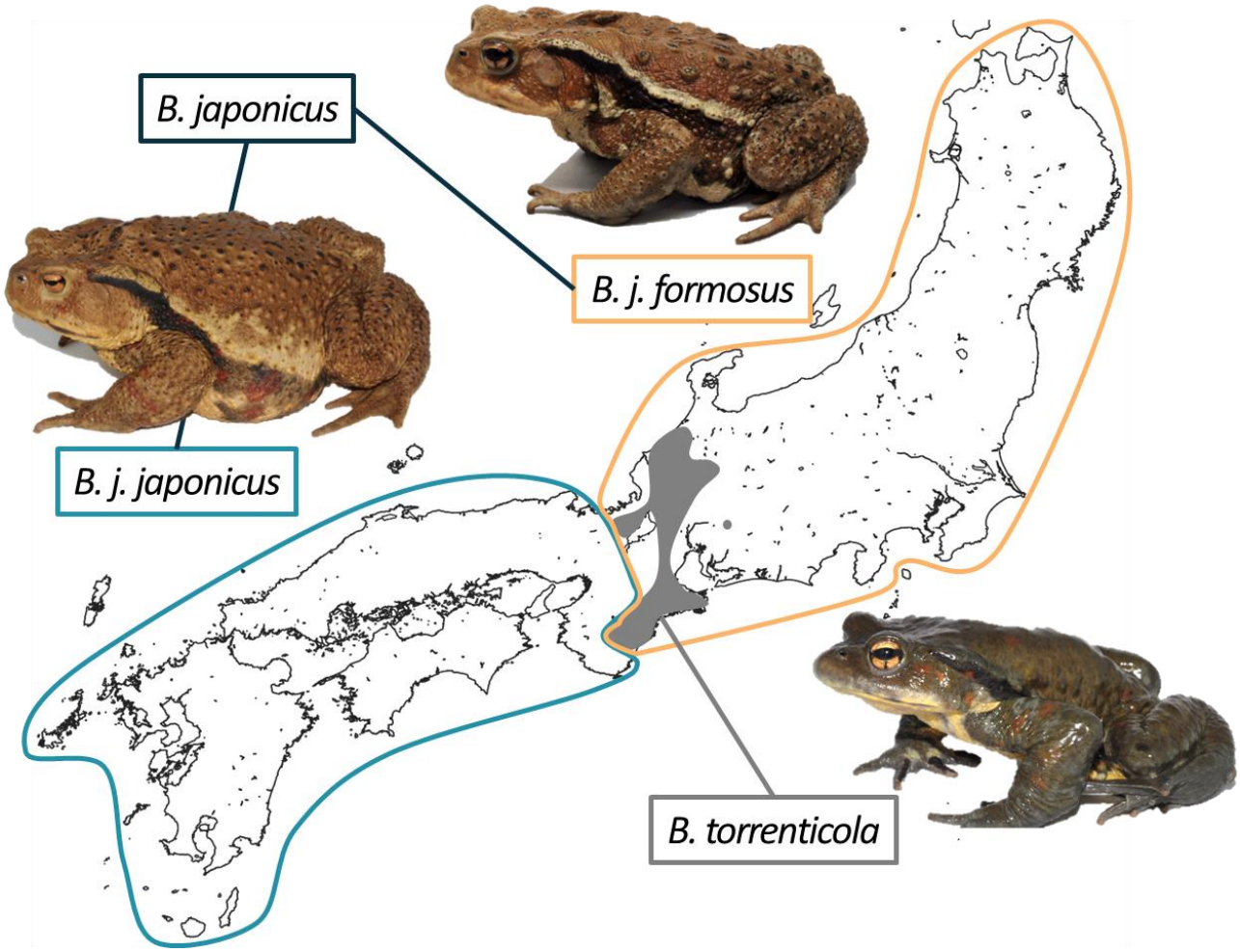

The distribution of *Bufo japonicus* and *B. torrenticola* excluding introduced populations (Matsui & Maeda, 2018)

Chapter 1

Mitochondrial DNA genealogy in the Japanese toads (*Bufo japonicus* and *B. torrenticola*)

1-1. Introduction

The genus *Bufo* Garsault, 1764, occurs in temperate Eurasia, Japan, North Africa, the Middle East, northern Indochina, and north-eastern South Asia. In Japan, there are three species: *B. japonicus* Temminck et Schlegel, 1838, *B. torrenticola* Matsui, 1976, which are endemic to Japan, and *B. gargarizans miyakonis* Okada, 1931, which occurs on Miyako Islands in the Ryukyu Archipelago (Matsui and Maeda, 2018). *Bufo japonicus* is widely distributed in Honshu, Shikoku, Kyushu, and some adjacent islands and has a habit of lentic breeding as most other congeneric species. The species is divided into two subspecies, *B. j. japonicus* from western Japan and *B. j. formosus* Boulenger, 1883 from eastern Japan. Another species from mainland Japan, *B. torrenticola*, occurs only in the mountainous area of central Honshu, with the lotic breeding habits exceptional for *Bufo* (Matsui, 1976). The two subspecies of *B. japonicus* are distributed parapatrically, and *B. torrenticola* is distributed sympatrically with *B. j. formosus* in some areas of central Honshu (Matsui and Maeda, 2018). The tympanum size can roughly identify these three: *B. torrenticola* has a small and indistinct tympanum, whereas the tympanum of *B. j. formosus* is approximately twice as large in diameter as that of *B. j. japonicus* (Matsui, 1984).

Based on analyses of external morphology, Matsui (1984) recognized three species/subspecies in toads of the Japanese mainland: *B. j. japonicus, B. j. formosus,* and *B. torrenticola*. Based on electrophoretic analyses of enzymes and blood proteins, Kawamura et al. (1990) suggested that the toad populations in the Japanese mainland were divided into two major groups, the western and eastern groups that corresponded to *B. j. japonicus* and *B. j. formosus,* respectively. Subsequent phylogenetic analysis based on mtDNA sequences supported the division of two groups, each further diverging into some subgroups (Igawa et al., 2006). However, the problem is that all Japanese toads were relegated as subspecies of *B. japonicus*, including *B. torrenticola*, even *B. bankorensis* Barbour, 1908 from Taiwan, and *B. gargarizans* Cantor, 1842 from mainland China (Nishioka et al., 1990; Kawamura et al., 1990; Igawa et al., 2006). For Japanese toads, they adopted the old names of *B. vulgaris*

montanus Okada, 1937 from the Tohoku region, and *B. v. yakushimensis* Okada, 1928 from Yakushima Island. These taxonomic treatments were made simply from the localities of toads sampled and without adequate examination. Regarding the phylogenetic position of *B. torrenticola*, only a few samples from limited localities were analyzed.

Over the last few decades, mtDNA has been the most commonly used molecular marker in animal systematics and has played a significant role in revolutionizing molecular systematics (Wilson et al., 1985; Avise et al., 1987; Moritz, Dowling & Brown, 1987). The increased effort to sequence widespread taxa at a finer genetic and geographical scale will bring a renewed understanding of the complex genetic diversity patterns and evolutionary history. Even in the age of genomics, mtDNA-driven systematic research remains relevant, especially for generating preliminary.

In the present study, I thoroughly investigate phylogenetic relationships and estimate the historical demography of the toads using the sequence of mitochondrial cytochrome *b* with sufficient sampling toward a future taxonomic revision of Japanese toads.

1-2. Materials & Methods

DNA sampling and sequencing

A total of 213 samples from 191 localities of *B. japonicus* and 27 samples from 25 localities of *B. torrenticola* were collected, covering each distribution range (Fig. 1-1 and 1-2; Table 1-1). The Animal Experimentation Ethics Committee at the Graduate School of Human and Environmental Studies, Kyoto University provided full approval for this research (20-A-5, 20-A-7). I extracted DNA from frozen or ethanol-preserved tissue samples (e.g., muscle, liver, or skin) with the Qiagen DNeasy Blood and Tissue Kit (Qiagen) according to the manufacturer's instructions.

I amplified mitochondrial DNA from the 3' region in *tRNA-Glu* to cytochrome *b*. I used the newly designed primer set (5'-TTCCTACAAGGACTTTAACCTAGAC-3'; 5'-GTTGGGCTAGTTTGTTCTCTG-3') for PCR. PCR amplification was conducted in a reaction volume of 10 µl containing 1 µl of 10 × PCR Buffer for Blend Taq (TOYOBO, Osaka, Japan), 1.0 µl of the dNTPs mixture (2 mM of each), 0.25 U of Blend Taq DNA polymerase (TOYOBO), 0.5 µl of each primer (25 µM), 0.5 µl of the DNA template, and 6.4 µl of distilled water. The PCR protocol followed 2 min of initial denaturation at 94° C, followed by 33 cycles of denaturation at 94° C for 15 s, 15 s of annealing at 53° C, and 90 s

of extension at 72° C, and a final extension at 72° C for 4 min. Primers, dNTPs, and polymerase were separated from successfully amplified PCR products by precipitation with polyethylene glycol. I performed cycle sequencing reactions (CSR) using the BigDye Terminator v.3.1 Cycle Sequencing Kit (Applied Biosystems, Carlsbad, CA, USA). The same primers used for PCR and two newly designed internal primers (5'-CGAACTTGTTCAATGAATCTGAG-3', 5'-CTTGTCGAAGTTGGGGTTAAG-3') were employed for CSR, and the products obtained were purified by ethanol precipitation. Amplified fragments were sequenced on an ABI PRISM 3130 Genetic Analyzer (Applied Biosystems, Carlsbad, CA, USA), assembled with ChromasPro v.1.34 (Technelysium Pty Ltd., South Brisbane, Queensland, Australia), and aligned with MAFFT v7.222 (default parameters: Katoh & Standley, 2013). I aligned 1,071-bp cytochrome *b* sequences and submitted the haplotypes identified in the present study to the DNA Data Bank of Japan (DDBJ: accession numbers are LC581513–LC581757; Table 1-1). Cytochrome *b* regions were extensively used in previous studies on Japanese toads and sufficiently showed variations within Japanese *Bufo* populations (e.g., Hase, Shimada & Nikoh, 2012; Iwaoka et al., 2021); therefore, I used the same gene fragment to allow for comparisons with previous studies.

Phylogenetic analyses

I built phylogenetic trees using the maximum likelihood (ML) and Bayesian inference (BI) methods. I selected the optimum substitution models for each partition by Kakusan4 (Tanabe, 2011) based on the Akaike information criterion (Akaike, 1974) for the ML analysis and Schwarz's Bayesian information criterion (Schwarz, 1978) for the BI analysis. The best-fit substitution models chosen for ML and BI analyses were GTR+G models. I performed the ML analysis with estimation node supports by 1,000 bootstrapping replications using RAxML v.8.2 (Stamatakis, 2014). In the BI analysis, I conducted two independent runs of three million generations, each with four Markov chains, and sampled the resulting trees every 100 generations by MrBayes v3.2.6 (Ronquist et al., 2012). I checked the parameter estimates and convergence using Tracer v.1.7 (Rambaut et al., 2018). The initial 10% of trees were discarded as burn-in. Sequences from *B. gargarizans gargarizans*, *B. g. miyakonis*, and *B. bankorensis* were used as outgroups because these sister lineages are the closest relatives of Japanese toads (Matsui, 1984, 1986; Igawa et al., 2006; Table 1-1).

Estimation of divergence time

Divergence dates for Japanese toads were estimated using BEAST v.2.6 (Bouckaert et al., 2019). I used two calibration points, a secondary calibration obtained from a previous study and fossil evidence. I selected two representative samples from each clade as appeared in my ML phylogeny as described by Garcia-Porta et al. (2012). To introduce calibration points, I added the sequences of four *Bufo* species and one species belonging to the family Bufonidae as outgroups. The Genbank accession numbers for the outgroups are NC_008410 (*B. gargarizans*; Cao et al., 2006), NC_027686 (*B. stejnegeri*; Dong & Yang, 2015), MN432913 (*B. bufo*; *Özdemir et al., 2020*), MN432915 (*B. verrucosissimus*; Özdemir et al., 2020), JN647474 (*B. eichwaldi*; Recuero et al., 2012), and MT483697 (*Epidalea calamita*; https://www.ncbi.nlm.nih.gov/nuccore/MT483697).

Two external nodes of Japanese toads were calibrated: (1) the split between *B. bufo* and *B. gargarizans* species complexes 12.33 million years ago (Mya; 95% highest posterior density [HPD], 8.81–16.36 Mya) according to the timetree of Garcia-Porta et al. (2012) used a normal prior (mean = 12.3 Ma, standard deviation = 1.93); (2) the oldest fossil record attributable to *B. verrucosissimus* (1.81–2.59 Mya) used a log-normal prior (offset = 1.81 Ma, mean = 1.0, standard deviation = 0.21) as described by Recuero et al. (2012). The analysis was run for 50 million generations, sampling every 100,000 using the HKY+G model estimated in jModelTest 2.1.10 (Guindon & Gascuel, 2003; Darriba et al., 2012) with the uncorrelated lognormal relaxed clock model. I assessed the stationarity and effective sample size above 200 for all estimated parameters using Tracer v.1.7 (Rambaut et al., 2018). I then generated a maximum clade credibility consensus tree with mean node heights using TreeAnnotator v 2.6 (Bouckaert et al., 2019), discarding the first 10% of the trees as burn-in.

1-3. Results

Phylogeny and divergence time

My phylogenetic analyses of mitochondrial cytochrome *b* (1,071-bp) recovered the monophyly of *B. japonicus* and *B. torrenticola*, which diverged from the other Asian *Bufo* species 7.13 Mya (HPD: 4.31–9.88 Mya; Fig. 1-3). The monophyly included six mitochondrial clades, five of which corresponded to *B. japonicus* and the other to *B. torrenticola*, with varying degrees of divergence (Fig. 1-1). ML and BI phylogenetic trees within Japanese toads were mainly congruent topologies and similar to previous findings (Igawa et al., 2006; Hase, Shimada & Nikoh, 2012). I also resolved possible geographic

boundaries between clades with higher resolution than in previous studies (Fig. 1-1). Molecular dating estimations revealed that the basal split of Japanese toads between clades A and B occurred at 5.66 Mya (HPD: 3.48–8.52 Mya), and the geographic boundary between the two clades was located on the west side of Lake Biwa in the Kinki region (Fig. 1-1).

The first clade (A) has a wide distribution across the eastern parts of the Japanese mainland and corresponds to *B. j. formosus* (Fig. 1-1). This main clade is further subdivided into three clades, which are distributed in the northern Tohoku region (clade A1), from the southern Tohoku to northern Kanto regions (clade A2), and from the southern Tohoku to Kinki regions (clade A3). The common ancestor of clades A1 and A2 diverged from clade A3 1.76 Mya (HPD: 0.85–2.62 Mya), and clades A1 and A2 diverged 0.81 Mya (HPD: 0.34–1.33 Mya). Two samples from Toyama and Ishikawa prefectures (locality 81, 84; Table 1-1), which were morphologically identified as *B. torrenticola*, had the haplotype of clade A3, indicating that the potential genetic introgression of *B. j. formosus* mtDNA occurred at the boundary between *B. j. formosus* and *B. torrenticola*, as suggested in previous studies (Yamazaki et al., 2008; Iwaoka et al., 2021).

The second clade (B) is widely distributed across the western parts of the Japanese mainland (Fig. 1-1). This main clade is subdivided into three clades: two clades correspond to *B. j. japonicus* and one to *B. torrenticola.* Regarding *B. j. japonicus*, one clade is distributed in the Kinki, Chugoku, and Shikoku regions (clade B1), which diverged 3.17 Mya (HPD: 1.83–4.64 Mya), and another in the western end of Honshu to Kyushu (clade B2). The clade of *B. torrenticola* is distributed along the mountain range northwest of Lake Biwa and from Hokuriku to the Kii Peninsula. Clade B2 and *B. torrenticola* made a sister group that diverged 2.25 Mya (HPD: 1.11–3.28 Mya), and, thus, *B. j. japonicus* is paraphyletic.

Our phylogenetic analysis reconfirmed previously suggested artificially introduced populations in Hokkaido, Izu Islands, and the Kanto region (Matsui, 1984; Kawamura et al., 1990; Igawa et al., 2006; Hase, Shimada & Nikoh, 2012; Matsui & Maeda, 2018; Suzuki et al., 2020; Fig. 1-1).

1-4. Discussion

Divergence history

The divergence time between clades A and B (5.7 Mya; Fig. 1-1) fell within the timeframe of the divergence between Eastern and Western clades for other Japanese amphibians (7–5 Mya;

Nishizawa et al., 2011; Tominaga et al., 2013; Dufresnes et al., 2016). The ancient basins, described as a divergence factor in a previous study (Igawa et al., 2006), were dammed in the middle Miocene under warm and humid climates by the strength of the East Asia summer monsoon (Hatano & Yoshida, 2017). These dammed ancient basins would likely limit the route between eastern and western Japan. In addition to the ancient basins, global cooling in the late Miocene, related to an intensified East Asian winter monsoon (Herbert et al., 2016; Matsuzaki, Suzuki & Tada, 2020), may also have restricted the activities of amphibians. Japanese amphibians may have diverged into eastern and western populations by being allopatrically isolated.

The divergence pattern and time within clade A are equivalent to those of the northern lineages of *Cynops pyrrhogaster*, a lentic breeder similar to *B. japonicus*, which diverged with glacial cycles (Tominaga et al., 2013). The dry climate at the Last Glacial Maximum (LGM) may have affected lentic-breeding amphibians by limiting breeding places.

Due to the paraphyly of *B. j. japonicus* between clades B1 and B2, difficulties are associated with estimating the phylogeography within clade B. Paraphyly may result from incomplete lineage sorting caused by recent speciation or ancient hybridization (Maddison, 1997; Funk & Omland, 2003; McKay & Zink, 2010; Toews & Brelsford, 2012). Divergence times within clade B were estimated from the late Pliocene to early Pleistocene (3.2–2.2 Mya); however, these may be overestimation if there was incomplete lineage sorting (Angelis & Reis, 2015) and underestimation if there was gene flow (Leaché et al., 2014). The other limitations are that I set the calibration only on the external nodes of Japanese toads (Ho et al., 2008) and used a single mitochondrial marker; however, divergence times were similar to those for other amphibians distributed in western Japan (Tominaga et al., 2006, 2013; Nishizawa et al., 2011).

Figure legends

Figure 1-1. Phylogenetic relationships and distribution map of *Bufo japonicus* and *B. torrenticola* based on mitochondrial cytochrome *b* haplotypes.

Bootstrap supports (maximum-likelihood)/posterior probabilities (Bayesian inference) are provided for major nodes. Arrows indicate estimated divergence times and 95% HPD (Mya). The scale bar indicates substitutions per site. Enlarged maps with locality numbers are available in Fig. 1-2. The tree was visualized by iTOL v6 (Letunic & Bork, 2021). The map was created by QGIS 3.16 (https://qgis.org). The administrative areas dataset was obtained from the GADM database (www.gadm.org, version 3.4) and the inland water dataset from the Digital Chart of the World available at the DIVA-GIS online resource (www.diva-gis.org). The elevation layer was created by editing the source data from the Geospatial Information Authority of Japan (https://maps.gsi.go.jp/development/ichiran.html).

Figure 1-2. Maps of the Japanese mainland (A) and sampling localities of five clades of *Bufo japonicus* and *B. torrenticola* in each region (B)–(H).

Clade A1, white circles; clade A2, black circles; clade A3, gray circle; clade B1, black inverted triangle; clade B2, white inverted triangle; *B. torrenticola*, white diamond. Stars indicate localities with the sympatry of several clades of *B. japonicus* or *B. torrenticola*. Asterisks indicate localities with identified introduced haplotypes. Regarding locality information, see Table 1-1. Maps were created by QGIS 3.16 (https://qgis.org).

Figure 1-3. Time tree of Japanese toads and outgroups.

Divergence times were estimated with two calibrations. Estimated divergence times and 95% HPD (Mya) are shown around the main nodes. Nodes are placed based on mean node ages. Asterisks represent nodes with posterior probabilities with values over 0.95. Two triangles indicate the calibration points used to obtain the time tree. The scale bar indicates substitutions per site. The tree was visualized by iTOL v6 (Letunic & Bork, 2021).

Table 1-1. List of samples used to generate the phylogenetic tree of *Bufo* species with information on vouchers, collection locality, and GenBank accession numbers.

KUHE, Graduate School of Human and Environmental Studies, Kyoto University; TMP, temporary number.

Locality No.	mtDNA clade/species	Voucher (KUHE)	Genbank accession No.	Locality	Prefecture	Region/Country
1	A1	27583	LC581732	Sai	Aomori	Tohoku
2	A1	TMP_20120617	LC581640	Mutsu	Aomori	Tohoku
3	A1	27584	LC581733	Higashidori	Aomori	Tohoku
4	A1	27792	LC581651	Nakadomari	Aomori	Tohoku
5	A1	TMP_T3127	LC581638	Kitaakita	Akita	Tohoku
5	A1	31943	LC581657	Kitaakita	Akita	Tohoku
6	A1	59671	LC581659	Kamaishi	Iwate	Tohoku
7	A1	27748	LC581735	Kamaishi	Iwate	Tohoku
8	A1	TMP_NY499	LC581693	Nishiwaga	Iwate	Tohoku
9	A1	35275	LC581637	Ichinoseki	Iwate	Tohoku
10	A1	24027	LC581514	Yurihonjo	Akita	Tohoku
11	A1	TMP_NY500	LC581710	Yuza	Yamagata	Tohoku
12	A1	TMP_NY501	LC581709	Tsuruoka	Yamagata	Tohoku
13	A2	TMP_NY2924	LC581706	Hakodate	Hokkaido	Hokkaido
13	A2	59647	LC581707	Hakodate	Hokkaido	Hokkaido
14	A2	43074	LC581658	Nikaho	Akita	Tohoku
15	A2	45519	LC581634	Sendai	Miyagi	Tohoku
16	A2	43201	LC581635	Nagai	Yamagata	Tohoku
17	A2	48108	LC581660	Yonezawa	Yamagata	Tohoku
18	A2	TMP_NY2463	LC581708	Oguni	Yamagata	Tohoku
19	A2	48110	LC581636	Yonezawa	Yamagata	Tohoku
20	A2	39607	LC581663	Kitashiobara	Fukushima	Tohoku
21	A2	TMP_NY1939	LC581704	Nishiaizu	Fukushima	Tohoku
22	A2	59301	LC581664	Otama	Fukushima	Tohoku
23	A2	49931	LC581713	Inawashiro	Fukushima	Tohoku
24	A2	TMP_NY1195	LC581697	Koriyama	Fukushima	Tohoku
25	A2	43072	LC581662	Koriyama	Fukushima	Tohoku
26	A2	TMP_20130702	LC581686	Koriyama	Fukushima	Tohoku
27	A2	43355	LC581661	Aizuwakamatsu	Fukushima	Tohoku
28	A2	TMP_NY843	LC581703	Tamura	Fukushima	Tohoku
29	A2	TMP_NY2805	LC581696	Iwaki	Fukushima	Tohoku
30	A2	21647	LC581632	Shirakawa	Fukushima	Tohoku
31	A2	TMP_NY458	LC581699	Tadami	Fukushima	Tohoku

Table 1-1.
Continued.

32	A2	TMP_NY457	LC581698	Tadami	Fukushima	Tohoku
33	A2	TMP_NY1289	LC581722	Tadami	Fukushima	Tohoku
33	A3	TMP_NY1290	LC581700	Tadami	Fukushima	Tohoku
34	A2	TMP_NY2143	LC581730	Tadami	Fukushima	Tohoku
34	A3	TMP_NY2144	LC581731	Tadami	Fukushima	Tohoku
35	A2	TMP_NY29	LC581725	Tadami	Fukushima	Tohoku
35	A2	TMP_NY1	LC581705	Tadami	Fukushima	Tohoku
35	A2	TMP_NY30	LC581726	Tadami	Fukushima	Tohoku
35	A3	TMP_NY48	LC581727	Tadami	Fukushima	Tohoku
35	A3	TMP_NY50	LC581729	Tadami	Fukushima	Tohoku
35	A3	TMP_NY49	LC581728	Tadami	Fukushima	Tohoku
35	A3	TMP_NY28	LC581723	Tadami	Fukushima	Tohoku
35	A3	TMP_NY36	LC581724	Tadami	Fukushima	Tohoku
36	A2	4017	LC581712	Nikko	Tochigi	Kanto
37	A2	45058	LC581665	Nikko	Tochigi	Kanto
38	A2	TMP_NY211	LC581695	Kanuma	Tochigi	Kanto
39	A2	TMP_20140423-5	LC581513	Sano	Tochigi	Kanto
40	A2	43354	LC581684	Minakami	Gunma	Kanto
40	A3	43353	LC581628	Minakami	Gunma	Kanto
41	A2	3236	LC581738	Mito	Ibaraki	Kanto
42	A2	TMP_NY372	LC581692	Tsukuba	Ibaraki	Kanto
43	A2	4063	LC581630	Tsuchiura	Ibaraki	Kanto
43	A2	4065	LC581689	Tsuchiura	Ibaraki	Kanto
44	A2	29976	LC581653	Niijima	Tokyo	Kanto
45	A2	21851	LC581652	Kouzushima	Tokyo	Kanto
46	A3	59328	LC581670	Asasahikawa	Hokkaido	Hokkaido
47	A3	43568	LC581669	Ebetsu	Hokkaido	Hokkaido
48	A3	45062	LC581633	Fukushima	Fukushima	Tohoku
49	A3	TMP_NY2714	LC581702	Tadami	Fukushima	Tohoku
50	A3	TMP_NY2713	LC581701	Tadami	Fukushima	Tohoku
51	A3	56048	LC581611	Minamiuonuma	Niigata	Chubu
52	A3	TMP_TS320	LC581690	Joetsu	Niigata	Chubu
53	A3	30687	LC581679	Itoigawa	Niigata	Chubu
54	A3	30677	LC581610	Itoigawa	Niigata	Chubu
55	A3	46513	LC581620	Nagano	Nagano	Chubu
56	A3	22929	LC581715	Naganohara	Gunma	Kanto
57	A3	55120	LC581623	Karuizawa	Nagano	Chubu
58	A3	3301	LC581745	Tatebayashi	Gunma	Kanto
59	A3	3813	LC581747	Fujimino	Saitama	Kanto
60	A3	3189	LC581749	Tokorozawa	Saitama	Kanto
60	A3	3175	LC581748	Tokorozawa	Saitama	Kanto
61	A3	46584	LC581757	Itabashi	Tokyo	Kanto

Table 1-1.
Continued.

62	A3	36924	LC581676	Narashino	Chiba	Kanto
63	A3	46176	LC581629	Ichihara	Chiba	Kanto
64	A3	60025	LC581718	Yokohama	Kanagawa	Kanto
65	A3	46298	LC581627	Machida	Tokyo	Kanto
66	A3	3981	LC581742	Sagamihara	Kanagawa	Kanto
67	A3	33239	LC581560	Nabari	Mie	Kinki
67	A3	56760	LC581711	Oshima	Tokyo	Kanto
67	B1	32002	LC581626	Oshima	Tokyo	Kanto
68	A3	TMP_HA-B-1	LC581741	Hachijo	Tokyo	Kanto
69	A3	TMP_MY140508-1	LC581737	Yamanashi	Yamanashi	Chubu
70	A3	58953	LC581625	Minobu	Yamanashi	Chubu
71	A3	59383	LC581631	Shizuoka	Shizuoka	Chubu
72	A3	32662	LC581619	Ina	Nagano	Chubu
73	A3	49583	LC581622	Ina	Nagano	Chubu
74	A3	26572	LC581618	Kiso	Nagano	Chubu
75	A3	24414	LC581621	Nakatsugawa	Gifu	Chubu
76	A3	32020	LC581562	Shitara	Aichi	Chubu
77	A3	55199	LC581601	Toei	Aichi	Chubu
78	A3	36750	LC581599	Shinshiro	Aichi	Chubu
79	A3	42071	LC581602	Takayama	Gifu	Chubu
80	A3	UN	LC581683	Suzu	Ishikawa	Chubu
81	A3	TMP_T3061	LC581590	Nanto	Toyama	Chubu
82	A3	TMP_S556	LC581608	Nanto	Toyama	Chubu
83	A3	13226	LC581609	Nanto	Toyama	Chubu
84	A3	36670	LC581588	Kanazawa	Ishikawa	Chubu
85	A3	28804	LC581607	Kanazawa	Ishikawa	Chubu
86	A3	55735	LC581605	Shirakawa	Gifu	Chubu
87	A3	33038	LC581587	Hakusan	Ishikawa	Chubu
88	A3	56769	LC581606	Hakusan	Ishikawa	Chubu
89	A3	49465	LC581589	Hakusan	Ishikawa	Chubu
90	A3	56072	LC581582	Katsuyama	Fukui	Chubu
91	A3	39854	LC581600	Inuyama	Aichi	Chubu
92	A3	TMP_T3600	LC581604	Tajimi	Gifu	Chubu
93	A3	14561	LC581598	Kounan	Aichi	Chubu
94	A3	TMP_TS1827	LC581691	Tahara	Aichi	Chubu
95	A3	16178	LC581649	Kuwana	Mie	Kinki
96	A3	40438	LC581596	Ikeda	Fukui	Chubu
96	*torrenticola*	40440	LC581581	Ikeda	Fukui	Chubu
97	A3	33504	LC581595	Echizen	Fukui	Chubu
98	A3	28711	LC581743	Ibigawa	Gifu	Chubu
99	A3	42147	LC581603	Ibigawa	Gifu	Chubu

Table 1-1.
Continued.

100	A3	36533	LC581592	Ogaki	Gifu	Chubu
101	A3	45949	LC581597	Tsuruga	Fukui	Chubu
102	A3	41497	LC581593	Nagahama	Shiga	Kinki
103	A3	40384	LC581594	Takashima	Shiga	Kinki
104	A3	59527	LC581614	Otsu	Shiga	Kinki
105	A3	59625	LC581617	Takashima	Shiga	Kinki
106	A3	59624	LC581616	Nantan	Kyoto	Kinki
106	B1	59076	LC581533	Nantan	Kyoto	Kinki
106	*torrenticola*	32681	LC581574	Nantan	Kyoto	Kinki
107	A3	58939	LC581522	Kyoto	Kyoto	Kinki
108	A3	48045	LC581525	Kyoto	Kyoto	Kinki
108	A3	59593	LC581526	Kyoto	Kyoto	Kinki
109	A3	57793	LC581529	Kyoto	Kyoto	Kinki
110	A3	59043	LC581523	Kyoto	Kyoto	Kinki
111	A3	34845	LC581650	Koka	Shiga	Kinki
112	A3	39945	LC581548	Koka	Shiga	Kinki
113	A3	59594	LC581615	Ujitawara	Kyoto	Kinki
114	A3	27791	LC581559	Iga	Mie	Kinki
115	A3	TMP_T3347	LC581561	Matsusaka	Mie	Kinki
116	A3	27790	LC581558	Nabari	Mie	Kinki
117	A3	25525	LC581551	Uda	Nara	Kinki
118	A3	25552	LC581552	Uda	Nara	Kinki
119	A3	29388	LC581553	Totsukawa	Nara	Kinki
120	A3	59641	LC581654	Tanabe	Wakayama	Kinki
121	A3	59642	LC581655	Tanabe	Wakayama	Kinki
122	B1	TMP_20140617-9	LC581681	Suginami	Tokyo	Kanto
123	B1	32712	LC581680	Chiyoda	Tokyo	Kanto
124	B1	TMP_NY1684	LC581694	Koto	Tokyo	Kanto
125	B1	28921	LC581515	Atsugi	Kanagawa	Kanto
126	B1	57792	LC581531	Kyoto	Kyoto	Kinki
127	B1	59047	LC581527	Kyoto	Kyoto	Kinki
128	B1	58938	LC581567	Otsu	Shiga	Kinki
129	B1	56161	LC581524	Kyoto	Kyoto	Kinki
130	B1	47011	LC581528	Kameoka	Kyoto	Kinki
131	B1	UN	LC581687	Mino	Osaka	Kinki
132	B1	3687	LC581550	Gose	Nara	Kinki
133	B1	24065	LC581554	Izumi	Osaka	Kinki
134	B1	24521	LC581555	Hannan	Osaka	Kinki
135	B1	42180	LC581556	Hidakagawa	Wakayama	Kinki
136	B1	59381	LC581656	Shirahama	Wakayama	Kinki
136	B1	TMP_20140423-2	LC581675	Shirahama	Wakayama	Kinki
137	B1	58940	LC581557	Kozagawa	Wakayama	Kinki

Table 1-1.
Continued.

138	B1	44246	LC581530	Kyotamba	Kyoto	Kinki
139	B1	59522	LC581612	Ayabe	Kyoto	Kinki
140	B1	59523	LC581613	Fukuchiyama	Kyoto	Kinki
141	B1	55655	LC581532	Ine	Kyoto	Kinki
142	B1	TMP_T3294	LC581591	Toyooka	Hyogo	Kinki
143	B1	36832	LC581541	Mimasaka	Okayama	Chugoku
144	B1	36471	LC581546	Sayo	Hyogo	Kinki
145	B1	44459	LC581547	Kamigori	Hyogo	Kinki
146	B1	30055	LC581545	Awaji	Hyogo	Kinki
147	B1	37045	LC581542	Kagamino	Okayama	Chugoku
148	B1	TMP_20140423-3	LC581543	Kibichuo	Okayama	Chugoku
149	B1	TMP_20140423-4	LC581544	Takahashi	Okayama	Chugoku
150	B1	36833	LC581540	Daisen	Tottori	Chugoku
151	B1	46529	LC581539	Izumo	Shimane	Chugoku
152	B1	48111	LC581538	Unnan	Shimane	Chugoku
153	B1	59644	LC581624	Akitakata	Hiroshima	Chugoku
154	B1	47276	LC581537	Akiota	Hiroshima	Chugoku
155	B1	42978	LC581536	Hatsukaichi	Hiroshima	Chugoku
156	B1	3430	LC581746	Hatsukaichi	Hiroshima	Chugoku
157	B1	60509	LC581753	Iwakuni	Yamaguchi	Chugoku
158	B1	60444	LC581750	Hagi	Yamaguchi	Chugoku
159	B1	38739	LC581534	Hagi	Yamaguchi	Chugoku
159	B1	60494	LC581535	Hagi	Yamaguchi	Chugoku
160	B1	30833	LC581668	Anan	Tokushima	Shikoku
161	B1	22348	LC581648	Kamiyama	Tokushima	Shikoku
162	B1	3186	LC581740	Takamatsu	Kagawa	Shikoku
163	B1	40176	LC581520	Ino	Kochi	Shikoku
164	B1	TMP_20130515-2	LC581518	Nakatosa	Kochi	Shikoku
165	B1	60495	LC581751	Yanai	Yamaguchi	Chugoku
166	B1	TMP_20140519-1	LC581685	Yawatahama	Ehime	Shikoku
167	B1	30658	LC581519	Tosashimizu	Kochi	Shikoku
168	B2	60501	LC581752	Nagato,	Yamaguchi	Chugoku
169	B2	59946	LC581719	Shimonoseki	Yamaguchi	Chugoku
169	B2	59947	LC581720	Shimonoseki	Yamaguchi	Chugoku
169	B2	59945	LC581716	Shimonoseki	Yamaguchi	Chugoku
170	B2	27809	LC581736	Kitakyushu	Fukuoka	Kyushu
171	B2	TMP_KE0364	LC581667	Kitakyushu	Fukuoka	Kyushu
172	B2	TMP_S906	LC581645	Kunisaki	Oita	Kyushu
173	B2	29252	LC581647	Kama	Fukuoka	Kyushu
174	B2	TMP_KPC319	LC581717	Iki	Nagasaki	Kyushu
175	B2	33214	LC581646	Karatsu	Saga	Kyushu
176	B2	24427	LC581516	Tara	Saga	Kyushu

Table 1-1.
Continued.

177	B2	TMP_NY1703	LC581721	Nagasaki	Nagasaki	Kyushu
178	B2	45171	LC581517	Shinkamigoto	Nagasaki	Kyushu
179	B2	47012	LC581639	Goto	Nagasaki	Kyushu
180	B2	TMP_120229-4	LC581754	Goto	Nagasaki	Kyushu
181	B2	3820	LC581739	Bungoono	Oita	Kyushu
182	B2	24067	LC581643	Takachiho	Miyazaki	Kyushu
183	B2	59659	LC581682	Mashiki	Kumamoto	Kyushu
184	B2	3929	LC581744	Amakusa	Kumamoto	Kyushu
185	B2	TMP_19890812	LC581644	Amakusa	Kumamoto	Kyushu
186	B2	27681	LC581734	Kobayashi	Miyazaki	Kyushu
187	B2	19033	LC581688	Miyazaki	Miyazaki	Kyushu
188	B2	32078	LC581642	Kanoya	Kagoshima	Kyushu
189	B2	45485	LC581755	Minamiosumi	Kagoshima	Kyushu
190	B2	UN	LC581666	Satsumasendai	Kagoshima	Kyushu
191	B2	45123	LC581641	Nishinoomote	Kagoshima	Kyushu
192	B2	56563	LC581672	Yakushima	Kagoshima	Kyushu
193	B2	32014	LC581671	Yakushima	Kagoshima	Kyushu
194	*torrenticola*	TMP_20130729-1	LC581714	Gujo	Gifu	Chubu
195	*torrenticola*	40364	LC581580	Ikeda	Fukui	Chubu
196	*torrenticola*	26657	LC581583	Ibigawa	Gifu	Chubu
197	*torrenticola*	44509	LC581586	Motosu	Gifu	Chubu
198	*torrenticola*	36024	LC581585	Ibigawa	Gifu	Chubu
199	*torrenticola*	34648	LC581584	Ibigawa	Gifu	Chubu
200	*torrenticola*	TMP_T3736	LC581549	Takashima	Shiga	Kinki
201	*torrenticola*	31959	LC581565	Higashiomi	Shiga	Kinki
202	*torrenticola*	34976	LC581564	Higashiomi	Shiga	Kinki
203	*torrenticola*	56747	LC581566	Takashima	Shiga	Kinki
204	*torrenticola*	3586	LC581563	Otsu	Shiga	Kinki
205	*torrenticola*	24066	LC581573	Kyoto	Kyoto	Kinki
206	*torrenticola*	43390	LC581579	Tsu	Mie	Kinki
207	*torrenticola*	27085	LC581577	Matsusaka	Mie	Kinki
208	*torrenticola*	43385	LC581578	Odai	Mie	Kinki
209	*torrenticola*	36890	LC581569	Kamikitayama	Nara	Kinki
209	*torrenticola*	TMP_S1090	LC581521	Kamikitayama	Nara	Kinki
210	*torrenticola*	43391	LC581571	Kamikitayama	Nara	Kinki
211	*torrenticola*	41016	LC581570	Tenkawa	Nara	Kinki
212	*torrenticola*	36644	LC581568	Shimokitayama	Nara	Kinki
213	*torrenticola*	28564	LC581572	Tanabe	Wakayama	Kinki
213	*torrenticola*	58941	LC581576	Tanabe	Wakayama	Kinki
214	*torrenticola*	56750	LC581575	Tanabe	Wakayama	Kinki
OUTGROUP	*g. miyakonis*	32507	LC581673	Miyako Isl.	Okinawa	

Table 1-1. Continued.

OUTGROUP	*g. gargarizans*	4093	LC581677	Sakhalin	Russia
OUTGROUP	*g. gargarizans*	4119	LC581678	Khabarovsk	Russia
OUTGROUP	*g. gargarizans*	26598	LC581674		South Korea
OUTGROUP	*bankorensis*	46294	LC581756	Taichung	Taiwan

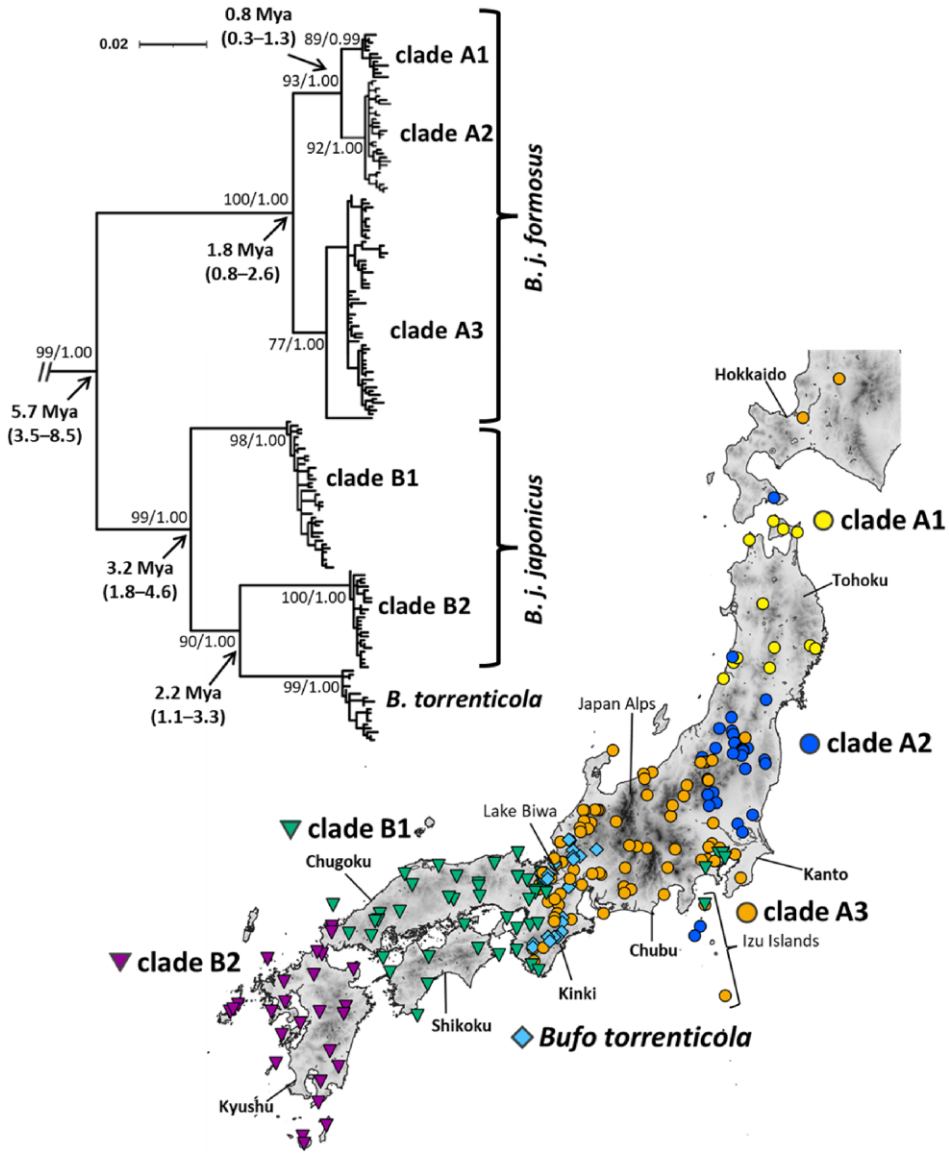
0.02
0.8 Mya
(0.3–1.3)
89/0.99
clade A1
93/1.00
clade A2
92/1.00
100/1.00
1.8 Mya
(0.8–2.6)
clade A3
77/1.00
B. j. formosus
99/1.00
5.7 Mya
(3.5–8.5)
98/1.00
clade B1
99/1.00
3.2 Mya
(1.8–4.6)
100/1.00
clade B2
90/1.00
2.2 Mya
(1.1–3.3)
99/1.00
B. torrenticola
B. j. japonicus
Hokkaido
clade A1
Tohoku
Japan Alps
clade A2
Lake Biwa
clade B1
Chugoku
Kanto
clade A3
Chubu
Izu Islands
clade B2
Kinki
Shikoku
Bufo torrenticola
Kyushu

Figure 1-1

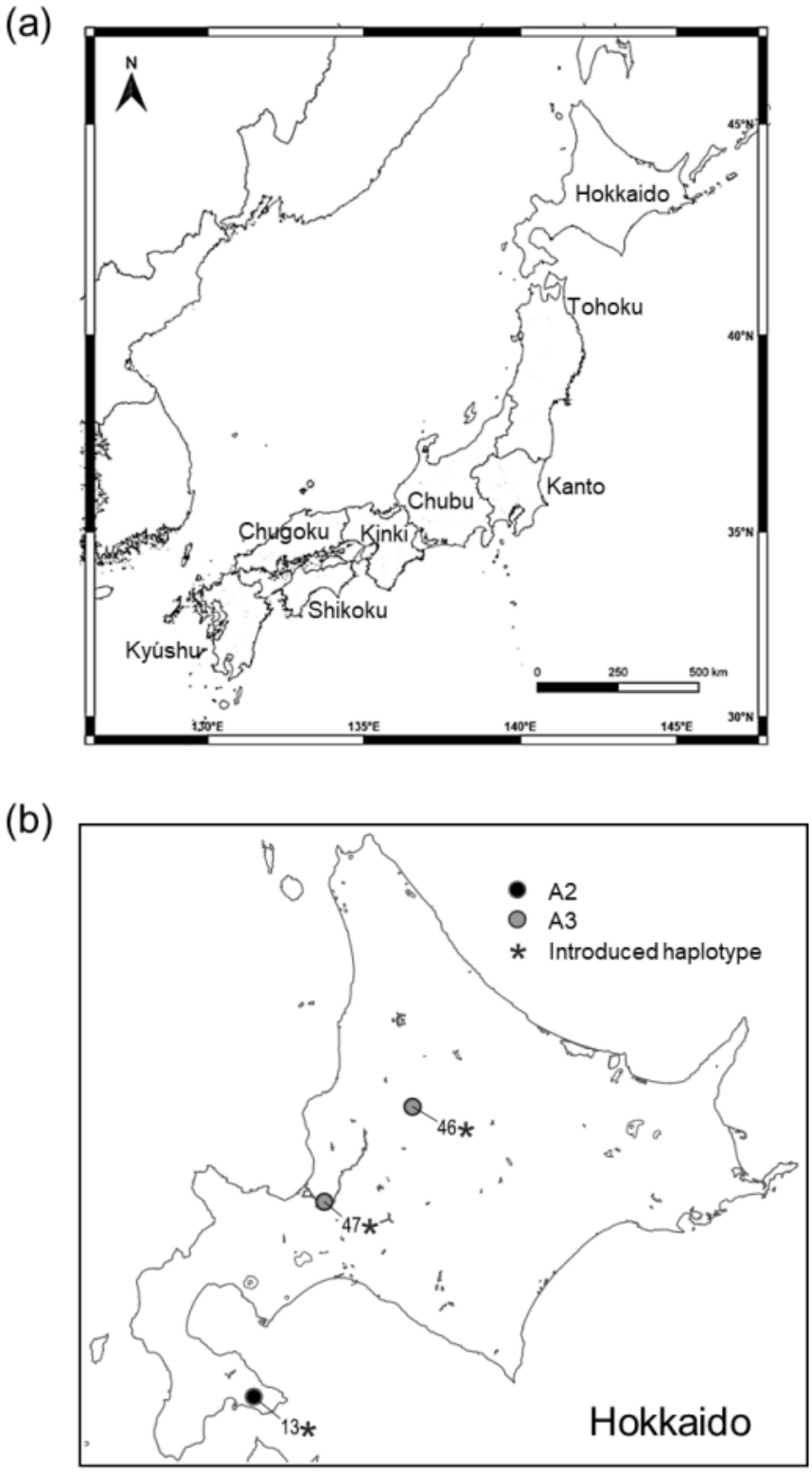
(a)
N
45°N
40°N
35°N
30°N
130°E
135°E
140°E
145°E
Hokkaido
Tohoku
Kanto
Chubu
Kinki
Chugoku
Shikoku
Kyúshu
0
250
500 km
(b)
A2
A3
Introduced haplotype
46
47
13
Hokkaido

Figure 1-2

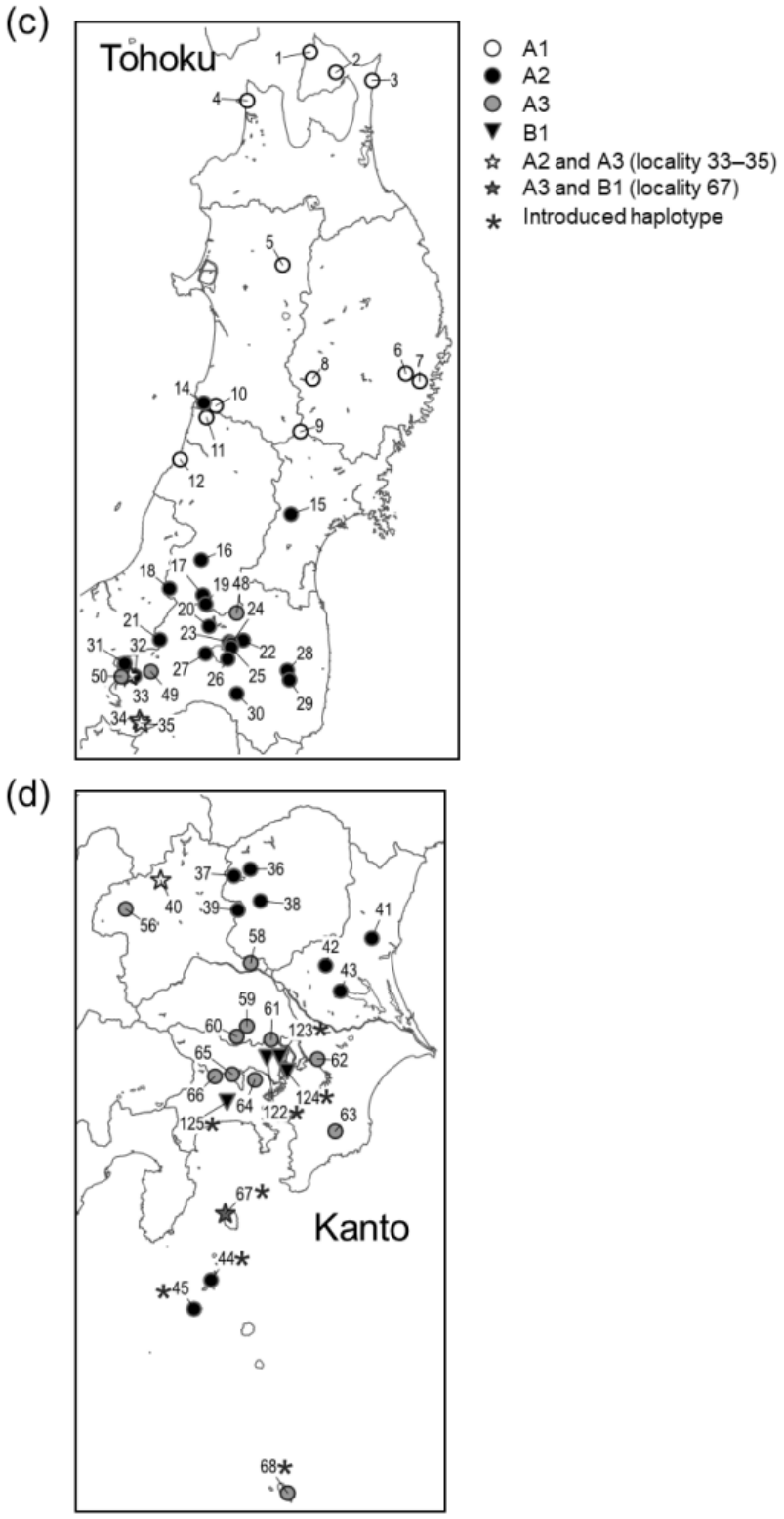

Figure 1-2 Continued.

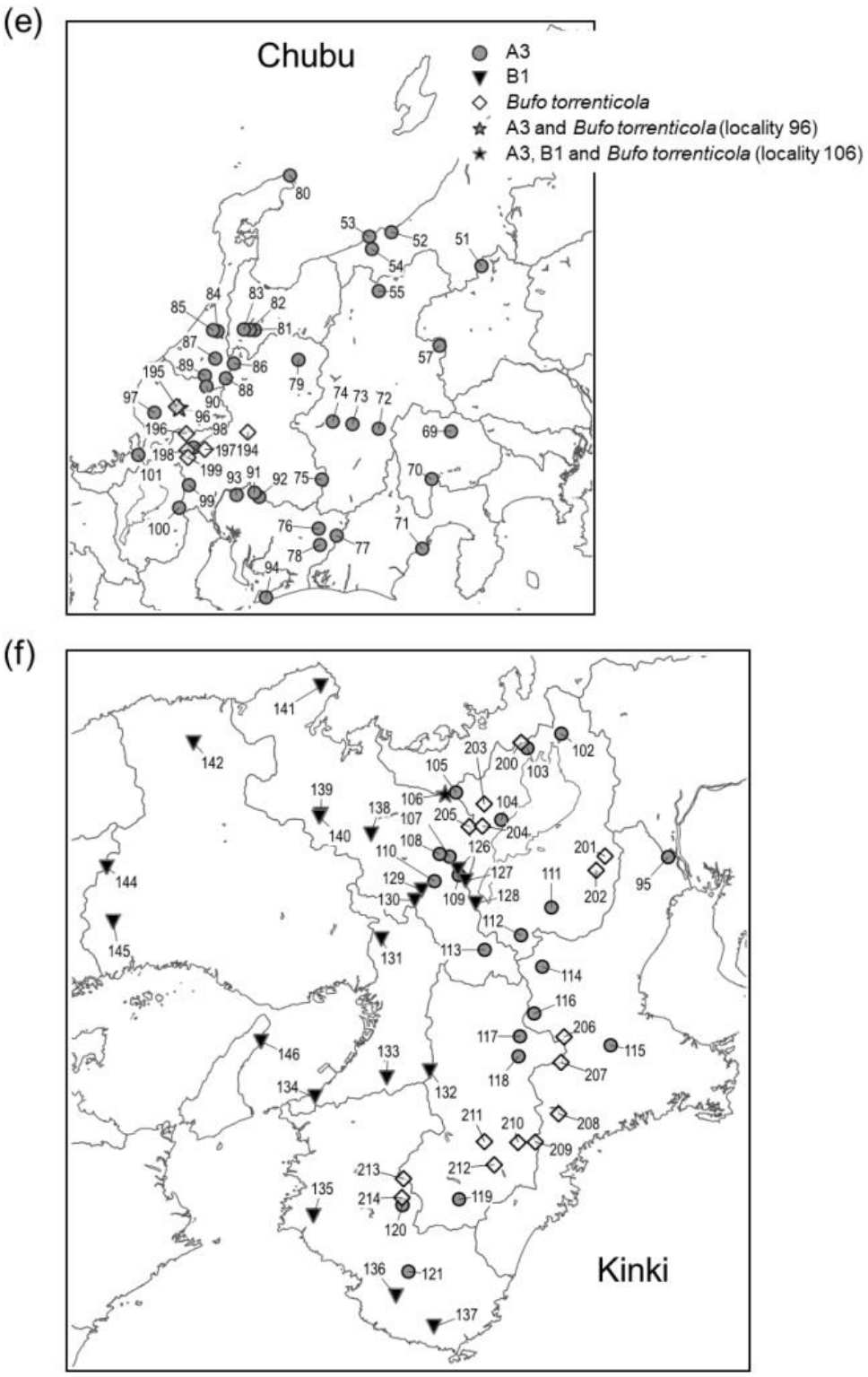

Figure 1-2 Continued.

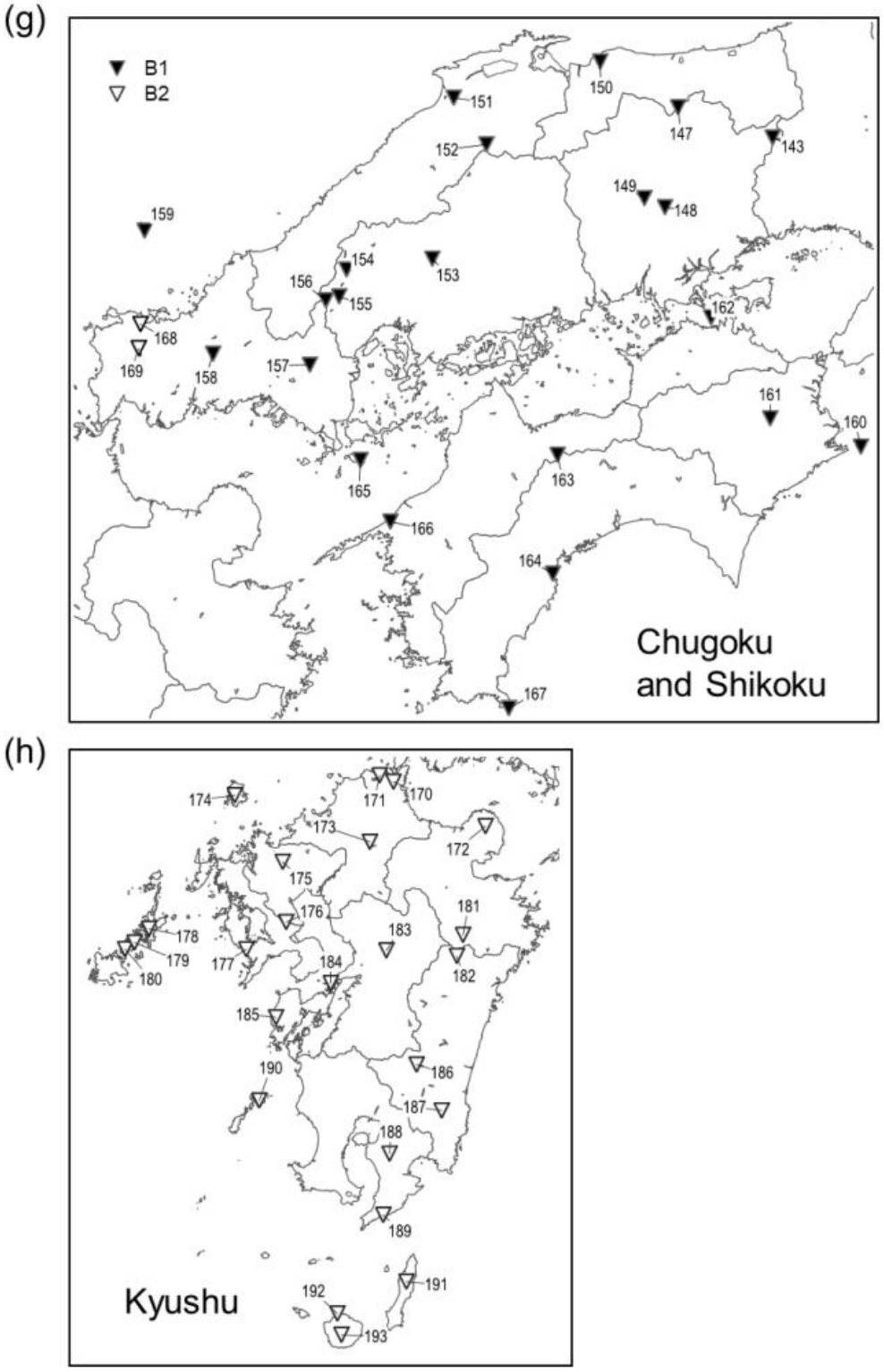

Figure 1-2 Continued.

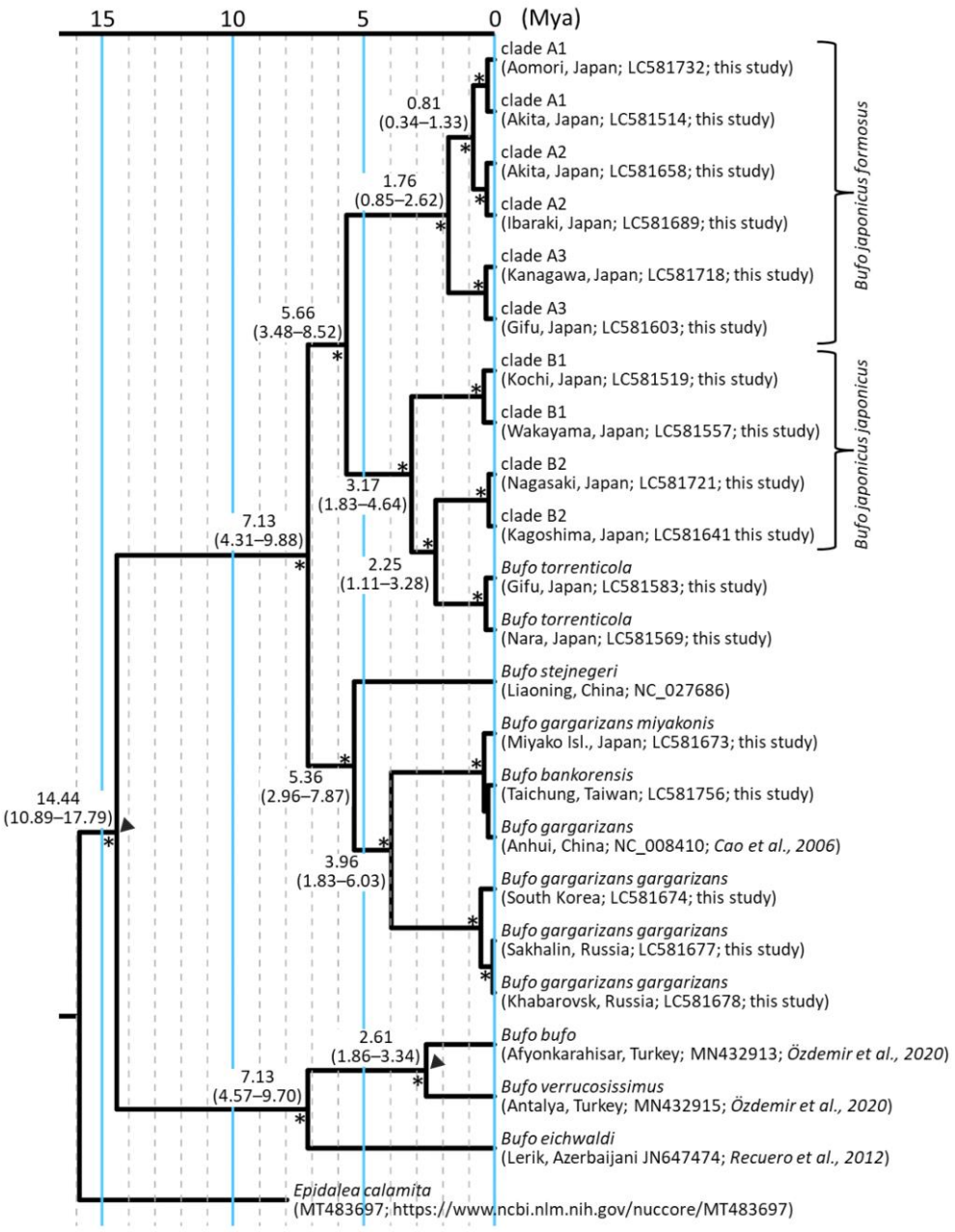
15
10
5
0 (Mya)
clade A1
(Aomori, Japan; LC581732; this study)
clade A1
(Akita, Japan; LC581514; this study)
clade A2
(Akita, Japan; LC581658; this study)
clade A2
(Ibaraki, Japan; LC581689; this study)
clade A3
(Kanagawa, Japan; LC581718; this study)
clade A3
(Gifu, Japan; LC581603; this study)
Bufo japonicus formosus
clade B1
(Kochi, Japan; LC581519; this study)
clade B1
(Wakayama, Japan; LC581557; this study)
clade B2
(Nagasaki, Japan; LC581721; this study)
clade B2
(Kagoshima, Japan; LC581641 this study)
Bufo japonicus japonicus
Bufo torrenticola
(Gifu, Japan; LC581583; this study)
Bufo torrenticola
(Nara, Japan; LC581569; this study)
Bufo stejnegeri
(Liaoning, China; NC_027686)
Bufo gargarizans miyakonis
(Miyako Isl., Japan; LC581673; this study)
Bufo bankorensis
(Taichung, Taiwan; LC581756; this study)
Bufo gargarizans
(Anhui, China; NC_008410; Cao et al., 2006)
Bufo gargarizans gargarizans
(South Korea; LC581674; this study)
Bufo gargarizans gargarizans
(Sakhalin, Russia; LC581677; this study)
Bufo gargarizans gargarizans
(Khabarovsk, Russia; LC581678; this study)
Bufo bufo
(Afyonkarahisar, Turkey; MN432913; Özdemir et al., 2020)
Bufo verrucosissimus
(Antalya, Turkey; MN432915; Özdemir et al., 2020)
Bufo eichwaldi
(Lerik, Azerbaijani JN647474; Recuero et al., 2012)
Epidalea calamita
(MT483697; https://www.ncbi.nlm.nih.gov/nuccore/MT483697)
0.81
(0.34–1.33)
1.76
(0.85–2.62)
5.66
(3.48–8.52)
3.17
(1.83–4.64)
7.13
(4.31–9.88)
2.25
(1.11–3.28)
5.36
(2.96–7.87)
3.96
(1.83–6.03)
14.44
(10.89–17.79)
2.61
(1.86–3.34)
7.13
(4.57–9.70)

Figure 1-3

Chapter 2

Genetic diversity and demography of *Bufo japonicus* and *B. torrenticola* (Amphibia: Anura: Bufonidae) influenced by the Quaternary climate

2-1. Introduction

Biogeographic studies have provided important information on the effects of the Quaternary climate on various species because glacial-interglacial repeated cycles led to their distribution changes, thereby affecting the present distribution (e.g., Taberlet et al., 1998; Hewitt, 2004). Since amphibians are ectotherms and their reproduction is markedly affected by climate factors, they are particularly vulnerable to climate variability (e.g., Carey & Alexander, 2003; Blaustein et al., 2010; Ficetola & Maiorano, 2016). Therefore, the glacial climate had an impact on the present species richness of amphibians by limiting their activities and subsequently restoring the diversity of herpetofauna after LGM (Araújo et al., 2008; Zeisset & Beebee, 2008; Martínez-Monzón et al., 2021).

Japan has rich amphibian fauna with many taxa and high endemism (Nishikawa, 2017). Areas with high species richness may have acted as refugia in the glacial period due to climate stability (Sandel et al., 2011). Furthermore, high endemism may have occurred as a result of *in situ* diversification by island-specific environments (Kubota, Shiono & Kusumoto, 2015; Kubota et al., 2017). As a result of climate variability in the Quaternary period, multiple refugia for plants, insects, and mammals formed in the Japanese mainland (Hokkaido, Honshu, Shikoku, and Kyushu) during glacial periods, mainly in areas of low elevation, such as coastal areas (e.g., Tomaru et al., 1998; Nunome et al., 2010; Aoki, Kato & Murakami, 2011). Among amphibians widely distributed on the Japanese mainland, the present geographic distribution patterns have been affected by the locations of the refugia, and genetic diversity was increased by isolating to refugia (Tominaga et al., 2013; Dufresnes et al., 2016; Matsui et al., 2019a).

In the present study, I focused on the phylogeography of Japanese toads (Genus *Bufo* Garsault, 1764, Bufonidae Gray, 1825). There are two endemic *Bufo* species on the Japanese mainland, *Bufo japonicus* Temminck and Schlegel, 1838 and *B. torrenticola* Matsui, 1976 (Matsui & Maeda, 2018). Although the effects of the Quaternary climate on European toads

have been examined in detail (e.g., Garcia-Porta et al., 2012; Arntzen et al., 2017; Chiocchio et al., 2021), limited information is currently available on *B. japonicus* and *B. torrenticola*.

Studies combining ecological niche models (ENM) with phylogeography have become mainstream in biogeographic research. The combination of gene-based estimates and analyses of environmental effects provides more robust data (Waltari et al., 2007; Hickerson et al., 2010; Alvarado-Serrano & Knowles, 2014). These methods have helped to resolve the phylogeography of some Japanese anuran species (Komaki et al., 2015; Dufresnes et al., 2016). Since few quaternary fossils of Japanese toads have been found on the Japanese mainland, the combination of genetic and environmental analyses will provide more powerful insights into their Quaternary biogeography. Furthermore, these analyses will help clarify the factors that maintain the high endemism of Japanese amphibians. In the present study, I describe the biogeographic processes that contributed to the diversification of Japanese toads and discuss the effects of the Quaternary climate using genetic analyses and ENM.

2-2. Materials & Methods

Demographic analyses

I used the same mtDNA sequence data for Chapter 2 as used in Chapter 1.

Haplotype diversity (H_d) and nucleotide diversity (π) within each main clade estimated in Chapter 1 were calculated using DnaSP v.6 (Rozas et al., 2017). To examine deviations from neutrality, which are expected with population expansion, I calculated Fu's F_S (Fu, 1997) with 10,000 permutations for significance using Arlequin ver 3.5 (Excoffier & Lischer, 2010). Mismatch distribution analyses were conducted by computing observed pairwise differences to distributions simulated under demographic (Rogers & Harpending, 1992) and range expansion models (Ray, Currat & Excoffier, 2003; Excoffier, 2004) implemented in Arlequin. Observations were compared to model predictions based on 10,000 permutations of data. I also tested the goodness-of-fit of the simulated distribution with the expected distributions using a population expansion model by calculating the sum of the square deviation (SSD).

Genetic Landscape Shape interpolation analyses were performed using Alleles In Space (AIS: Miller, 2005; Miller et al., 2006) to obtain spatial patterns in genetic diversity. The analysis produced three-dimensional surface plots of interpolated genetic distances with X and Y coordinates corresponding to geographical locations on the rectangular grid, and

surface plot heights (Z) reflecting genetic distances. I performed an analysis of each clade estimated in Chapter 1 with a grid of 150×150 and a distance weighting value of 1.0. All analyses implemented in AIS used sequences as the input matrix (raw genetic distances) and Universal Transverse Mercator coordinates.

I estimated past changes in the effective population size of each clade estimated in Chapter 1 in Japanese toads using Bayesian skyline plots (BSP; Drummond et al., 2005) in BEAST v.2.6 (Bouckaert et al., 2019). I employed a calibrated rate for BSP based on the calibration of the demographic transition method (CDT; Hoareau, 2016). This calibration method is an advancement of expansion dating (Crandall et al., 2012) based on the two-epoch demographic model (Shapiro et al., 2004). The commonly used older (>1 Mya) or interspecific phylogenetic calibration often leads to incorrect estimates for intraspecific demographic parameters (Ho & Larson, 2006; Grant, 2015). CDT helps to overcome this issue by using the timing of late glacial climatic warming between 20 and 10 thousand years ago (kya) to calibrate expansion times. I applied CDT on clade A1 following default CDT procedures (Hoareau, 2016) using Beast v1.8.4 (Drummond et al., 2012) because clade A1 was the most likely to be affected by the glacial period and expand during the warming period. I considered the low sample size of clade A1 to have no effect on inferring the past population size because I collected samples to cover their distribution range. BSP analyses were performed for each clade of Japanese toads using the CDT rate based on the clade A1. I applied the HKY model of molecular evolution as described by Drummond et al. (2005), and a strict molecular clock model for BSP analyses as described by Hoareau (2016). Analyses consisted of one Markov chain Monte Carlo analysis with chain runs for 50 million generations, sampling every 100,000 generations and discarding 10% as burn-in. I verified the effective sample sizes for each parameter and the convergence of chains in Tracer v.1.7 (Rambaut et al., 2018).

ENM

I constructed ENM for each clade of Japanese toads and predicted their ranges under the present and LGM conditions. I gathered distribution localities with the known occurrence of *B. japonicus* and *B. torrenticola*, combining my sampling localities used for phylogenetic analyses in the present study. This initial dataset was filtered to avoid spatial autocorrelation and duplication by randomly selected occurrence points more than 1 km apart from each

other in 10 replicates using the R package spThin (Aiello-Lammens et al., 2015). The final dataset comprised 422 records for *B. japonicus* and 26 records for *B. torrenticola*, respectively. I assigned the records for *B. japonicus* to the clades obtained in phylogenetic analyses in Chapter 2 based on their locations.

I extracted 19 bioclimatic layers representative of the climatic date from 1970 to 2000 from the WorldClim v.2.1 (Fick & Hijmans, 2017), featuring 30 arc seconds of spatial resolutions: 11 layers related to temperature and eight layers related to precipitation. Pearson's correlation coefficients for all pairs of bioclimatic variables were calculated using ENMTools v.1.4.4 (Warren, Glor & Turelli, 2010) to eliminate predictor collinearity before generating the model. The variables of correlated pairs with $|r| > 0.85$ were excluded because they were biologically less important based on the known preferences of Japanese toads. The resulting data set contained eight bioclimatic variables: BIO 2 (mean diurnal range), BIO 3 (isothermality; BIO 2/BIO 7), BIO 8 (mean temperature of the wettest quarter), BIO 10 (mean temperature of the warmest quarter), BIO 11 (mean temperature of the coldest quarter), BIO 15 (precipitation seasonality), BIO 18 (precipitation of the warmest quarter), and BIO 19 (precipitation of the coldest quarter).

Distribution models were built with ten replicates using the default setting in Maxent v.3.4.4 (Phillips, Anderson & Schapire, 2006). I used the areas under the receiving operator characteristics curve (AUC) to evaluate the performance of models. ENM were constructed according to current environmental factors and projected for the present and LGM. To project the current ecological niches of Japanese toads on climate conditions in LGM (21,000 years ago), I applied two widely-used general circulation climate models with a 2.5 arc-minute spatial resolution and species-specific masks: the Community Climate System (CCSM4; Gent et al., 2011), and the Model for Interdisciplinary Research on Climate (MIROC-ESM 2010; Watanabe et al., 2011) from WorldClim version 1.4 (https://www.worldclim.org/data/v1.4/worldclim14.html). The logistic thresholds of the 10-percentile training presence generated in Maxent v.3.4.4 (Phillips, Anderson & Schapire, 2006) were used to define the minimum probabilities of suitable habitats.

I also tested niche overlaps among the clades. I used Schoener's *D* (Schoener, 1968) and Hellinger's *I* metric (Warren, Glor & Turelli, 2008) to test for niche conservatism and divergence. These metrics were computed from climatic variations under present conditions in ENMTools v.1.4.4 (Warren, Glor & Turelli, 2010). I built niche models of identity and background tests based on 100 pseudoreplicates generated from a random sampling of data

points pooled for each pair of clades. Schoener's *D* and Hellinger's *I* of the true calculated niche between clades were compared with the null distribution by two-tailed *t*-tests.

I included the putative populations of the introduced origin (see below in Results) for the phylogenetic analysis to identify their haplotypes, but excluded them for the demographic analysis and ENM because they may hinder estimations of the actual demography and suitable distribution area.

2-3. Results

Demographic analyses

The high haplotype diversities (H_d = 0.967–0.995), low nucleotide diversities (π = 0.00486–0.00805), and significantly negative Fu's F_S values for all clades of *B. japonicus* and *B. torrenticola* supported the pattern of historical demographic expansion (Fu, 1997; Grant & Bowen, 1998; Table 2-1).

I demonstrated possible patterns of demographic expansions, which indicated the presence of glacial refugia at LGM. The ragged mismatch distribution for clade B1 suggested demographic equilibrium, whereas the unimodal distribution for clades A1, A2, and B2 indicated recent population expansion (Harpending, 1994; Fig. 2-1). Two peaks for clade A3 and *B. torrenticola* suggested the inclusion of multiple populations, each undergoing bottlenecks followed by expansion (Hayes et al., 2008). SSD values did not reject the demographic expansion of clades A1 and A3 or the spatial expansion of clades A1, A3, and *B. torrenticola* (p >0.05; Fig. 2-1).

Genetic Landscape Shape interpolation analyses revealed the geographic gradient of genetic variation in each clade (Fig. 2-2). I show areas with higher genetic diversity in warmer colors and those with lower genetic diversity in cooler colors. High genetic diversity areas for clade A1 were distributed in the southern and western ranges, while those for clade A2 had higher genetic diversity in the southern range. The areas with high genetic diversity in clade A3 were distributed in areas of low elevation on both sides of the Japan Alps (Hida, Kiso and Akaishi Mountains) at the center of Honshu. Clade B1 had high genetic diversity in the western side of their distribution and in the central areas of the Chugoku and Kinki regions, and clade B2 had high genetic diversity in the northern region. *Bufo torrenticola* had high genetic diversity, mainly in the southern area and scattered northwestern, northwestern, and central regions. Since populations that remained in refugia during the glacial period have

a longer dynamic history and greater genetic diversity than those that expanded after the glacial age (Comes & Kadereit, 1998; Taberlet et al., 1998), regions with high genetic diversity may be regarded as refugia.

The CDT rate based on clade A1 was high at 0.166 changes/site/million years, but was consistent with the findings of Hoareau (2016) and other evolutionary rates estimated for a recent time scale for mitochondrial cytochrome *b* (Ho et al., 2005; Suzuki et al., 2015). BSP reconstructed the demographic histories of the mtDNA clades of Japanese toads from the most recent common ancestor (Fig. 2-1). All of the clades presented signals of population expansion. Population expansion occurred at different times: between 20 and 10 kya, used for CDT, in clades A1, A2, and B2, before 20 kya in clade B2, and after 10 kya in clade A3 and *B. torrenticola*. Increases in the effective population size (N_e) were larger (more than a 10-fold increase) for *B. japonicus* (clades A and B) than for *B. torrenticola* (less than a 10-fold increase; Fig. 2-1).

ENM

Each ENM estimated under current climate conditions had mean test AUC values ≥0.9, indicating a better than random prediction. The predicted potential niche models for each clade of Japanese toads under the climate conditions in LGM are shown in Fig. 2-3, and those under the present climate conditions are shown in Fig. 2-4.

The extent of suitable range in LGM in clade A varied depending on the global circulation model. Predicted distributions showed that the suitable range in LGM for clade A1 almost vanished from all areas based on MIROC, while some small parts of coastal areas by the Japan Sea remained based on CCSM. According to the CCSM model, suitable environmental conditions in LGM for clade A2 were distributed in some areas along the coast of the Sea of Japan and the Pacific Ocean, whereas based on MIROC, suitable conditions were expanded distributed along the Pacific coast from southern Tohoku to Shikoku. Regarding clade A3, the predicted suitable distribution range in LGM mainly expanded from Chubu and Kinki according to the CCSM and MIROC models. On the other hand, the CCSM and MIROC models for each clade in clade B both suggested that the projected potential niche models for LGM were significantly limited southward of their ranges.

Niche overlap under the present climate conditions between clades ranged between 0.04 and 0.59 for Schoener's *D* and between 0.18 and 0.85 for Hellinger's *I* metrics (Table 2-

2). The null hypotheses of the niche identity test were rejected for all pairs of clades ($p <$ 2.2e-16), indicating that the environmental niches of the all pairs were not equivalent.

The null hypotheses of the similarity test were not rejected between clades A1 and A2 based on the direction that tested the known localities of clade A2 to the background range of clade A1 for Schoener's *D* and based on both directions for Hellinger's *I* (Table 2-3). Additionally, the null hypotheses of the similarity test were not rejected between clades A2 and A3 based on the direction that tested the known localities of clade A2 to the background range of clade A3 for Hellinger's *I*. The observed niche overlaps were significantly higher than expected under the null hypotheses between each pair of *B. japonicus* (except for between clades A3 and B2 and the not rejected pairs of clades described above) and between clade A1 and *B. torrenticola*, indicating that each clade was more similar than expected (Table 2-3). The contrasting results of the identity test and similarity test are false positive; the identity test is more likely to unduly reject the null hypothesis of niche identity (Peterson, 2011). In addition, the background test is known to be more suitable for understanding speciation than the identity test (Smith & Donoghue, 2010). Therefore, I focused on the similarity test, similar to Collart et al. (2021), because the null hypotheses of identity tests were rejected for all of the clades in the present study.

The environmental niches of *B. japonicus* (except for clade A1) and *B. torrenticola* were more similar than expected based on the habitat available to *B. japonicus*, but diverged more than expected based on the habitat available to *B. torrenticola* (Table 2-3). These contrasting results were also confirmed between clades A3 and B2. This counterintuitive result is likely to be driven by differences in the heterogeneity of the environmental background for the two species (Nakazato, Warren & Moyle, 2010), and their overall similarity was indicated to be low.

2-4. Discussion

Phylogeography of Japanese toads

The results of ENM recognized suitable areas in CCSM for clade A1 in LGM along the Japan Sea coast in the northern Tohoku region, consisting of a region with high genetic diversity (Fig. 2-2 and 2-3). I also found a high genetic diversity area of clade A1 in the southern part of the distribution; however, this southern area was not suitable in LGM. The southeastern area of the present distribution of clade A1 on the Pacific Ocean side was also an unsuitable

area despite the actual distribution. There may have been areas that were not suitable for clade A1 based on climate factors, but were inhabitable. The suitable areas during LGM for clade A2 were varied between CCSM and MIROC; however, judging from the area with high genetic diversity, the refugia for clade A2 might be along the Pacific coast in the southern Tohoku region. The divergence time between clades A1 and A2 (0.8 Mya; Chapter 1) fell within the middle Pleistocene transition when glacial cooling became more severe (1.25–0.7 Mya; Lisiecki & Raymo, 2005; Clark et al., 2006) and a significant flora change also occurred on the Japanese mainland (Momohara, 2016). By assuming that refugia in the glacial age before LGM during the Quaternary climate were consistent with those in LGM, clades A1 and A2 may have diverged by isolation into different refugia along the coastal areas of the Japan Sea and the Pacific Ocean, respectively, followed by genetic drift (Provan & Bennett, 2008).

Although refugia in slightly different locations may have been sufficient to allow divergence, I cannot conclude that a common ancestor of clades A1 and A2 diverged from clade A3 in different refugia because the refugia of clades A2 and A3 were located close to each other.

Regarding the taxonomic treatment of clade B, the genetic diversity and niche differences between *B. j. japonicus* (clades B1 and B2) and *B. torrenticola* strongly support their distinct species status, in addition to differences in their morphology and breeding behavior. On the other hand, there is sufficient mitochondrial genetic diversity for a heterospecific level between clades B1 and B2. Although niche similarity between clades B1 and B2 suggests a conspecific relationship, in addition to the lack of differences in morphology or breeding behavior, it is not possible to reach a concrete conclusion on their taxonomic statuses without examining reproductive isolation.

Niche similarity between clades B1 and B2 indicates their allopatric divergence (Wiens & Graham, 2005). On the other hand, niche dissimilarity between *B. japonicus* and *B. torrenticola* may suggest the possibility of sympatric speciation (Via, 2001); however, I presently have no data for supporting that possibility. Adaptation to the different ecological niches between *B. japonicus* and *B. torrenticola* may have allowed *B. torrenticola* to speciate in a short period (2.2 Myr; Schluter, 2009). *Bufo torrenticola* and its sister clade, clade B2, are now distributed allopatrically, which may be attributed to the complex phylogeography associated with the formation and transition of the Seto Inland Sea.

Demography from LGM to the present

Clades A1 and A2, distributed in the Tohoku region, shrank their ranges into refugia and expanded after the glacial period (Fig. 2-1, 2-2, and 2-3). Some amphibians with overlapping distribution with toads also diverged in the Tohoku region (Sumida & Ogata, 1998; Yoshikawa et al., 2008; Aoki, Matsui & Nishikawa, 2013; Tominaga et al., 2013; Yoshikawa & Matsui, 2014; Matsui et al., 2020). Although divergence times did not coincide, the maintenance of genetic structures within the Tohoku region suggests the presence of multiple refugia for amphibians in this region. Amphibians that diverged in the Tohoku region developed tolerance to the cold and may have survived in multiple refugia by moving to areas of lower elevation during glacial periods. On the other hand, some amphibians did not diverge genetically in the Tohoku region (Nishizawa et al., 2011; Matsui et al., 2019). They may have been unable to live in the cold and dry environments of the glacial period, and only had one refugium in the southern region even when there were refugia in the Tohoku region. These differences may reflect current ecological characteristics, such as habitat elevations and breeding seasons.

A region with high genetic diversity for clade A3 was found on both sides of areas of high elevation in central Japan, particularly on the eastern side (Fig. 2-2). This was also demonstrated by the bimodal mismatch distribution (Fig. 2-1), indicating a contemporary geographic barrier to gene flow (Bremer et al., 2005). The central areas were also shown as unsuitable in LGM for clade A3 in ENM (Fig. 2-3). Areas of high elevation in central Japan were covered with glaciers followed by volcanic activity (Ono et al., 2005; Shiba, 2021), which may have prevented clade A3 from expanding its distribution soon after LGM. Even if the population of clade A3 was fragmented, I did not find any phylogroup in the clade (Chapter 1), which may have been due to high mobility when their spatial and population expansion, as suggested for many other *Bufo* species (Yu, Lin & Weng, 2014; Borzée et al., 2017; Dufresnes et al., 2020a).

Suitable areas for *B. torrenticola* in LGM vanished except for the southern end of their distribution (Fig. 2-3). The narrow suitable habitats at LGM for clades in clade B (including *B. torrenticola*) may be because they were estimated based only on western Japan's current temperature and precipitation. If the present habitats are limited more by factors such as interactions with other populations than solely by climate factors, then suitable habitats in LGM may have been underestimated. A Genetic Landscape Shape interpolation analysis suggested that the area with the highest genetic diversity was a

southern area; however, genetic diversity was also high in the northern area, and these regions may have become refugia (Fig. 2-2). The lower degree of expansion of the effective population size for *B. torrenticola* than that for *B. japonicus* (Fig. 2-1) indicated that *B. torrenticola* may have been affected less by the glacial climate than *B. japonicus*, which may have been because lotic environments were more available than lentic environments under the dry climate in the glacial period. Since the northern and southern ends of the distribution became refugia, the undistributed central region with high genetic diversity suggested a separation between the northern and southern populations. *Bufo torrenticola* and clade A3 had been geographically separated, followed by the expansion after 10 kya, and then, the niche dissimilarity may have enabled their present overlaying.

I identified high genetic diversity for clade B1 on the western side of their distribution and in the central areas of the Chugoku and Kinki regions (Fig 2-2), although these areas were not identified as a suitable habitat for clade B1 (Fig 2-3). These areas with high genetic diversity coincided with the region of paleo-rivers (Sakaguchi et al., 2021), indicating that clade B1 maintained its population along paleo-rivers.

In contrast to the results of ENM, which showed the almost vanished suitable area with only a few remaining in the southern parts (Fig 2-3), areas with high genetic diversity were distributed in the northern and southern Kyushu (Fig 2-2). Volcanic activity in the central Kyushu (Mahony et al., 2011) may have prevented clade B2 from inhabiting this region, which was also suggested by the increase in the effective population size after LGM. Vegetation in central Kyushu was also affected by volcanic activity around LGM, which contributed to the cool climate (Miyabuchi, Sugiyama & Nagaoka, 2012; Miyabuchi & Sugiyama, 2020).

Refugia have been consistent with stable climate areas since LGM, and frequently harbor highly endemic fauna (Sandel et al., 2011). Climate stability between LGM and the present day has been proposed as a better predictor of species richness in European amphibian species (Araújo et al., 2008). However, Lehtomäki et al. (2018) suggested that climate stability was of relatively minor importance for Japanese amphibians; nevertheless, these findings do not reflect the characteristics of each species. They also indicated that historical climate stability was very important for plant species richness. The identified refugia of Japanese toads appeared to coincide with areas of plant species richness reported by Lehtomäki et al. (2018). Accordingly, the distribution patterns of each clade of Japanese toads may have been affected by climate stability after expansion from refugia.

Figure legends

Figure 2-1. Demographic analyses of each clade of *Bufo japonicus* and *B. torrenticola* based on mitochondrial sequencing data.

Left charts display the distribution of observed (histograms) and expected (orange solid lines: under demographic expansion, and green solid lines: under spatial expansion models) pairwise nucleotide differences. The sums of squared deviations (SSD) and p-values are shown for demographic and spatial expansion models. Asterisks indicate significant *p*-values ($p < 0.05$). Right charts display Bayesian skyline plots (BSP) showing the evolution of an effective population size (N_e) over time (blue solid lines: median estimates, and blue dashed lines: 95% confidence intervals of highest posterior densities). Vertical lines show the time to the most recent common ancestor (solid lines: median, and dotted lines: lower estimates).

Figure 2-2. Results of Genetic Landscape Shape interpolation analyses of each clade of *Bufo japonicus* and *B. torrenticola*.

The geographic distribution patterns of genetic diversity are shown for each clade. Areas with higher genetic diversity are shown in warmer colors, and those with lower genetic diversity are shown in cooler colors. Open circles indicate the localities of samples used for Genetic Landscape Shape interpolation analyses. Maps were created by QGIS 3.16 (https://qgis.org).

Figure 2-3. Predicted suitable distributions under the Last Glacial Maximum (LGM; CCSM and MIROC scenarios) for *Bufo japonicus* and *B. torrenticola*.

Warmer colors indicate higher probabilities of occurrence. Navy blue zones, land areas at LGM; grey zones, oceanic areas; white lines, the present land areas. Maps were created using R package map data version 2.3.0 (Becker, Wilks & Brownrigg, 2018).

Figure 2-4. Predicted present suitable distributions for *Bufo japonicus* and *B. torrenticola*.

Warmer colors indicate higher probabilities of occurrence. Navy blue zones, land areas; grey zones, oceanic areas. Maps were created using R package map data version 2.3.0 (Becker, Wilks & Brownrigg, 2018).

Table 2-1. Genetic diversity indices and neutrality tests for each clade of *Bufo japonicus* and *B. torrenticola* based on cytochrome *b* sequences.

		N	N_a	H_d ± SD	π ± SD	Fu's F_S	
						F_S	*p*-value
Bufo japonicus	clade A1	13	12	0.99 ± 0.04	0.006 ± 0.003	-5.46*	0.0061
	clade A2	33	29	0.99 ± 0.01	0.006 ± 0.003	-24.10*	0
	clade A3	83	57	0.98 ± 0.01	0.007 ± 0.004	-24.83*	0
	clade B1	45	36	0.99 ± 0.01	0.008 ± 0.004	-23.06*	0
	clade B2	28	26	0.99 ± 0.01	0.005 ± 0.003	-24.34*	0
Bufo torrenticola		25	19	0.97 ± 0.02	0.006 ± 0.003	-8.15*	0.0018

N, number of individuals; N_a, number of haplotypes; H_d, haplotype diversity; π, nucleotide diversity; SD, standard deviation. Asterisks indicate significant *p*-values ($p < 0.01$).

Table 2-2. Niche similarity scores of Schoener's *D* (above the diagonal) and Hellinger's *I* (below the diagonal) obtained from known occurrences between lineages of *Bufo japonicus* and *B. torrenticola*.

	A1	A2	A3	B1	B2	*torrenticola*
A1		0.45	0.26	0.22	0.04	0.20
A2	0.72		0.57	0.47	0.16	0.37
A3	0.52	0.83		0.59	0.21	0.48
B1	0.48	0.77	0.85		0.37	0.51
B2	0.18	0.41	0.49	0.68		0.25
torrenticola	0.46	0.69	0.76	0.78	0.53	

Table 2-3. Results of background similarity tests.

The *t*- and *p*-values in two-tailed *t*-tests and whether the observed niche similarities are more or less similar than expected by chance ($p < 0.01$) are shown.

			lineage for the background distribution								
			A1			A2			A3		
			t-value	*p*-value	similarity	*t*-value	*p*-value	similarity	*t*-value	*p*-value	similarity
lineage for the observed distribution	Schoener's *D*	A1				-4.06	1.E-04	more	-8.48	2.E-13	more
		A2	0.36	0.72	NS				-3.43	9.E-04	more
		A3	-20.32	2.E-16	more	-8.69	8.E-14	more			
		B1	-15.20	2.E-16	more	-837.44	2.E-16	more	-29.88	2.E-16	more
		B2	-32.92	2.E-16	more	-29.73	2.E-16	more	-13.25	2.E-16	more
		torrenticola	-26.40	2.E-16	more	-23.64	2.E-16	more	-69.19	2.E-16	more
	Hellinger's *I*	A1				-1.10	0.27	NS	-3.20	2.E-03	more
		A2	-1.44	0.15	NS				1.52	0.13	NS
		A3	-16.50	2.E-16	more	-5.79	8.E-08	more			
		B1	-15.08	2.E-16	more	-434.87	2.E-16	more	-25.06	2.E-16	more
		B2	-37.04	2.E-16	more	-27.28	2.E-16	more	-10.02	2.E-16	more
		torrenticola	-22.78	2.E-16	more	-20.86	2.E-16	more	-56.47	2.E-16	more

			lineage for the background distribution								
			B1			B2			*B. torrenticola*		
			t-value	*p*-value	similarity	*t*-value	*p*-value	similarity	*t*-value	*p*-value	similarity
lineage for the observed distribution	Schoener's *D*	A1	-43.23	2.E-16	more	32.67	2.E-16	more	-17.43	2.E-16	more
		A2	-37.68	2.E-16	more	-5.29	7.E-07	more	15.41	2.E-16	less
		A3	-20.50	2.E-16	more	13.92	2.E-16	less	31.92	2.E-16	less
		B1				-15.64	2.E-16	more	53.89	2.E-16	less
		B2	-7.63	1.E-11	more				4.45	2.E-05	less
		torrenticola	-36.69	2.E-16	more	-24.64	2.E-16	more			
	Hellinger's *I*	A1	-38.55	2.E-16	more	-19.32	2.E-16	more	-20.14	2.E-16	more
		A2	-30.82	2.E-16	more	-7.38	5.E-11	more	7.02	3.E-10	less
		A3	-19.02	2.E-16	more	12.98	2.E-16	less	35.61	2.E-16	less
		B1				-18.25	2.E-16	more	63.10	2.E-16	less
		B2	-4.01	1.E-04	more				10.53	2.E-16	less
		torrenticola	-30.27	2.E-16	more	-25.15	2.E-16	more			

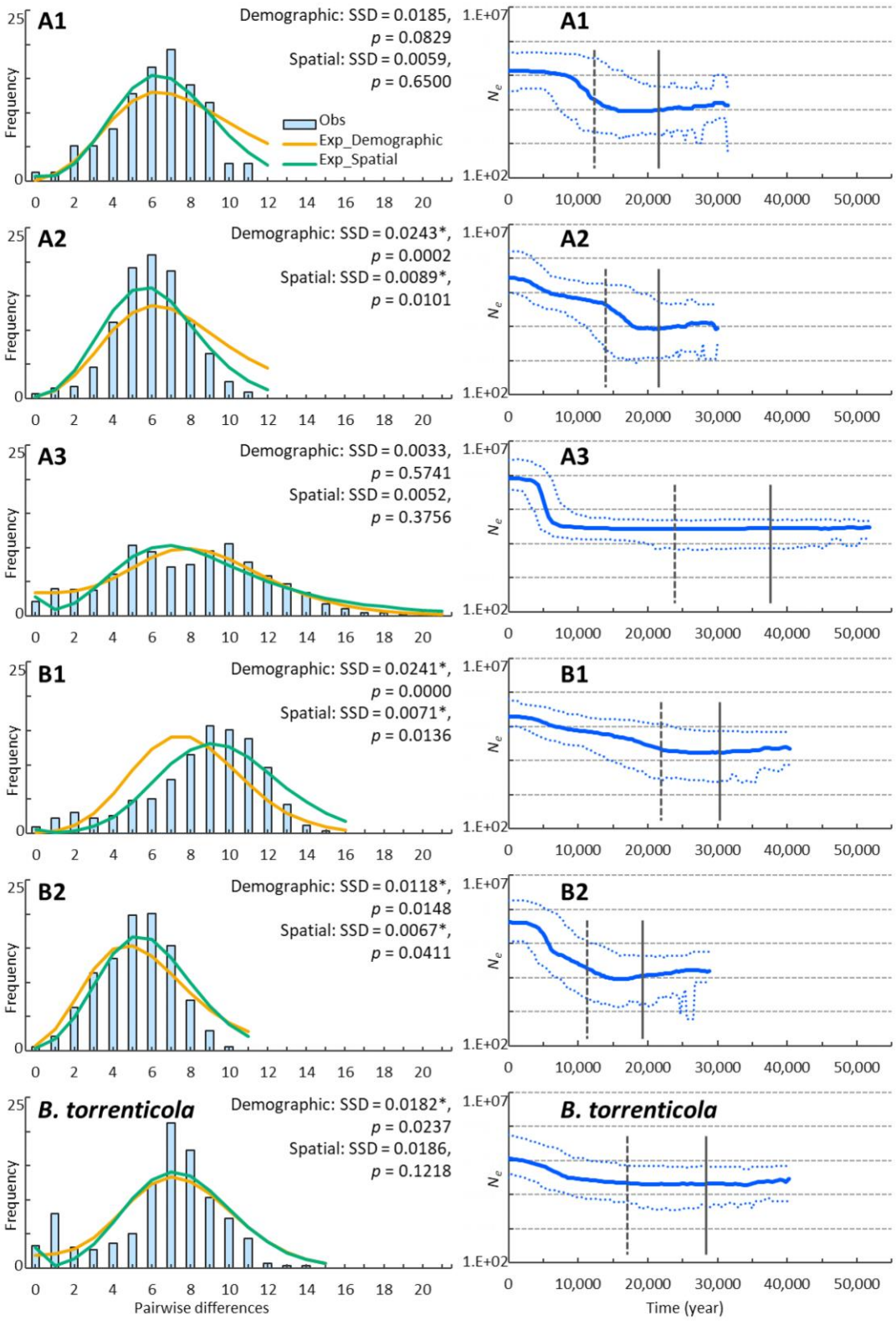
A1
Demographic: SSD = 0.0185,
p = 0.0829
Spatial: SSD = 0.0059,
p = 0.6500
Obs
Exp_Demographic
Exp_Spatial
A2
Demographic: SSD = 0.0243*,
p = 0.0002
Spatial: SSD = 0.0089*,
p = 0.0101
A3
Demographic: SSD = 0.0033,
p = 0.5741
Spatial: SSD = 0.0052,
p = 0.3756
B1
Demographic: SSD = 0.0241*,
p = 0.0000
Spatial: SSD = 0.0071*,
p = 0.0136
B2
Demographic: SSD = 0.0118*,
p = 0.0148
Spatial: SSD = 0.0067*,
p = 0.0411
B. torrenticola
Demographic: SSD = 0.0182*,
p = 0.0237
Spatial: SSD = 0.0186,
p = 0.1218
Frequency
Pairwise differences
Ne
Time (year)

Fig. 2-1

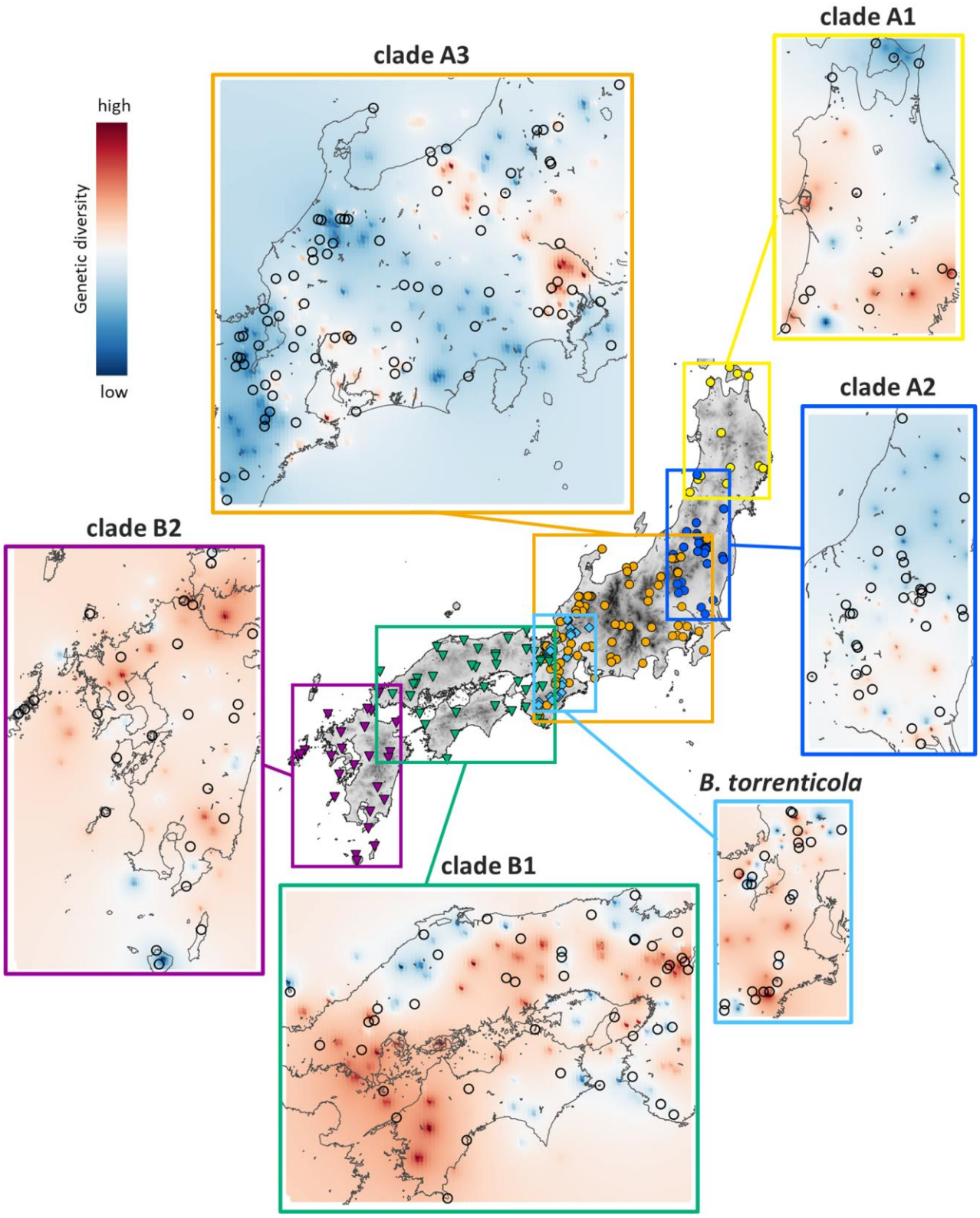
clade A1
clade A3
high
Genetic diversity
low
clade A2
clade B2
B. torrenticola
clade B1

Fig. 2-2

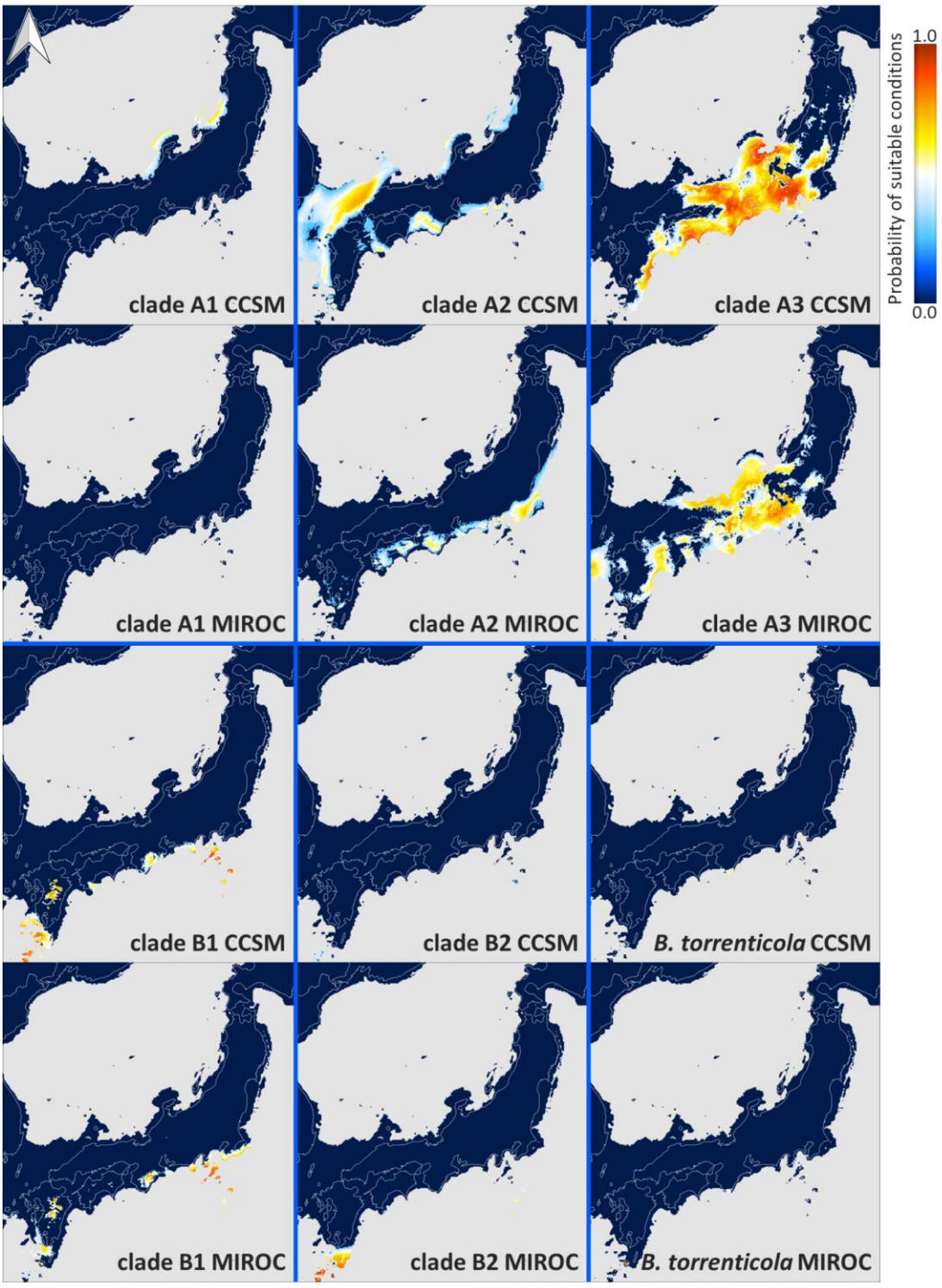
clade A1 CCSM
clade A2 CCSM
clade A3 CCSM
clade A1 MIROC
clade A2 MIROC
clade A3 MIROC
clade B1 CCSM
clade B2 CCSM
B. torrenticola CCSM
clade B1 MIROC
clade B2 MIROC
B. torrenticola MIROC
Probability of suitable conditions
1.0
0.0

Fig. 2-3

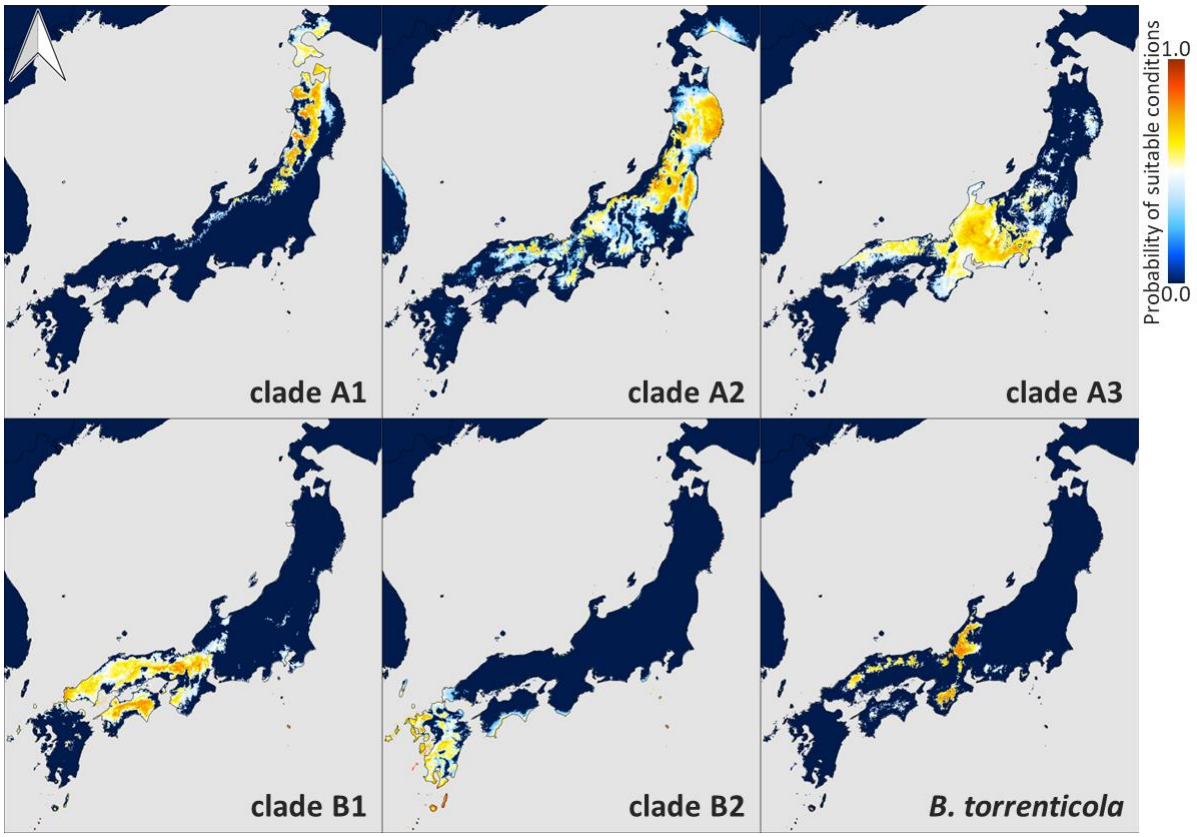
clade A1
clade A2
clade A3
clade B1
clade B2
B. torrenticola
Probability of suitable conditions
1.0
0.0

Fig. 2-4

Chapter 3

Population genetic structure and hybrid zone analyses for species delimitation in the Japanese toad (*Bufo japonicus*)

3-1. Introduction

Hybrid zones are natural laboratories that offer many insights into speciation processes, thereby contributing to a more detailed understanding of evolution (Barton & Hewitt, 1985; Hewitt, 1988; Abbott et al., 2013). Hybridization following secondary contact may produce different outcomes depending on the extent to which genetic diversity and reproductive barriers have accumulated during isolation. This results in a reduction in differentiation as well as the fusion of gene pools. Alternatively, an increase in the strength of the genetic barrier may lead to complete reproductive isolation (Barton & Hewitt, 1985; Wu, 2001).

Hybridization is frequent and evolutionarily significant in amphibians (Burbrink and Ruane, 2021). There are well-described studies on amphibians for the hybrid zone of fire-bellied toads (*Bombina bombina* and *B. variegata*; e.g., Szymura & Barton, 1986, 1991; Yanchukov et al., 2006), green toads (*Bufotes viridis* subgroups; e.g., Stöck et al., 2006; Colliard et al., 2010; Dufresnes et al., 2014), and, more recently, European common toads (*Bufo bufo* and *B. spinosus*; e.g., Arntzen et al., 2016, 2018; Dufresnes et al., 2020a; Riemsdijk et al., 2023). In contrast to many other anuran species, the hybrid zone of Japanese toads has not yet been examined in detail (*Bufo japonicus* subspecies; Miura, 1995). However, they have the advantage of comprising distinct genetic lineages representing different stages of the speciation process because several contact zones of the different genetic lineages have been recognized (Chapter 1). Regarding amphibian cases, the extent of natural hybridization in contact zones has been correlated with divergence times (Hickerson, Meyer & Moritz, 2006; Dufresnes et al., 2021).

Bufo japonicus Temminck and Schlegel, 1838 is widely distributed in the Japanese archipelago, Honshu, Shikoku, Kyushu, and some adjacent islands. This species is divided into two subspecies, *B. j. japonicus* from western Japan and *B. j. formosus* Boulenger, 1883 from eastern Japan. These two subspecies are parapatrically distributed with the boundary in the Kinki region of central Japan (Matsui & Maeda, 2018). Matsui (1984) concluded that *B. j. japonicus* and *B. j. formosus* showed a climatic cline in their morphometric characteristics, which was insufficient to distinguish them as different species because of their identity in the

fundamental patterns of modes of life. However, Dufresnes & Litvinchuk (2021) recently proposed elevating *B. j. japonicus* and *B. j. formosus* to the species level based on the Miocene split estimated by mtDNA markers. However, they refrained from taxonomic changes because mitochondrial distances may not reflect actual species distances. Other studies proposed the Kinki region as a hybrid zone of *B. j. japonicus* and *B. j. formosus* by a C-banding analysis of chromosomes (Miura, 1995).

The sympatric distribution of mitochondrial haplotypes of *B. j. japonicus* and *B. j. formosus* was also found in the Kinki region (Chapter 1). Furthermore, several contact distributions of the genetic lineages in the two subspecies were identified. These findings indicate the necessity of analyzing the degree of hybridization between the two subspecies and other genetic lineages for taxonomic revision.

The delimitation of species must be connected to a species concept. I used the integrative species concept (de Queiroz, 2007, 2020) that considers both aspects, phylogeny and the reproductive isolation mechanism.

In this study, I applied multiplexed ISSR genotyping by sequencing (MIG-seq: Suyama & Matsuki, 2015) to achieve the fine-scale resolution of genetic clusters in *B. j. japonicus* and *B. j. formosus*. MIG-seq has been effectively used to study molecular phylogenetic taxonomy for various taxa (see Suyama et al., 2022).

I performed cline analyses to elucidate the degree of gene flows. The results of cline analyses explained the transition between the characteristics of interbreeding species across the hybrid zone and will contribute to a more detailed understanding of the mechanisms maintaining species boundaries (Barton & Hewitt, 1985). Valid species need to exhibit significant divergence and narrow transition zones. In contrast, insufficiently diverged lineages that remained conspecific need to admix freely across broad genetic areas. I revised the taxonomic status of *B. j. japonicus* and *B. f. formosus* based on phylogenetic and hybrid zone analyses.

3-2. Materials & Methods

Sampling and MIG-seq

A total of 155 individuals of *B. japonicus* and 13 of *B. torrenticola* Matsui, 1976 were collected, covering the complete distribution range. The Animal Experimentation Ethics Committee in the Graduate School of Human and Environmental Studies, Kyoto University

approved this research (20-A-5, 20-A-7, 22-A-2). DNA was extracted from frozen or ethanol-preserved tissue samples (e.g., muscle, liver, or skin) with the Qiagen DNeasy Blood and Tissue Kit following the manufacturer's instructions.

I prepared two genomic libraries and sequenced them separately for the convenience of the experiment, and the data obtained were analyzed together as described below. Library 1 included 121 DNA samples of *B. japonicus* and 13 of *B. torrenticola*, while library 2 had 40 DNA samples of *B. japonicus*, with six of *B. japonicus* overlapping in both libraries. The two genomic libraries were prepared following the protocol described by Matsui et al. (2019b) for library 1 and that described by Watanabe et al. (2020) for library 2. Amplicons in libraries 1 and 2 were purified and sequenced on the Illumina MiSeq Sequencer (Illumina San Diego, CA, USA) using the MiSeq Reagent Kit v3 (150 cycles, Illumina). Two libraries were prepared and sequenced separately for the convenience of the molecular experiment, and the raw sequence data obtained were combined for subsequent data analyses.

The raw sequence reads of MIG-seq data were deposited in the DNA Data Bank of Japan (DDBJ) Sequence Read Archive (DRA) under accession number DRA016475 (BioProject ID; PRJDB15971: BioSample ID; SAMD00622809–SAMD00622982).

Raw paired-end sequences (reads 1 and 2) were filtered by fastp version 0.23.2 (Chen et al., 2018) to trim the first 14 base sequences of read 2 and the primer regions of reads 1 and 2 and to discard reads shorter than 80 bp and low-quality sequences with phred quality Q <30 according to Suyama and Matsuki (2015). I then mapped the filtered reads to reference sequences because mapping obtains more loci than a *de novo* analysis of MIG-seq data (Takata et al., 2021). As the reference genome sequence for Japanese toads, I used the genome assembly of their closely related species, *B. gargarizans* (RefSeq assembly accession number: GCF_014858855.1; https://www.ncbi.nlm.nih.gov/data-hub/genome/GCF_014858855.1/). The assembly contained 11 chromosome-level contigs and unplaced scaffolds. I ultimately mapped the filtered reads to the indexed reference sequences by bwa-mem2 version 2.2.1 (Vasimuddin et al., 2019) to make SAMfiles, which were then converted to BAM files and sorted with a minimum mapping quality of 20 using *samtools* version 1.15 (Li et al., 2009).

Genotyping

I prepared the following datasets: dataset I, data from samples of *B. japonicus* and *B. torrenticola* to examine the genetic structure of Japanese toads, and dataset II, data from samples of *B. j. japonicus* and *B. j. formosus* to investigate the degree of reproductive isolation between the two subspecies. I excluded the 11 samples from these two datasets that were considered to be from artificially introduced populations based on the results in Chapter 1. I instead prepared dataset III, which included these 11 samples with dataset II to verify their genetic assignment in the population.

The reference-based analysis pipeline with the *gstacks* program followed by the *populations* program in Stacks v2.60 (Rochette, Rivera-Colón & Catchen, 2019) was applied to the mapped reads of all datasets to call SNPs and genotypes. The following filters were used for the *populations* program in Stacks. I initially kept variant sites with a minimum allele count of three (--min-mac 3) to ensure that an allele was in at least two diploid samples (Rochette, Rivera-Colón & Catchen, 2019). I then set up the maximum observed heterozygosity at 0.5 (--max-obs-het 0.50) because heterozygosity for a biallelic SNP was expected to be <0.5, and SNPs with values above this threshold may belong to paralogous loci or multilocus contigs (Hohenlohe et al., 2011; Willis et al., 2017). Subsequently, only one random SNP per locus was extracted (--write-random-snp) to avoid any effect of linkages among SNPs on the multivariate analysis (Gargiulo, Kull & Fay, 2020). In the population designation in a *population map*, I set two populations corresponding to *B. japonicus* and *B. torrenticola* for dataset I. In datasets II and III, I set two populations based on the admixture proportion (*q*-value, with *q*-value = 0.5 as a boundary) at the optimal number of clusters (*K*) = 2 in the Structure analysis (see below: Pritchard, Stephens & Donnelly, 2000) of dataset I. I ultimately only processed the loci present in at least 80% of samples in a population (*-r* = 0.80) and those present in two populations for all datasets (*-p* = 2). In the following stacks program, the two parameters, *-r* and *-p*, varied, and the others were common for each analysis.

Estimation of genetic structures

To estimate the population genetic structures of *B. japonicus* and *B. torrenticola*, I performed three different methods using SNP genotyping information and compared grouping among these methods: a discriminate analysis of principal components (DAPC; Jombart, Devillard &

Balloux, 2010), Structure 2.3.4 (Pritchard, Stephens & Donnelly, 2000), and a principal component analysis (PCA; Cavalli-Sforza, 1966). DAPC was used to infer the number of clusters. I used Structure analyses to perform a Bayesian clustering analysis. In addition, complementary to Structure analyses, I performed PCA.

DAPC was performed on dataset I in the R package *adegenet* 2.1.8 (Jombart, 2008; Jombart, Devillard & Balloux, 2010; Jombart & Ahmed, 2011). This method maximizes the variance among groups while minimizing variations within groups without making assumptions about the underlying population genetic model. This approach transforms multilocus genotype data using PCA to derive uncorrelated variables that are input for a discriminate analysis. The optimal groups were initially assessed using the *de novo* clustering method, *find.cluster*, testing *K* values from 1 to 8, and the best *K* value was selected with the Bayesian information criterion (BIC) method. This *de novo* clustering method and initial DAPC using the *dapc* function were run. The *optim.a.score* was then used to assess the optimal number of principal components (PCs) to retain. Once the optimal number of PCs was selected, a second DAPC analysis was conducted using this value.

The program Structure 2.3.4 (Pritchard, Stephens & Donnelly, 2000) performed the analysis by an admixture model with correlated allele frequencies based on the Bayesian clustering method to infer the population structure. Since excessive uneven sampling may increase bias on admixture proportions in the Structure analysis (Toyama, Crochet & Leblois, 2020), I reduced the sample size in Yakushima and Tanegashima from dataset I, called dataset I-2, and conducted Structure analyses. Structure analyses were performed for the number of clusters *K* from 1 to 8, with ten runs for each *K* value. Markov chain Monte Carlo (MCMC; Metropolis et al., 1953; Hastings, 1970) iterations of 100,000 were implemented for each run after an initial burn-in of 100,000. The parallelization of Structure 2.3.4 calculations was achieved using EasyParallel (Zhao et al., 2020) to reduce the computational time. The optimal number of clusters was inferred in StructureSelector (Li & Liu, 2018) with the Delta *K* (Δ*K*; Evanno, Regnaut & Goudet, 2005), MedMeaK, MaxMeaK, MedMedK, and MaxMedK (Puechmaille, 2016). StructureSelector integrated the CLUMPAK program (Kopelman et al., 2015) to cluster and merge data from independent runs and generate graphical representations of the results. In a Structure analysis, an admixed ancestry is modeled by assuming that an individual has inherited some proportion of its genome from its ancestors in the population (Pritchard, Stephens & Donnelly, 2000).

PCA was performed on dataset I using the R package *adegenet* 2.1.8 (Jombart, 2008; Jombart & Ahmed, 2011), and the first two eigenvectors were plotted in two dimensions.

Moreover, I conducted a Structure analysis of dataset III to identify the assignment of genomic clusters for samples from introduced populations, reducing the sample size in Yakushima and Tanegashima for the above reason as dataset III-2. A Structure analysis was performed on the number of clusters *K* from 1 to 6, and other parameters were the same as above.

Phylogenetic estimations

I used SNAPP 1.5.2 (Bryant et al., 2012) implemented in Beast v 2.6.7 (Bouckaert et al., 2019) to estimate phylogenetic relationships among population groups identified by my clustering. I selected four individuals for each population group and applied them to the stacks program (*-r* = 1.0 and *-p* = 5). I ran SNAPP for 10,000,000 iterations with mutation rates *u* and *v* = 1.0, a gamma distribution with *alpha* = 2 and *beta* = 200 for the lambda prior, and *alpha* = 1, *beta* = 250, *kappa* = 1, and *lambda* = 10 for *snapprior*, sampling every 1,000 steps. Convergence was examined using Tracer 1.7.2 (Rambaut et al., 2018), and the results obtained were visualized by Densitree 2.2.7 with a burn-in of 10%. The maximum clade credibility tree with posterior probability was calculated using TreeAnnotator version 2.6.7 (Bouckaert et al., 2019). To perform comparisons, I reconstructed a mitochondrial phylogenetic tree using the mitochondrial cytochrome *b* sequences from Chapter 1 of the same individuals used to construct the SNP tree adding the sequence of *B. g. gargarizans* as the outgroup. RAxML version 8.2.12 (Stamatakis, 2014) was employed for 1,000 bootstrap iterations with the GTRGAMMA model to infer a maximum likelihood phylogenetic tree based on mitochondrial sequences.

Effective estimates of migration surfaces

I visualized the spatial patterns of gene flow using Fast Estimation of Effective Migration Surfaces (FEEMS; Marcus et al., 2021) to assess the genomic context and geographic location of any historical barriers to migration in *B. japonicus*. FEEMS is an improvement of Estimated Effective Migration Surfaces (Petkova, Novembre & Stephens, 2016) and uses a Gaussian Markov Random Field model in a penalized likelihood framework. This method uses locality information and pairwise dissimilarity matrices calculated from SNP data to

identify regions where genetic similarity decays more quickly than expected under isolation by distance (Petkova, Novembre & Stephens, 2016). To estimate effective migration parameters, I used the genotype data of dataset II as well as the coordinate information of each individual as inputs. A polygon grid was prepared using QGIS 3.28. Cross-validation was performed and the lambda with the lowest cross-validation value was used to generate the final plot.

Hybrid zone analyses

To estimate the geographic gradient of genomic differences between adjacent clusters of *B. japonicus*, I calculated the steepness of the cline of genetic differences. Assuming similar dispersal abilities among the individuals of each cluster and no geographic barriers to gene flow at their transitions, wide hybrid zones will be present for the younger pairs if they have not yet evolved significant reproductive isolation. In contrast, narrow transitions will be present for the older pairs if they represent distinct species.

I fit clines to the Structure *q*-value across the geographic transition between genetic clusters using the R package *hzar* version 0.2-7 (Derryberry et al., 2014). The admixture proportions inferred by the Structure program (Pritchard, Stephens & Donnelly, 2000) have frequently been used to fit a geographic consensus cline, from which the width of the hybrid zone is estimated (e.g., Tominaga et al., 2018; Dufresnes et al., 2020b). To avoid bias on the admixture proportions of Structure, I also reduced the sample size in Yakushima and Tanegashima from dataset II as dataset II-2. I also fit clines to mitochondrial haplogroup frequency data from my previous study (Chapter 1) for comparison with nuclear ancestry clines.

I performed the stacks program on this subset, setting four populations based on the results of DAPC on dataset II, with -*r* = 0.80 and -*p* = 4, and conducted a Structure analysis using the same parameters as above. This subset was divided into sub-datasets I, II, and III, based on the *q*-value at *K* = 4 with some samples overlapping. Each sub-dataset contained individuals of two pure clusters, considering a *q*-value >0.90 as pure individuals and admixed individuals between pure clusters. I applied the stacks program for each sub-dataset, setting three populations (two pure and one admixed population) with -*r* = 0.80 and -*p* = 3, and conducted a Structure analysis. The *q*-values on *K* = 2 for each sub-dataset were used to perform *hzar*. In addition to the three sub-datasets, I prepared sub-dataset III-2, which is data

excluding samples in Shikoku and Seto Inland Sea (see discussion) and performed a similar analysis to that for the other sub-datasets.

I reduced the two-dimensional space (latitude and longitude) into a single-dimensional distance from the center line of the hybrid zone. The probable center line of the admixture was estimated using R package *tess3r* version 1.1 (Caye, 2016, 2018) and considered to be the baseline for *hzar*. The minimum distances from the baseline to individuals were calculated in QGIS 3.28. I assigned a positive or negative sign to these distances depending on individual orientations to the baseline.

The shape of a cline is modeled by combining three equations (Szymura & Barton, 1986, 1991) that describe a sigmoid shape at the center of a cline (maximum slope) and two exponential decay curves on either side of the central cline (tails). I tested 15 different models, which combined three trait intervals and five fitting tails, for each cline plus a null model with no cline. The three possible combinations of trait intervals were used to scale clines by the minimum (p_{min}) and maximum (p_{max}) values in the cline: no scale (fixed to $p_{min} = 0$ and $p_{max} = 1$), observed values (fixed to p_{min} = minimum observed mean values, p_{max} = maximum observed mean values), and estimated values (p_{min} and p_{max} as the free parameter). The five possible combinations of fitting tails represent the cline shapes: no tails, right tail only, left tail only, symmetrical tails, mirror tails, and both tails estimated separately.

MCMC was performed for each model with the default values of 100,000 generations, each with a randomly selected seed and 10% of steps discarded as a burn-in. After each run, I compared the model performance using the Akaike information criterion score corrected for a small sample size (AICc; Anderson & Burnham, 2002). The model with the lowest AICc score was selected as the best-fit model to infer cline widths and centers along with a 95% confidence interval (CI). The stability and convergence of the cline parameters of the best-fit model were assessed by visualizing MCMC traces. I plotted the maximum-likelihood clines and 95% credible cline region for the best-fit model.

Introgression

I assigned individuals in each contact zone to hybrid classes to estimate whether gene flow is an ongoing or historic admixture. I temporarily designated individuals with *q*-values >0.98 for $K = 2$ in the Structure analysis of sub-datasets I, II, and III as parental individuals for each

cluster following Scordato et al. (2017). I identified ancestry-informative markers by calculating AMOVA F_{ST} for SNPs between pairs of parental clusters using the stacks program on the sub-datasets, setting three populations (two parental and one admixed population) and -*r* = 0.80 and -*p* = 3. The diagnostic loci, F_{ST} = 1, were selected as ancestry-informative markers segregating between each pair of parental clusters.

I used the R package INTROGRESS version 1.2.3 (Gompert & Buerkle, 2010) to calculate the maximum-likelihood estimates of the hybrid index for each individual and the average heterozygosity of each individual across informative loci. I compared genomic hybrid indices with heterozygosity to identify the individual hybrid classes. Pure individuals were defined by a hybrid index of 0 or 1 because only loci fixed in parental individuals with F_{ST} =1 were used. First-generation hybrids (F1) have an expected hybrid index of 0.5 and heterozygosity of 1.0. I regarded individuals with intermediate hybrid indices (>0.25 and <0.75) and high heterozygosity (≥0.5) as recent-generation hybrids, those with intermediate hybrid indices (>0.25 and <0.75) and low heterozygosity (<0.5) as later-generation hybrids, and those with low or high hybrid indices (≤0.25 or ≥0.75) as backcrossed to one or the other parental type according to previous studies (Milne & Abbott, 2008; Scordato et al., 2017; Slager et al., 2020).

Estimation of migration rates

Recent migration rates between parental and hybrid populations were calculated using the Bayesian inference approach by BayesAss3-SNPs v 1.1 (Wilson & Rannala, 2003; Mussmann et al., 2019). Using sub-datasets I, II, and III after applying for the stacks program with each setting for three populations (two parental and one admixed population) and -*r* = 0.80 and -*p* = 3, BA3-SNPs -autotune v2.1.2 (Mussmann et al., 2019) was performed with the default parameters to find mixing parameters for BA3-SNPs. BayesAss3-SNPs was conducted with ten million generations sampling every 100 generations using predefined mixing parameters. The first one million generations were discarded as a burn-in, and chain convergence was assessed in Tracer v 1.7.2 (Rambaut et al., 2018).

All analyses by R were conducted in R studio version 2022.07.2.576 (Rstudio Team 2022) using R version 4.2.2 (R Core Team 2022).

3-3. Results

Analyses of MIG-seq data

A total of 46,889,160 clean reads in 168 samples passed quality filtering, with the average percentage of reads that passed filtering for each sample being 77.6%. Among them, 17,644,888 reads were successfully mapped to the reference genome of *B. gargarizans* in the reference-mapping approach with an average mapping quality of 27.2%.

Genetic structure and phylogeny

A total of 839 variants were identified in dataset I of 157 samples of *B. japonicus* and *B. torrenticola*.

I retained all information (157 PCs) for the initial DAPC on dataset I. After running the initial steps, the first 21 PCs were retained following the result of the *optim.a.score* function (Fig. 3-7A). The BIC plot in DAPC displayed the lowest value at $K = 4$ and 5 (Fig. 3-7B), and both clearly identified three clusters corresponding to *B. j. formosus*, *B. j. japonicus*, and *B. torrenticola*. The results of $K = 4$ identified two subclusters within *B. j. japonicus*. In addition, two subclusters within *B. j. formosus* were recognized for $K = 5$. However, these defined subclusters within *B. j. japonicus* and *B. j. formosus* had markedly overlapping plots between subclusters (Fig. 3-1A).

A total of 570 variants were identified in dataset I-2 of 131 samples. A Structure analysis of dataset I-2 supported two peaks for the ΔK estimation, $K = 2$ and 5 (Fig. 3-8A), and the number of K estimated from MedMeaK, MaxMeaK, MedMedK, and MaxMedK values was 5 (Fig. 3-8B).

Therefore, $K = 5$ may be the valid cluster number in my results, leading to a similar grouping pattern to the DAPC (Fig. 3-1B). The five genetic clusters identified by DAPC and Structure analyses corresponded to northern *B. j. formosus* (NF), southern *B. j. formosus* (SF), eastern *B. j. japonicus* (EJ), western *B. j. japonicus* (WJ), and *B. torrenticola*. Cluster assignments for individuals by DAPC are shown in Fig. 3-1.

The Structure bar plot revealed that *B. torrenticola* has rare admixtures with *B. japonicus*, three samples of *B. torrenticola* had *q*-values from 0.85 to 0.9, and one sample of *B. j. formosus* had a *q*-value of 0.09 admixed with *B. torrenticola*. These samples appeared to be hybrid individuals based on the *q*-value threshold following Vähä & Primmer (2006).

Therefore, the admixed sample of *B. j. formosus* was excluded from the subsequent analysis of *B. japonicus* (datasets II, II-2, III, and III-2 and all sub-datasets).

Structure assignments also revealed hybridization between each adjacent cluster of *B. japonicus* (Fig. 3-1B). The admixture proportion assignment for each cluster of *B. japonicus* changed in steps. High levels of continuous admixtures were indicated across the geographic transition between NF and SF and between EJ and WJ. In contrast, hybrid individuals were limited to the boundary between SF and EJ.

The first PC axis explained 25.1% of the genomic covariance in PCA. It separated the two subspecies, *B. j. formosus* and *B. j. japonicus* (Fig. 3-1C). By the second PC axis, *B. torrenticola* had clearly split from *B. japonicus*. In addition, the second axis separated two continuous clusters within *B. j. japonicus*.

Based on SNAPP (290 SNPs), nuclear phylogeny confirmed deep splits between the five main clades (Fig. 3-2A). Mitochondrial cytochrome *b* phylogeny (1,071 bp) recovered the splits of the main clades confirmed in Chapter 1 (Fig. 3-2B).

Artificially introduced population

A total of 718 variants were identified in the 128 samples of dataset III-2, *B. japonicus,* including the 11 samples from the artificially introduced populations in Hokkaido, Izu Islands, and the Kanto region. Two individuals in Hokkaido (Asahikawa and Hakodate) had an admixture, mainly two clusters of NF and SF, similar to those in Niijima and Kouzushima (Fig. 3-9). Individuals in Tokyo and Kanagawa prefectures had four admixed clusters of NF, SF, EJ, and WJ. The individual in Oshima had three clusters of SF, EJ, and WJ, and one in Hachijojima had clusters of SF and EJ.

Effective estimates of migration surfaces

A total of 783 variants were identified in dataset II, 143 samples of *B. j. japonicus* and *B. j. formosus*. The estimated effective migration rates confirmed low migration rates between *B. j. formosus* and *B. j. japonicus* despite the absence of any geographic barrier that limits gene flow between subspecies (Fig. 3-3). Among *B. j. japonicus*, low migration rates were detected between Chugoku and Shikoku vs. Kyushu, and Kyushu vs. Yakushima, which appeared to be due to the presence of straits. In contrast, high migration rates were detected within them. On the other hand, among *B. j. formosus*, low migration rates were widely identified from

Tohoku to Chubu, likely due to fewer interactions between regions than among *B. j. japonicus*.

Hybrid zone analyses

Each sub-dataset consisted of cluster pairs, sub-dataset I (NF–SF) of 47 samples, sub-dataset II (SF–EJ) of 47 samples, sub-dataset III (EJ–WJ) of 59 samples, and sub-dataset III-2 (EJ–WJ excluding samples in Shikoku and Seto Inland Sea) of 48 samples. The geographic distribution of each cluster detected by *tess3r* on each sub-dataset ($K = 2$) did not significantly differ from that of Structure analyses by SNP data. The baselines across the three contact zones are shown in Fig. 3-4. Regarding the SNP data of sub-dataset SF–EJ and the mtDNA data of EJ–WJ, the best-supported model in *hzar* with the lowest AICc was that in which scaling was fixed to the minimum value of 0 and maximum value of 1, and no exponential tails were desired. In sub-datasets NF–SF and EJ–WJ and the mtDNA data of SF–EJ and NF–SF, the model selected was that in which scaling was fixed to the minimum and maximum observed mean values, and no exponential tails were desired.

Based on SNP data, the cline width decreased from NF–SF 170 (CI: 82–362) km to EJ–WJ 162 (CI: 63–330) km and SF–EJ 29 (CI: 24–76) km (Fig. 3-5). The estimated centers based on SNP data as the distance from the baseline were 0.6 (CI: -9.5–12) km for SF–EJ, 5.4 (CI: -42–58) km for NF–SF, and 7.0 (CI: -40–56) km for EJ–WJ.

Based on mtDNA data, the cline width decreased from NF–SF 86 (CI: 35–223) km to EJ–WJ 75 (CI: 31–212) km and SF–EJ 39 (CI: 18–106) km (Fig. 3-5). The estimated centers based on mtDNA data as distances from the baseline were 0.3 (CI: -12–15) km for SF–EJ, 23 (CI: -12–64) km for NF–SF, and -33 (CI: -75–-6.2) km for EJ–WJ.

In addition, in the sub-dataset EJ–WJ excluding samples in Shikoku and Seto Inland Sea (48 samples), the model selected for SNP and mtDNA data was that in which scaling was fixed to the minimum and maximum observed mean values, and no exponential tails were desired. Based on SNP data, the width was 99 (CI: 33–301) km and the distance from the baseline was -1.2 (CI: -38–53) km. Based on mtDNA data, the width was 79 (CI: 32–245) km and the distance from the baseline was -33 (CI: -76–-2.0) km (Fig. 3-5).

Introgression

I identified loci that were informative for assigning hybrid classes for each sub-dataset. There were 40 loci with F_{ST} >1.0 between parental SF and EJ, and six loci for the NF and SF pair and EJ and WJ pair. Comparisons of individual hybrid indices and average heterozygosity using these differentiated loci revealed that none of the pairs contained F1 individuals (Fig. 3-6). A recent-generation hybrid with high heterozygosity was detected in the NF–SF contact zone only, confirming ongoing gene flow. Later-generation hybrids were detected in all contact zones, and hybrid individuals with intermediate hybrid index values and heterozygosity of zero were identified in NF–SF and EJ–WJ contact zones, suggesting that old-origin hybrids survived. Backcrossed individuals with both parental populations were identified in the NF–SF and SF–EJ contact zones, while those with one parental population were detected in the EJ–WJ contact zone.

BayesAss directional migration

The mixing parameters for migration rates (-*m*), allele frequencies (-*a*), and inbreeding coefficients (-*f*) were selected using BA3-SNPs-autotune for each sub-dataset: sub-dataset NF–SF, -*m* =0.2125, -*a* =0.55, -*f* =0.1; sub-dataset SF–EJ, -*m* = 0.2125,-*a* =0.55, -*f* =0.1281; sub-dataset EJ–WJ, -*m* = 0.1563, -*a* =0.325, -*f* =0.1.

All estimated migration rates between populations are shown in Table 3-1. In the sub-dataset NF–SF, the self-recruitment estimate of the parental population of SF was high at >95%, while that of the parental population of NF and the hybrid populations were slightly lower (90–95%). Northward migration rates through the hybrid zone, from the parental SF to the hybrid (5.9%) and from the hybrid to the parental NF (3.6%), were higher than migration rates in the opposite direction, from the parental NF to the hybrid (1.5%) and from the hybrid to the parental SF (1.7%).

In the sub-dataset SF–EJ, self-recruitments within both parental populations were estimated to be high at >95%. In contrast, the hybrid population had low self-recruitment rates at 76.2%. Correspondingly, outward migration rates from the hybrid population into parental populations were low (2.0% to parental SF and 1.3% to parental EJ efflux). In contrast, migration rates into hybrid populations were high (16.7% from parental SF and 7.1% from parental EJ influx).

In the sub-dataset EJ–WJ, the self-recruitment of both parental populations was high at >95%, while that of the hybrid population was intermediate at 80.1%. The estimations of migration rates from hybrids into both parental populations were low (1.3% to parental EJ and 1.4% to parental WJ efflux). In contrast, migration rates into hybrid populations were high (7.3% from parental EJ and 12.6% from parental WJ influx). The migration rates among each parental population were estimated to be very low, ranging between 1.3 and 2.6%.

3-4. Discussion

Genetic clustering and phylogeny

Previous studies reported that Japanese toads diverged into six mitochondrial lineages from the late Miocene to the middle Pleistocene (Igawa et al., 2006; Chapter 1). The two subspecies, *B. j. japonicus* and *B. j. formosus*, were recommended for elevation to the species level given their Miocene split. However, the findings of these studies were insufficient for the taxonomic conclusion because they were based solely on mitochondrial analyses (Dufresnes & Litvinchuk, 2021). Given the contact between the distribution zones of the two subspecies (Chapter 1) and the possible presence of a hybrid zone between them (Miura, 1995), identifying the status of the zone is necessary for the study of the taxonomic status of Japanese toads because I followed the integrative species concept that considers phylogeny and reproductive isolation.

I used SNP markers of samples covering virtually the complete distribution ranges of *B. j. japonicus*, *B. j. formosus*, and *B. torrenticola* and presented the clustering and phylogenetic relationship between the identified clusters. I then showed the results of a fine-scale analysis of gene flow across the secondary contact zones of *B. j. formosus* and *B. j. japonicus*.

The consensus across independent methods suggested that $K = 5$ most accurately described the population structure of *B. japonicus* and *B. torrenticola*. This SNP clustering was roughly concordant with the five main mitochondrial clades in Chapter 1, except for the lesser diverged mitochondrial clade in the Tohoku region (NF). Based on SNP data, phylogeny confirmed the splits between the five main clades. However, the topology was discordant with the mitochondrial phylogenetic topology for the clades in western Japan (Fig. 3-2). The SNP phylogenetic tree showed EJ and WJ as sister clades and supported the monophyly of *B. j. japonicus*. However, in the mitochondrial phylogenetic tree, *B. j.*

japonicus was paraphyletic because *B. torrenticola* and WJ were identified as sister clades with a high node support (Fig. 3-2). One explanation is that *B. torrenticola* and the ancestor of EJ and WJ may all simultaneously diverge. Alternatively, discordance may stem from ancestral mitochondrial introgression between *B. torrenticola* and WJ after they diverged. These hypotheses need to be tested explicitly in future phylogenetic studies.

The hybrid zone between *B. j. japonicus* and *B. j. formosus*

I found that mitochondrial and SNP marker cline positions and shapes varied for the three contact zones between four clusters of *B. j. japonicus* and *B. j. formosus* and showed different patterns of gene flow.

The hybrid zone between *B. j. japonicus* and *B. j. formosus* showed a sharp genetic transition, with concordant and coinciding clines between mtDNA and SNP (Fig. 3-5B). The cline width depended, in part, on whether the hybrid zone was structured primarily by selection or by a neutral process (Mallet et al., 1990). The cline width without any form of selection may be calculated using the following diffusion approximation from Barton & Gale (1993): $w = 2.51\sigma\sqrt{T}$, where w, cline width, T, number of generations since secondary contact, and σ, average lifetime dispersal. While the lifetime dispersal distance for *B. japonicus* currently remains unknown, the maximum dispersal distance recorded for native *B. j. formosus* between the breeding pond and the summer home range is 0.26 km and the generation time is three years (Kusano, Maruyama & Kaneko, 1995). At a dispersal of 0.78 km per generation, cline width exceeds the 29.4 km width of the hybrid zone in *ca.* 677 years of unrestricted diffusion. Based on their paleo distribution, these toads came into contact with expansion after LGM at the latest (Chapter 2). Therefore, contact between the subspecies is arguably markedly older than 677 years. The cline width may have been kept narrow over a long time despite the absence of geographic barriers to dispersal, presumably through selection against hybrids, suggesting that the two subspecies formed a tension zone (Key, 1968; Barton & Hewitt, 1985) in the Kinki region. In addition, all hybrid individuals were classified by INTROGRESS as layer-generation hybrids or backcrosses, suggesting the relatively ancient origin of their contact.

The hybrid zone within *B. j. japonicus*

Based on the refugia distributions proposed by Chapter 2, the mitochondrial boundary of EJ and WJ may have been maintained at the western edge of the Chugoku region from LGM to the present. Therefore, EJ and WJ likely shared refugia during the glacial period, resulting in admixture. Admixed individuals may have spread to the Shikoku region and surrounding islands through the Seto Inland Sea, which covered a terrestrial and freshwater environment due to the lower sea level during the glacial period until 13,000 years ago between the western part of Chugoku and Shikoku regions (Yashima, 1994).

While the strait between the Chugoku and Kyushu regions formed 8,000 years ago (Yashima, 1994), which was later than that between the Chugoku and Shikoku regions, admixed individuals were identified in the Shikoku region, but not in the Kyushu region, suggesting asymmetric introgression. Furthermore, this asymmetric introgression may have resulted in discordance in mtDNA and nuclear cline positions between EJ and WJ (Fig. 3-5C), where the mitochondrial cline center shifted approximately 40 km west from the nuclear cline center, with partially overlapping CI. The incongruity of clines inferred from different sets of molecular markers is a common phenomenon of terrestrial vertebrate hybrid zones, including amphibians (e.g., Dufresnes et al., 2014; Arntzen et al., 2017; Sequeira et al., 2020). Prezygotic or postzygotic effects may explain the discordance in mtDNA and nuclear cline position. Sex-biased asymmetries (Toews & Brelsford, 2012) and an environmental gradient acting on mtDNA (Cheviron & Brumfield, 2009) as prezygotic effects and Haldane's rule (Haldane, 1922; Orr, 1997) and Dobzhansky–Muller incompatibilities (Dobzhansky, 1936; Muller, 1942) as postzygotic effects may have produced discordance in mtDNA and nuclear clines. Future field and genomic studies are needed to test these hypotheses and identify the factors that caused admixed individuals to spread mainly to the east of the mtDNA boundary at the time of secondary contact during the glacial period.

Regarding the width of the cline, including Shikoku, 20,490 years are needed to reach 161.8 km using the above formula, and the width of the cline, not including Shikoku, is 88.6 km which requires 6,144 years to reach, suggesting that selection may not act specifically in the Shikoku region. Furthermore, the range of present suitable habitats for EJ and WJ in Chapter 2 was consistent with the actual distribution boundaries within the Chugoku region, indicating exogenous environmental factors. However, Matsui (1984) did not identify morphological differences between EJ and WJ. Moreover, the distribution of hybrid

individuals in the Shikoku region suggests that EJ and WJ are the same species, despite the different degrees of admixture on the transect in the Chugoku and Shikoku regions.

The toad population in Yakushima was once considered to be a different subspecies of *B. japonicus* (as *vulgaris* Okada, 1928), but is now recognized as the same species based on morphology (Matsui 1984). Based on mitochondrial phylogeny in Chapter 1, morphologically defined groups were not monophyletic and did not form a single cluster in this study. There may have been interbreeding between the Kyushu, Yakushima, and Tanegashima populations when the straits between Yakushima, Tanegashima and Kagoshima were terrestrial during the glacial period (Ikehara, 1992). Geographic isolation after LGM may have led to the deviation from isolation by distance (Fig. 3-2).

The hybrid zone within *B. j. formosus*

I identified the hybrid zone between NF and SF as the widest in the present study (Fig. 3-5A), which was an expected result because of their recent evolutionary histories (Chapters 1 and 2). Widespread gene flow and recent hybridization indicate the absence of endogenous reproductive barriers between NF and SF. Furthermore, the mtDNA and SNP clines between NF and SF had an almost concordant center (Fig. 3-5A), suggesting the absence of selection (Toews & Brelsford, 2012). In contrast, the SNP cline was wider than the mitochondrial cline across the transition between NF and SF due to the lower effective population size of mitochondrial DNA than nuclear markers (Toews & Brelsford, 2012).

The time needed to reach the 170 km width of the SNP cline between NF and SF without selection was calculated to be 22,619 years, suggesting a prominent role for neutral processes. According to my previously predicted distributions during the glacial period, NF and SF may have shared their refugia around the southern Tohoku to northern Kanto regions (Chapter 2). The expansion of distribution after LGM may have led to widespread hybridization. An expansive hybrid zone consisting of late-generation hybrids and backcrosses is consistent overall with a prolonged period of neutral expansion. Although I did not find any asymmetry for the hybrid class assignment in the triangle plots (Fig. 3-6), the results obtained on the direction of migration were predominantly from SF to NF through the hybrid population (Table 3-1), indicating that this hybrid zone will lead to the formation of a hybrid swarm in the future.

Taxonomic revision of *B. japonicus*

Based on the above discussion, I reviewed the taxonomy of *B. japonicus*. SNP clustering based on DAPC supported four cluster numbers for *B. japonicus*, and nuclear phylogeny according to SNAPP confirmed deep splits between the five main clades.

However, based on PCA, these defined subclusters had markedly overlapping plots between NF and SF and between EJ and WJ. Additionally, hybrid zone analyses between NF and SF and between EJ and WJ indicated weak or no selection against hybrids that was insufficient for them to be regarded as different species.

In contrast, at the hybrid zone between *B. j. japonicus* and *B. j. formosus*, there was sufficient selection against hybrids for them to be regarded as different species. Hybridization persisted over time as parentals moved into the hybrid zone (Table 3-1). In contrast, introgression was limited by negative selection against hybrids (Table 3-1), allowing species to maintain their genetic distinctiveness (Barton & Hewitt, 1985). These results call for a taxonomic revision of *B. j. japonicus* and *B. j. formosus*. Therefore, I consider the eastern Japanese common toad *B. formosus* as a distinct species as originally described (Boulenger, 1883) and not a subspecies of the western Japanese common toad *B. japonicus* as currently considered (e.g., Matsui & Maeda, 2018).

I validated the two Japanese common toads, the western Japanese toad *Bufo japonicus* Temminck and Schlegel, 1838 (type locality: Japan [for discussion, see Matsui, 1984]) distributed in south-western Japan, and the eastern Japanese toad *Bufo formosus* Boulenger, 1883 (type locality: Yokohama, Japan) distributed in north-eastern Japan.

Morphometric variation analyses of these two species were conducted by Matsui (1984). However, intermediate forms were not detected in the Kinki region, and the morphological boundary extended more westerly to the Chugoku region (Matsui, 1984). The discordant patterns in morphological and genetic markers warrant further study.

Speciation with gene flow is common in anurans (Dufresnes et al., 2021). For example, a previous study on two European *Bufo* species, *B. bufo* and *B. spinosus*, which diverged in the Late Miocene, showed limited gene flow across a narrow hybrid zone (width of approximately 30 km) in the northwest of France even with the absence of barriers to dispersal (Arntzen et al., 2016). Despite the presence of a hybrid zone for *B. formosus* and *B. japonicus*, the identity of the parental species is distinctive and appears to have been unaffected. These two species could be considered to remain in partial reproductive isolation over a long period (cf. Servedio and Hermisson, 2020). Cline coupling may have progressed

further toward reproductive isolation after secondary contact, and it may still be ongoing throughout the hybrid zone (Harrison & Larson, 2014; Butlin & Smadja, 2018).

I also found that the geographic location of the hybrid zone between the two species appeared to be independent of the environment. Ecological niche modeling in Chapter 2 showed that environmental conditions were suitable for both species across the hybrid zone identified in this study, suggesting that environment-associated selection may not act directly to keep the hybrid zone. Many anuran speciation processes are initiated through the gradual accumulation of multiple barrier loci scattered across the genome, which reduces hybrid fitness by intrinsic postzygotic isolation (Dufresnes et al., 2021). Similarly, for *B. formosus* and *B. japonicus*, many genomic regions may represent local barriers to gene flow. I will attempt to elucidate the genomic mechanism that induces speciation in future studies.

Figure legends

Figure 3-1. Population structure using (A) DAPC, (B) Structure, and (C) PCA based on SNPs datasets, dataset I for DAPC and PCA, and dataset I–2 for Structure. (D) The distribution map of individuals colored by the cluster assignments by DAPC.

The four different genetic clusters, northern *Bufo japonicus formosus* (NF), southern *B. j. formosus* (SF), eastern *B. j. japonicus* (EJ), western *B. j. japonicus* (WJ), are displayed with *B. torrenticola*. (A) DAPC plot shows the best fit for K = 5 clusters. The axes represent the first two linear discriminants (LD), and the dots represent individuals colored by their groups in DAPC. (B) Structure bar plots show individual ancestry to the five clusters (K = 5). (C) PC1 and PC2 are plotted. Each dot corresponds to an individual colored according to their genetic cluster found in DAPC. The first axis distinguishes *B. j. formosus* and *B. j. japonicus*, and the second axis distinguishes *B. japonicus* and *B. torrenticola* and reflects intraspecific structure within *B. japonicus*. (D) The map was created by QGIS 3.28 (https://qgis.org). The administrative areas dataset was obtained from the GADM database (www.gadm.org, version 3.4) and the inland water dataset from the Digital Chart of the World available at the DIVA-GIS online resource (www.diva-gis.org).

Figure 3-2. (A) Densitree diagram representing the species tree obtained from SNAPP using SNPs. (B) The phylogenetic tree using mitochondrial cytochrome *b* sequences.

(A) All nodes were supported by posterior probabilities of 1.0. (B) Asterisks on each node indicate bootstrap supports are more than 85%.

Figure 3-3. Effective migration rates for the lowest cross-validation lambda estimated by FEEMS (Fast Estimation of Effective Migration Surfaces) using dataset II.

The figure shows the fitted parameters in the log scale, with lower effective migration shown in orange and higher effective migration shown in blue. Dots represent individuals.

Figure 3-4. Maps showing sampling localities with pie charts for three different contact zones of subdatasets, (A) SF–EJ, (B) NF–SF, and (C) EJ–WJ.

Pie charts show the *q*-values inferred by the Structure program for each individual. The dotted lines indicate the baselines used for *hzar*.

Figure 3-5. The maximum-likelihood clines fitted on nuclear genomic average ancestry and mitochondrial allele frequencies along three different transects of sub-datasets, (A) SF–EJ, (B) NF–SF, and (C) EJ–WJ.

The grey areas show the 95% credible cline region. The x-axis represents distances (km) from the baselines shown in Fig. 3-4. Crosses indicate the observed values for individuals.

Figure 3-6. Triangle plots of the hybrid index versus heterozygosity of individuals based on selected ancestry-informative SNP markers (*F*st = 1) for sub-datasets, (A) SF–EJ, (B) NF–SF, and (C) EJ–WJ.

Individual with intermediate hybrid indices (>0.25 and <0.75) and high heterozygosity (≥0.5) was considered as recent-generation hybrid (a gray square), and those with intermediate hybrid indices (>0.25 and <0.75) and low heterozygosity (<0.5) as later-generation hybrids (gray triangles). Those with low or high hybrid indices (≤0.25 or ≥0.75) were considered as backcross to one or the other parental type (triangles colored by parental assignments). Each colored circle indicates the pure individuals.

Figure 3-7. (A) Numbers of retained principal components (PCs) versus α-score values. (B) Bayesian Information Criterion (BIC) values for different numbers of clusters for DAPC.

Figure 3-8. Structure clustering results in the estimation of the most likely number of population clusters. (A) Delta K. (B) MedMed K, MedMean K, MaxMed K and MaxMean.

Figure 3-9. Maps showing sampling localities with pie charts for 11 samples from the artificially introduced population and around samples in (A) Hokkaido and (B) Kanto region and Izu Islands.

Pie charts show the *q*-values inferred by the Structure program for each individual. Color assignments for clusters were the same as in Fig. 3-4.

Table 3-1. Estimates of migrants from BayesAss3-SNPs analyses between population clusters, (A) NF-SF, (B) SF-EJ, and (C) EJ–WJ.

The row headers represent the populations into where the individuals migrated, and the column headers represent the populations from where the migrant derived. Standard deviations of the values are given in parentheses.

(A)

		Migration from		
		parental NF	Hybrid	parental SF
Migration into	parental NF	0.9407 (0.0349)	0.0355 (0.0290)	0.0238 (0.0221)
	Hybrid	0.0152 (0.0145)	0.9262 (0.0293)	0.0586 (0.0269)
	parental SF	0.0167 (0.0158)	0.0167 (0.0158)	0.9667 (0.0218)

(B)

		Migration from		
		parental SF	Hybrid	parental EJ
Migration into	parental SF	0.9607 (0.0253)	0.0196 (0.0185)	0.0196 (0.0185)
	Hybrid	0.1667 (0.0431)	0.7619 (0.0389)	0.0714 (0.0353)
	parental EJ	0.0133 (0.0128)	0.0133 (0.0128)	0.9733 (0.0178)

(C)

		Migration from		
		parental EJ	Hybrid	parental WJ
Migration into	parental EJ	0.9683 (0.0209)	0.0133 (0.0151)	0.0159 (0.0152)
	Hybrid	0.0725 (0.0280)	0.8013 (0.0340)	0.1262 (0.0337)
	parental WJ	0.0139 (0.0133)	0.0139 (0.0133)	0.9722 (0.0184)

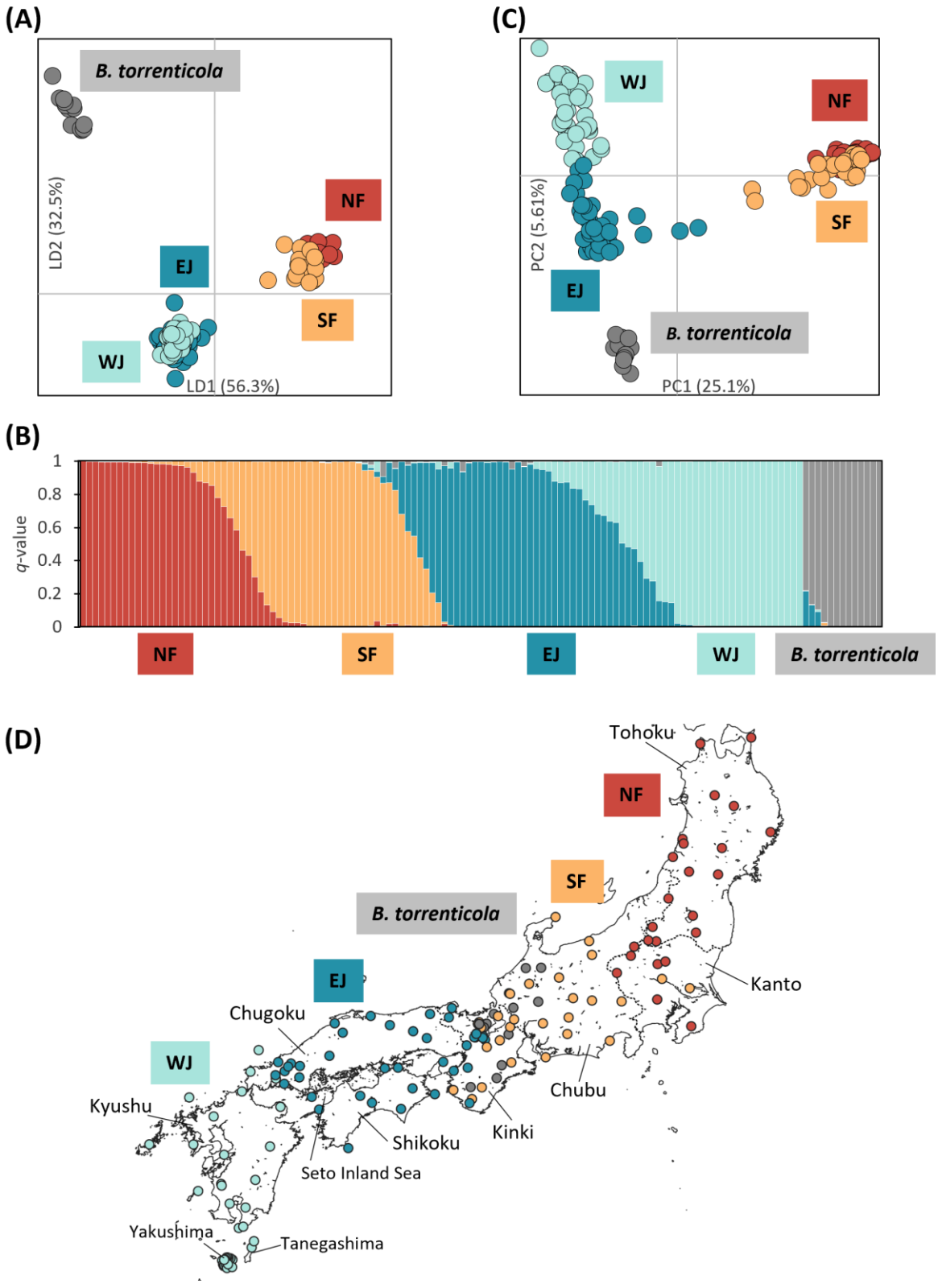
(A)
B. torrenticola
NF
EJ
SF
WJ
LD2 (32.5%)
LD1 (56.3%)
(C)
WJ
NF
SF
EJ
B. torrenticola
PC2 (5.61%)
PC1 (25.1%)
(B)
q-value
1
0.8
0.6
0.4
0.2
0
NF
SF
EJ
WJ
B. torrenticola
(D)
Tohoku
NF
SF
B. torrenticola
EJ
Kanto
Chugoku
WJ
Chubu
Kyushu
Kinki
Shikoku
Seto Inland Sea
Yakushima
Tanegashima

Fig. 3-1

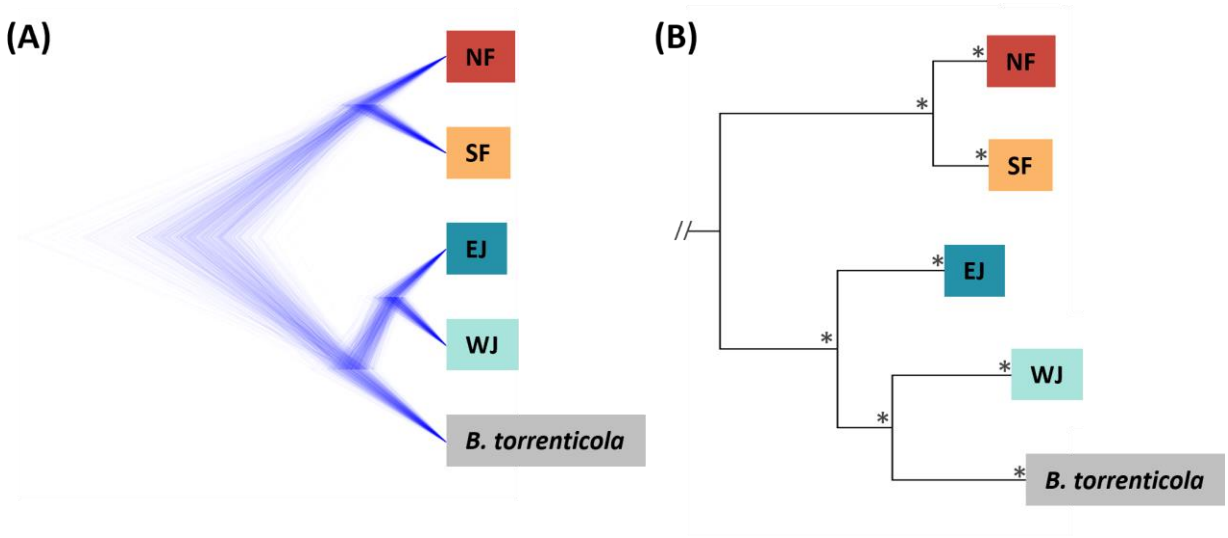
(A)
NF
SF
EJ
WJ
B. torrenticola
(B)
NF
SF
EJ
WJ
B. torrenticola

Fig. 3-2

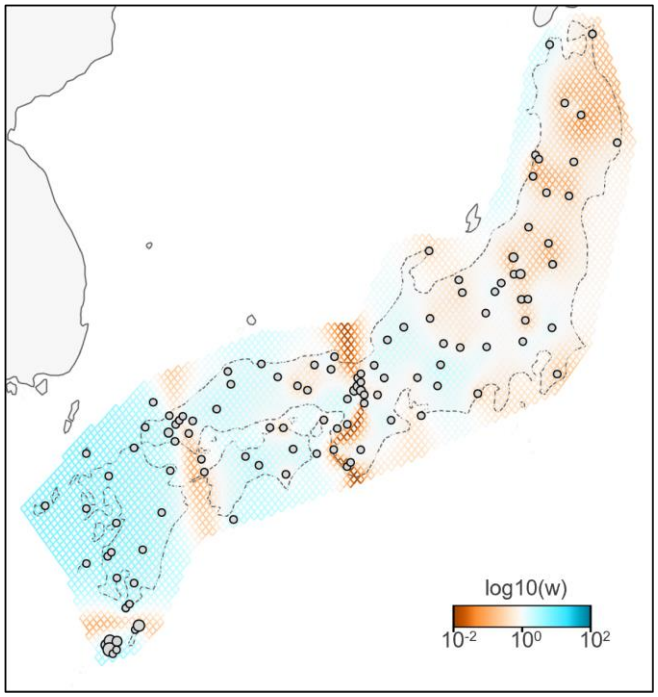
log10(w)
10-2
100
102

Fig. 3-3

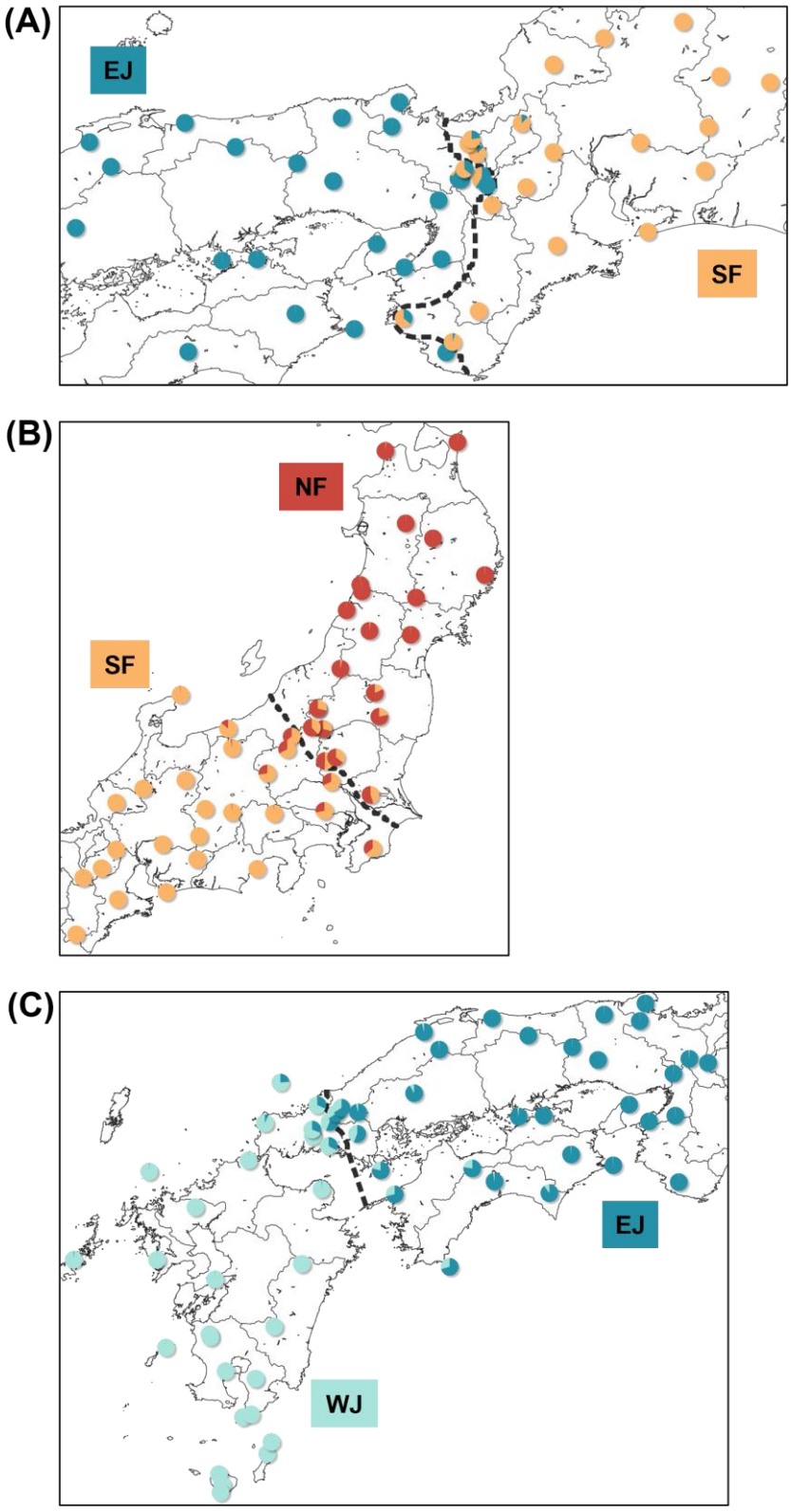

Fig. 3-4

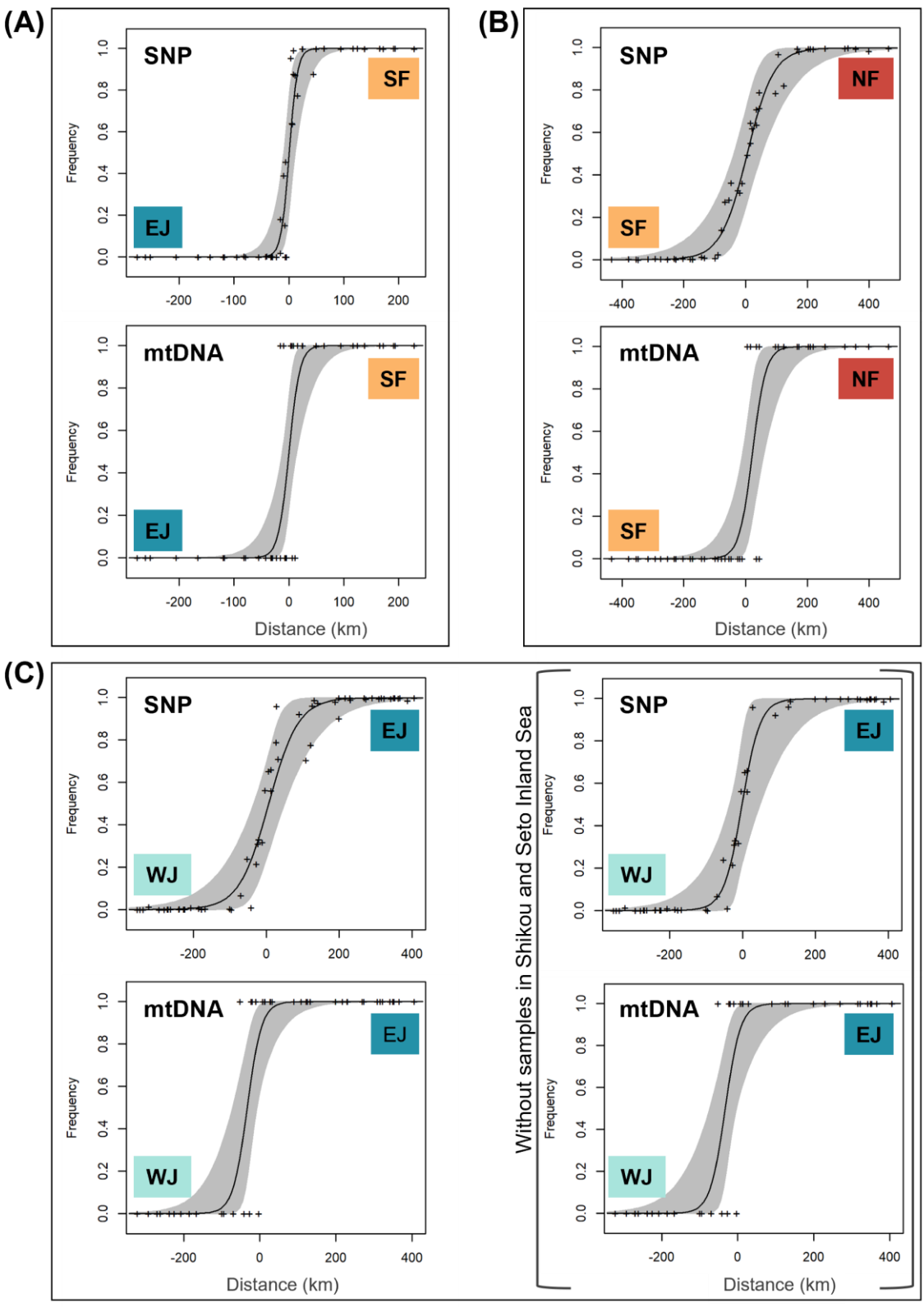
(A)
SNP
SF
EJ
mtDNA
SF
EJ
Frequency
Distance (km)
(B)
SNP
NF
SF
mtDNA
NF
SF
Frequency
Distance (km)
(C)
SNP
EJ
WJ
mtDNA
EJ
WJ
Without samples in Shikou and Seto Inland Sea
Frequency
Distance (km)

Fig. 3-5

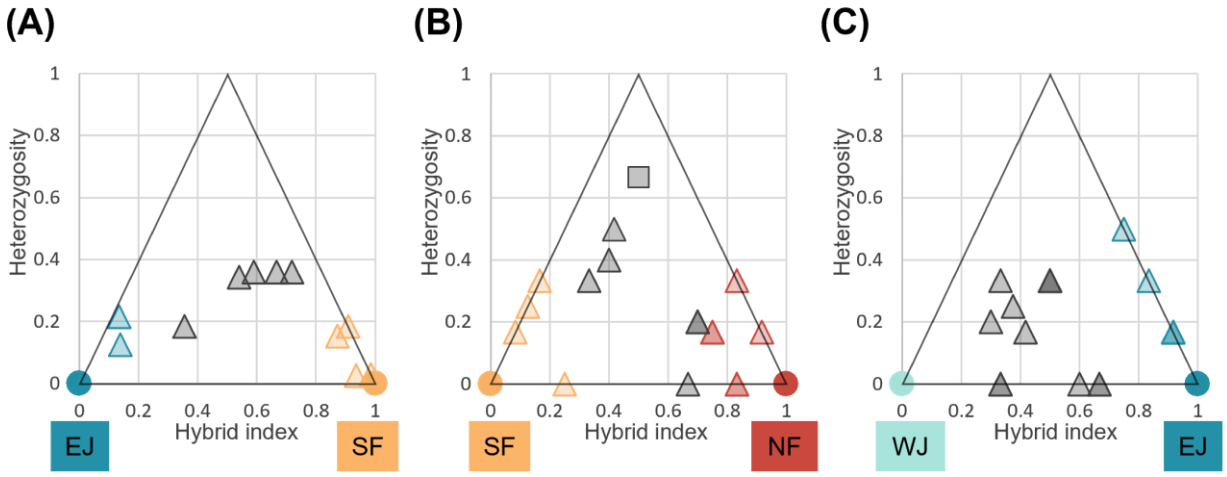
(A)
(B)
(C)
Heterozygosity
Hybrid index
EJ
SF
SF
NF
WJ
EJ

Fig. 3-6

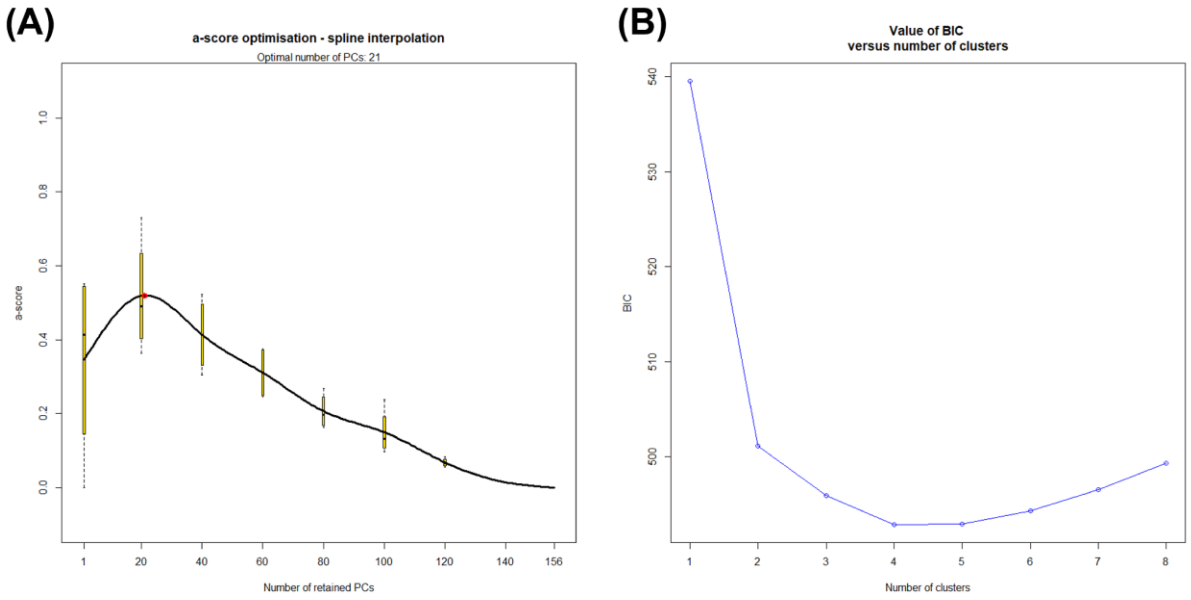
(A)
a-score optimisation - spline interpolation
Optimal number of PCs: 21
a-score
Number of retained PCs
(B)
Value of BIC
versus number of clusters
BIC
Number of clusters

Fig. 3-7

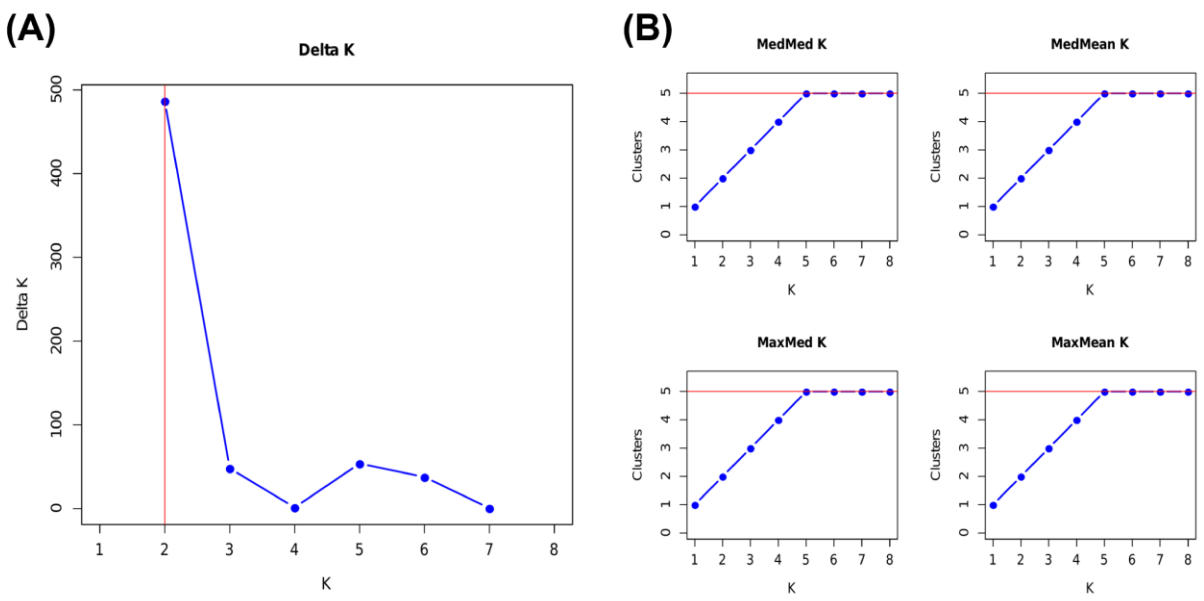
(A)
Delta K
Delta K
K
(B)
MedMed K
MedMean K
MaxMed K
MaxMean K
Clusters
K

Fig. 3-8

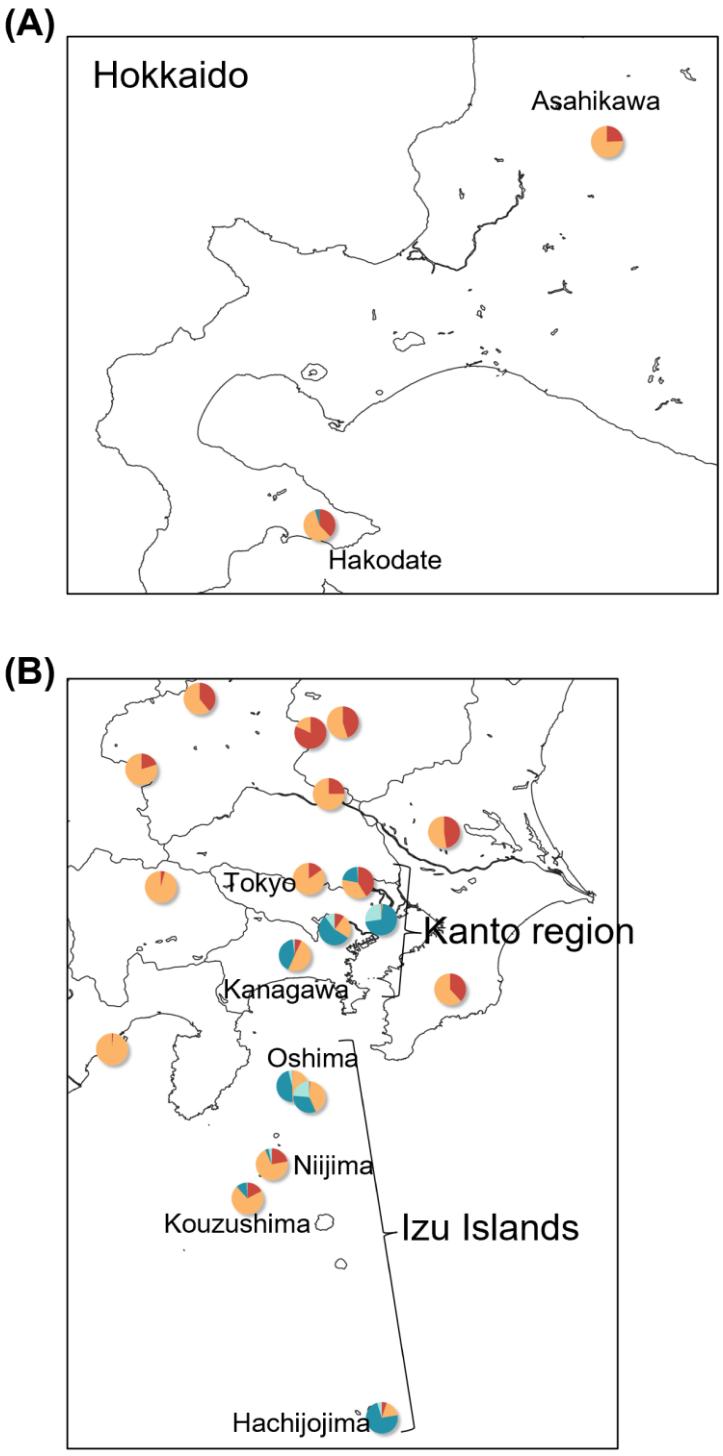
(A)
Hokkaido
Asahikawa
Hakodate
(B)
Tokyo
Kanto region
Kanagawa
Oshima
Niijima
Kouzushima
Izu Islands
Hachijojima

Fig. 3-9

General Discussion

My comprehensive geographic sampling and the mtDNA and genome-wide SNP analyses provided new insights into the phylogeny and structure of the hybrid zones, with implications for the taxonomy of the Japanese toads. This study first detailed the divergence patterns and phylogeography of the Japanese toads (Chapters 1 and 2) and characterized the inter- and intra-specific hybrid zone between *B. j. japonicus* and *B. j. formosus* (Chapter 3). In addition to the genetic data, my ecological niche modeling analyses give context to the demographic history, especially the location of refugia among *B. j. formosus*.

The hybrid zone between *B. japonicus* and *B. formosus* showed a narrow and steep cline without any apparent climatic or geographic barriers (Chapter 3). Therefore, the hybrid zone can be a tension zone maintained by balancing dispersal and negative selection against hybrids (Key, 1968; Barton & Hewitt, 1985). Therefore, based on the divergence time and hybrid zone analyses, I recommended that *B. j. japonicus* and *B. j. formosus* be elevated to the species levels. I validated the western Japanese toad *Bufo japonicus* Temminck and Schlegel, 1838 (type locality: Japan [for discussion, see Matsui, 1984]), and the eastern Japanese toad *Bufo formosus* Boulenger, 1883 (type locality: Yokohama, Japan).

Divergence processes of *B. japonicus* and *B. formosus*

Bufo japonicus and *B. formosus* were estimated to be allopatrically diverged in the late Miocene (5.7 Mya; Chapters 1 and 2). The niche similarities supported the allopatric speciation (Wiens & Graham, 2005; Chapter 2). Tectonic events during the formation of the Japanese archipelago geographically separated them into isolated two populations across the unsuitable niche, and the genetic drift caused the initial divergence. The two species expanded their distribution, and secondary contact occurred with subsequent environmental changes.

Divergence processes of *B. japonicus* and *B. torrenticola*

Both mtDNA and genome-wide SNP lineages are highly divergent, but the topologies of the phylogenies are discordant for the Japanese toads (Chapter 3). SNPs data group the Kyushu population and Chugoku/Shikoku population of *B. japonicus* as a sister clade. However, the topology obtained from mtDNA sequences indicated that *B. torrenticola* and the Kyushu population of *B. japonicus* are sister lineages despite their geographic isolation. The mito-

nuclear discordance pattern could occur as a consequence of ancient hybridization, incomplete lineage sorting, different selection regimes, or demographic dynamics (Maddison, 1997; Funk & Omland, 2003; McKay & Zink, 2010; Toews & Brelsford, 2012). The asymmetric introgression is unlikely because mitochondrial and nuclear markers suggest complete isolation of the lineages, also using a random mix of male and female samples to perform the phylogenetic reconstructions. Furthermore, The clear pattern in geographic distribution of mtDNA and SNP lineages of *B. japonicus* and *B. torrenticola* could rule out incomplete lineage sorting because the discordance that arises from incomplete lineage sorting is explained not to leave a predictable biogeographic pattern (Funk & Omland, 2003; Toews & Brelsford, 2012). The demographic dynamics could not be rejected because of the unknown complex topographic history of the Seto Inland Sea (Yoshida, 1992).

One more possibility for mito-nuclear discordance is the selective processes of mitochondrial protein-coding genes (Noll et al., 2022). Few studies have examined mitochondrial phylogenetic relationships among Japanese toads (Igawa et al. 2006). Examining the phylogenetic relationship of each protein-coding mitochondrial gene region in the future is necessary. It is unknown which ecological features are related to mitogenome adaptation. However, the amino acid changes in functionally important regions of cytochrome *b* promote metabolic or oxygen requirements and lead to local adaptation (Fonseca et al., 2008; Tieleman et al., 2009). The trigger of the positive selection of mitochondrial genes could be the stress of climate conditions or immune responses affected by pathogen or parasite factors. Research on parasites in Japanese toads has just begun (Marcaida et al., 2022), and more details will be elucidated in the future. By testing these hypothetical factors, I may be able to elucidate the causes of the mito-nuclear discordance.

Whether mitochondrial selection has led to the evolution of adaptation to the lotic environment in B. torrenticola is unknown. However, the niche divergence enables the overlapping distribution of *B. torrenticola* and *B. formosus.* The parapatric distribution between *B. torrenticola* and *B. japonicus* is probably due to the niche suitability. The primary suitable habitat of *B. torrenticola* was consistent with its actual distribution (Chapter 2). However, contacts between *B. torrenticola* and *B. japonicus* and *B. torrenticola* and *B. formosus* have been confirmed in some areas and will be discussed below.

The hybrid zones between *B. japonicus* and *B. formosus*

I showed that the hybrid zone between *B. japonicus* and *B. formosus* is a tension zone (Key, 1968; Barton & Hewitt, 1985), with a steep cline across narrow hybrid zones (Chapter 3). At the contact zone, intrinsic postzygotic barriers first reduce gene flow between sympatric species. As reinforcement, the intrinsic postzygotic barriers could evolve, lead to genetic incompatibilities, and promote the evolution of subsequent reproductive isolation (Coughlan & Matute, 2020). The contact zone between *B. japonicus* and *B. formosus* is the stable hybrid zone, in which selection against hybrids is balanced by the movement of parental species into the hybrid zone. I also identified the later hybrids and backcross to parental species at the hybrid zone (Chapter 3). The absence of recent-generation hybrids indicates that the hybridization between parental species could be prevented across the hybrid zone. The two species will diverge to continue until hybridization can no longer occur.

The climate oscillations during the Quaternary strongly affected the distributions of the Japanese toads, forming the present secondary contact zones. I identified the distribution of the refugia of the three Japanese toads (Chapter 2). *Bufo formosus* had the refugia on both sides of high-elevation areas in central Japan and was prevented from expanding its distribution soon after LGM. *Bufo japonicus* had refugia along the paleo-rivers in the Chugoku and Kinki regions. Given these refugia locations, I hypothesize two different contact zones between *B. japonicus* and *B. formosus* in the northern and southern Kinki regions.

Riemsdijk et al. (2023) recently suggested the difference in the hybrid zone between the northern and southern transect at the boundary between two European toads, *B. bufo* and *B. spinosus*. They suggested that the timing of the secondary contact made the difference in genetic characteristics between the northern and southern contact. In the Kinki region, *B. japonicus* have refugia mainly in the Kyoto prefecture, and from the region, they could expand their distribution southward. During postglacial expansion, secondary contact between *B. japonicus* and *B. formosus* would have first been established in the north of the Kinki region and progressed over time towards the southern Kinki region, where the geographic distance between refugia is larger than the northern contact zone. Due to the longer time from secondary contact of the north than of the south, there may have been sufficient ages for evolving intrinsic postzygotic barrier genes. I could not test this hypothesis of the differences between the northern and southern hybrid zones in the Kiniki region because of the small sample size in the southern Kinki region. The future genomic

comparison between the two hybrid zones could provide insight into the evolution of the genomic barriers leading to reproductive isolations.

The artificial introduction in the Kanto region also established the hybrid formation between *B. japonicus* and *B. formosus*. In the region, the native *B. formosus* and introduced *B. japonicus* have been crossed (Matsui, 1964; Hase, Nikoh & Shimada, 2013; Chapter 3). The hybridizations apart from the natural hybrid zone were some reported for the European amphibians, between the Northern crested newts, native *Triturus cristatus* and invasive *T. carnifex* (e.g., Brede, 2015; Wielstra et al., 2016; Hinneberg et al., 2022), between the European tree frogs, native *Hyla arborea* and invasive *H. intermedia* (Dufresnes et al., 2015). Instead of their deep divergence, between *T. cristatus* and *T. carnifex* occurred at ca. 9.3 Mya (Wielstra & Arntzen, 2011) and between *Hyla arborea* and invasive *H. intermedia* at ca. 4.2 Mya (Gvoždík et al., 2015), their artificial hybridization have occurred. The reason is that hybridization could occur more frequently in the introduced regions than in the native regions because of the less opportunity for assortative mate choice for the invasive species with initially low population density (Dufresnes et al., 2015). The current hybridization between *B. japonicus* and *B. formosus* in the Kanto region is probably in the early stages of contact, and genetic pollution (Butler, 1994) is expanding (Hase et al., 2022). Of course, the conservation to prevent genetic pollution from expansion is essential. Examining the progress of hybridization in the areas may provide insight into the process of developing reproductive isolation at the contact region (Mastrantonio et al., 2016).

The hybrid between *B. torrenticola* and *B. japonicus*

The contact between *B. japonicus* and *B. torrenticola* could be found in the northern and southern Kinki regions. There is no admixture between the two species in the northern Kinki region. However, in the Structure analysis, *B. torrenticola* in the southern Kinki region had a *q*-value >0.1 admixture with *B. japinicus* (Chapter 3). *Bufo japonicus* had refugia in the northern Kinki regions. *Bufo torrenticola* had refugia in the northern and southern parts of the distribution and are less affected by the glacial climate than *B. japonicus* and *B. formosus*. Given their refugia positions, the southern contact zone was constructed later than the northern contact zone by the southward expansion of *B. japonicus*. Similar to the contact zone between *B. japonicus* and *B. formosus*, the insufficient time to diverge the reproductive isolations possibly led to the admixture in the southern Kinki region.

The hybrid between *B. torrenticola* and *B. formosus*

Bufo torrenticola and *B. formosus* had been geographically separated, followed by the expansion, and then, the niche dissimilarity may have enabled their overlapping. The hybrids between *B. torrenticola* and *B. formosus* have not been identified in most distribution areas, except for at the edge of the distribution of *B. torrenticola* in the northeast Toyama and Ishikawa prefectures (Yamazaki et al., 2008; Iwaoka et al., 2021; Chapter 3). Topographical change by flooding abolished the *B. formosus* breeding environment, such as puddles along mountain streams, and led to their occasional contact. Moreover, half of the breeding seasons overlap between *B. torrenticola* and *B. formosus*, resulting in asymmetric mating between female *B. torrenticola* and male *B. formosus* (Yamazaki et al., 2008; Iwaoka et al., 2021). However, given that the environmental changes caused by flooding are not region-specific, some genetic barriers possibly prevent their admixture in other overlapping areas. I hypothesize that at the contact zone in the northern end of the distribution of *B. torrenticola*, genetic barriers have been incomplete because of the recent contact after the expansion.

Matsui (1977) showed by the cross experiments between *B. torrenticola* in Nara prefecture and *B. formosus* in Kyoto prefecture that the hatching rate of F1 hybrids between female *B. torrenticola* and male *B. formosus* was much lower than those between male *B. torrenticola* and female *B. formosus*. Both genetic barriers and the difference in the breeding season likely influence asymmetrical matings in Toyama and Ishikawa prefectures.

Moreover, one *B. formosus* individual in Gifu prefecture showed a slight admixture with *B. torrenticola* (Chapter 3). This region is located between the northern and southern refugia of *B. torrenticola*, and the shorter time to contact with *B. formosus* might lead to insufficient reproductive isolation and admixture.

The incomplete genetic reproductive isolation also brought controversy to the taxonomy of *B. torrenticola*. Kawamura, Nishioka & Ueda (1980) rejected the recognition of *B. torrenticola* based on fertility by laboratory crossing experiments, ignoring ecological reproductive isolation. They followed the classical species concept of biological species concept, defined as species being groups of actually or potentially interbreeding natural populations that are reproductively isolated from other similar groups (Mayr, 1942). However, species evolve their divergence through hybridization as explained above, in addition to the ecological reproductive isolation, such as breeding environment and season for *B. torrenticola*. Moreover, the divergence of the gene underlying adaptive trait to the lotic environment may also accelerate the speciation of *B. torrenticola*.

Reproductive isolation could be completed by a complex combination of genetic, morphological, ecological, and behavioral factors. In the process, the postzygotic genomic barriers reduce hybrid fitness by lowering viability and fertility. In the speciation continuum, reproductive isolation is continuous (Stankowski & Ravinet, 2021). By comparing multiple closely related species exhibiting different levels of reproductive isolation, I will identify factors that determine how the speciation process proceeds, including the strength of selection, loci under selection, and other factors such as demographic history.

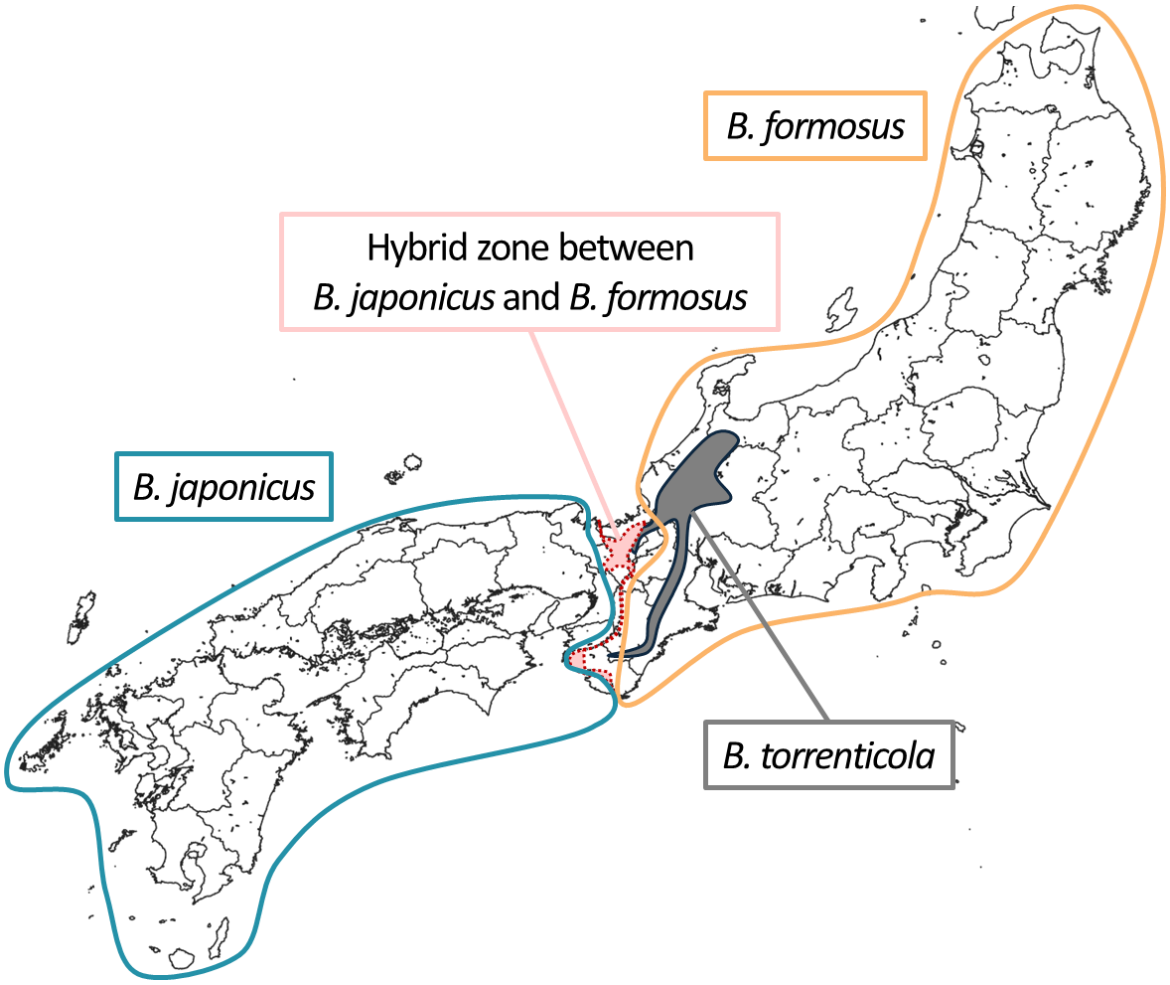

The distribution of *Bufo japonicus*, *B. formosus*, and *B. torrenticola* identified in this study

Acknowledgments

I thank my supervisors, Professor Dr. K. Nishikawa and Emeritus Professor Dr. M. Matsui, for their suggestions, direction, and encouragement throughout this study. I also thank the members of Professor Nishikawa's laboratory for their precious advice and support in the field and laboratory work. I fully acknowledge for collecting specimens, K. Eto, I. Fukuyama, R. Fukuyama, S. Ikeda, Y. Kawahara, K. Kimura, T. Matsuki, Y. Misawa, Y. Miyagata, S. Mori, T. Shimada, Z. Shimizu, T. Sugahara, T. Sugihara, Y. Tahara, H. Takeuchi, S. Tanabe, A. Tominaga, N. Yoshikawa, and many more collaborators. I thank Dung Van Tran for helping to conduct the ecological niche modeling in Chapter 2. I also thank N. Yoshikawa and Y. Fuke for helping to conduct MIG-seq and analyses in Chapter 3.

References

Abbott R, Albach D, Ansell S, Arntzen JW, Baird SJE, Bierne N, Boughman J, Brelsford A, Buerkle CA, Buggs R, Butlin RK, Dieckmann U, Eroukhmanoff F, Grill A, Cahan SH, Hermansen JS, Hewitt G, Hudson AG, Jiggins C, Jones J, Keller B, Marczewski T, Mallet J, Martinez-Rodriguez P, Möst M, Mullen S, Nichols R, Nolte AW, Parisod C, Pfennig K, Rice AM, Ritchie MG, Seifert B, Smadja CM, Stelkens R, Szymura JM, Väinölä R, Wolf JBW, Zinner D. 2013. Hybridization and speciation. *Journal of Evolutionary Biology* 26:229–246. DOI: 10.1111/j.1420-9101.2012.02599.x.

Aiello-Lammens ME, Boria RA, Radosavljevic A, Vilela B, Anderson RP. 2015. spThin: an R package for spatial thinning of species occurrence records for use in ecological niche models. *Ecography* 38:541–545. DOI: 10.1111/ecog.01132.

Akaike H. 1974. A new look at the statistical model identification. *IEEE Transactions on Automatic Control* 19:716–723. DOI: 10.1109/tac.1974.1100705.

Alvarado-Serrano DF, Knowles LL. 2014. Ecological niche models in phylogeographic studies: applications, advances and precautions. *Molecular Ecology Resources* 14:233–248. DOI: 10.1111/1755-0998.12184.

Anderson DR, Burnham KP. 2002. Avoiding pitfalls when using information-theoretic methods. *The Journal of Wildlife Management* 66:912. DOI: 10.2307/3803155.

Angelis K, Reis MD. 2015. The impact of ancestral population size and incomplete lineage sorting on Bayesian estimation of species divergence times. *Current Zoology* 61:874–885. DOI: 10.1093/czoolo/61.5.874.

Aoki K, Kato M, Murakami N. 2011. Phylogeography of phytophagous weevils and plant species in broadleaved evergreen forests: a congruent genetic gap between western and eastern parts of Japan. *Insects* 2:128–150. DOI: 10.3390/insects2020128.

Aoki G, Matsui M, Nishikawa K. 2013. Mitochondrial cytochrome b phylogeny and historical biogeography of the Tohoku Salamander, *Hynobius lichenatus* (Amphibia, Caudata). *Zoological Science* 30:167–173. DOI: 10.2108/zsj.30.167.

Araújo MB, Nogués-Bravo D, Diniz-Filho JAF, Haywood AM, Valdes PJ, Rahbek C. 2008. Quaternary climate changes explain diversity among reptiles and amphibians. *Ecography* 31:8–15. DOI: 10.1111/j.2007.0906-7590.05318.x.

Arntzen JW, McAtear J, Butôt R, Martínez-Solano I. 2018. A common toad hybrid zone that runs from the Atlantic to the Mediterranean. *Amphibia-Reptilia* 39:41–50. DOI: 10.1163/15685381-00003145.

Arntzen JW, Trujillo T, Butôt R, Vrieling K, Schaap O, Gutiérrez-Rodríguez J, Martínez-Solano I. 2016. Concordant morphological and molecular clines in a contact zone of the Common and Spined toad (*Bufo bufo* and *B. spinosus*) in the northwest of France. *Frontiers in Zoology* 13:52. DOI: 10.1186/s12983-016-0184-7.

Arntzen JW, Vries W, Canestrelli D, Martínez-Solano I. 2017. Hybrid zone formation and contrasting outcomes of secondary contact over transects in common toads. *Molecular Ecology* 26:5663–5675. DOI: 10.1111/mec.14273.

Avise JC, Arnold J, Ball RM, Bermingham E, Lamb T, Neigel JE, Reeb CA, Saunders NC. 1987. Intraspecific phylogeography: The mitochondrial DNA bridge between population genetics and systematics. *Annual Review of Ecology and Systematics* 18:489–522. DOI: 10.1146/annurev.es.18.110187.002421.

Barton NH, Gale K. 1993. Genetic analysis of hybrid zones. In: *Hybrid zones and the evolutionary process*. New York: Oxford University Press, 13–45.

Barton NH, Hewitt GM. 1985. Analysis of hybrid zones. *Annual Review of Ecology and Systematics* 16:113–148. DOI: 10.1146/annurev.es.16.110185.000553.

Becker RA, Wilks AR, Brownrigg R. 2018. *mapdata: Extra Map Databases. R Package Version 2.3.0*.

Blaustein AR, Walls SC, Bancroft BA, Lawler JJ, Searle CL, Gervasi SS. 2010. Direct and indirect effects of climate change on amphibian populations. *Diversity* 2:281–313. DOI: 10.3390/d2020281.

Borzée A, Santos JL, Sánchez-RamÍrez S, Bae Y, Heo K, Jang Y, Jowers MJ. 2017. Phylogeographic and population insights of the Asian common toad (*Bufo gargarizans*) in Korea and China: population isolation and expansions as response to the ice ages. *PeerJ* 5:e4044. DOI: 10.7717/peerj.4044.

Bouckaert R, Vaughan TG, Barido-Sottani J, Duchêne S, Fourment M, Gavryushkina A, Heled J, Jones G, Kühnert D, Maio ND, Matschiner M, Mendes FK, Müller NF, Ogilvie HA, Plessis L du, Popinga A, Rambaut A, Rasmussen D, Siveroni I, Suchard MA, Wu C-H, Xie D, Zhang C, Stadler T, Drummond AJ. 2019. BEAST 2.5: an advanced software platform for Bayesian evolutionary analysis. *PLoS Computational Biology* 15:e1006650. DOI: 10.1371/journal.pcbi.1006650.

Boulenger GA. 1883. Description of a new Species of *Bufo* from Japan. *Proceedings of the Zoological Society of London* 51:139–175. DOI: 10.1111/j.1469-7998.1883.tb06647.x.

Brede E. 2015. Beam Brook revisited: a molecular study of a historically introduced non-native amphibian (*Triturus carnifex*) and its limited introgression into native UK Triturus cristatus populations. *Amphibia-Reptilia* 36:287–299. DOI: 10.1163/15685381-00003006.

Bremer JRA, Viñas J, Mejuto J, Ely B, Pla C. 2005. Comparative phylogeography of Atlantic bluefin tuna and swordfish: the combined effects of vicariance, secondary contact, introgression, and population expansion on the regional phylogenies of two highly migratory pelagic fishes. *Molecular Phylogenetics and Evolution* 36:169–187. DOI: 10.1016/j.ympev.2004.12.011.

Bryant D, Bouckaert R, Felsenstein J, Rosenberg NA, RoyChoudhury A. 2012. Inferring species trees directly from biallelic genetic markers: bypassing gene trees in a full coalescent analysis. *Molecular Biology and Evolution* 29:1917–1932. DOI: 10.1093/molbev/mss086.

Burbrink FT, Ruane S. 2021. Contemporary philosophy and methods for studying speciation and delimiting species. *Ichthyology & Herpetology* 109:874–894. DOI: 10.1643/h2020073.

Butler D. 1994. Bid to protect wolves from genetic pollution. *Nature* 370:497–497. DOI: 10.1038/370497a0.

Butlin RK, Smadja CM. 2018. Coupling, reinforcement, and speciation. *The American Naturalist* 191:155–172. DOI: 10.1086/695136.

Cao S-Y, Wu X-B, Yan P, Hu Y-L, Su X, Jiang Z-G. 2006. Complete nucleotide sequences and gene organization of mitochondrial genome of *Bufo gargarizans*. *Mitochondrion* 6:186–193. DOI: 10.1016/j.mito.2006.07.003.

Carey C, Alexander MA. 2003. Climate change and amphibian declines: is there a link? *Diversity and Distributions* 9:111–121. DOI: 10.1046/j.1472-4642.2003.00011.x.

Cavalli-Sforza LL. 1966. Population structure and human evolution. *Proceedings of the Royal Society of London. Series B. Biological Sciences* 164:362–379. DOI: 10.1098/rspb.1966.0038.

Caye K, Deist TM, Martins H, Michel O, François O. 2016. TESS3: fast inference of spatial population structure and genome scans for selection. *Molecular Ecology Resources* 16:540–548. DOI: 10.1111/1755-0998.12471.

Caye K, Jay F, Michel O, François O. 2018. Fast inference of individual admixture coefficients using geographic data. *The Annals of Applied Statistics* 12:586–608. DOI: 10.1214/17-aoas1106.

Chen S, Zhou Y, Chen Y, Gu J. 2018. fastp: an ultra-fast all-in-one FASTQ preprocessor. *Bioinformatics* 34:i884–i890. DOI: 10.1093/bioinformatics/bty560.

Cheviron ZA, Brumfield RT. 2009. Migration-selection balance and local adaptation of mitochondrial haplotypes in Rufous-Collared Sparrows (*Zonotrichia capensis*) along an elevational gradient. *Evolution* 63:1593–1605. DOI: 10.1111/j.1558-5646.2009.00644.x.

Chiocchio A, Arntzen JanW, Martínez-Solano I, Vries W de, Bisconti R, Pezzarossa A, Maiorano L, Canestrelli D. 2021. Reconstructing hotspots of genetic diversity from glacial refugia and subsequent dispersal in Italian common toads (*Bufo bufo*). *Scientific Reports* 11:260. DOI: 10.1038/s41598-020-79046-y.

Clark PU, Archer D, Pollard D, Blum JD, Rial JA, Brovkin V, Mix AC, Pisias NG, Roy M. 2006. The middle Pleistocene transition: characteristics, mechanisms, and implications for long-term changes in atmospheric pCO_2. *Quaternary Science Reviews* 25:3150–3184. DOI: 10.1016/j.quascirev.2006.07.008.

Collart F, Hedenäs L, Broennimann O, Guisan A, Vanderpoorten A. 2021. Intraspecific differentiation: implications for niche and distribution modelling. *Journal of Biogeography* 48:415–426. DOI: 10.1111/jbi.14009.

Colliard C, Sicilia A, Turrisi GF, Arculeo M, Perrin N, Stöck M. 2010. Strong reproductive barriers in a narrow hybrid zone of West-Mediterranean green toads (*Bufo viridis* subgroup) with Plio-Pleistocene divergence. *BMC Evolutionary Biology* 10:232–232. DOI: 10.1186/1471-2148-10-232.

Comes HP, Kadereit JW. 1998. The effect of Quaternary climatic changes on plant distribution and evolution. *Trends in Plant Science* 3:432–438. DOI: 10.1016/s1360-1385(98)01327-2.

Coughlan JM, Matute DR. 2020. The importance of intrinsic postzygotic barriers throughout the speciation process. *Philosophical Transactions of the Royal Society B: Biological Sciences* 375:20190533. DOI: 10.1098/rstb.2019.0533.

Crandall ED, Sbrocco EJ, DeBoer TS, Barber PH, Carpenter KE. 2012. Expansion dating: calibrating molecular clocks in marine species from expansions onto the Sunda Shelf following the Last Glacial Maximum. *Molecular Biology and Evolution* 29:707–719. DOI: 10.1093/molbev/msr227.

Darriba D, Taboada GL, Doallo R, Posada D. 2012. jModelTest 2: more models, new heuristics and parallel computing. *Nature methods* 9:772. DOI: 10.1038/nmeth.2109.

Derryberry EP, Derryberry GE, Maley JM, Brumfield RT. 2014. hzar: hybrid zone analysis using an R software package. *Molecular Ecology Resources* 14:652–663. DOI: 10.1111/1755-0998.12209.

Dobzhansky T. 1936. Studies on hybrid sterility. II. Localization of sterility factors in *Drosophila pseudoobscura* hybrids. *Genetics* 21:113–135. DOI: 10.1093/genetics/21.2.113.

Dong B, Yang B. 2015. The complete mitochondrial genome of the *Bufo stejnegeri* (Anura: Bufonidae). *Mitochondrial DNA Part A: DNA Mapping, Sequencing, and Analysis* 27:2885–2886. DOI: 10.3109/19401736.2015.1060421.

Drummond AJ, Rambaut A, Shapiro B, Pybus OG. 2005. Bayesian coalescent inference of past population dynamics from molecular sequences. *Molecular Biology and Evolution* 22:1185–1192. DOI: 10.1093/molbev/msi103.

Drummond AJ, Suchard MA, Xie D, Rambaut A. 2012. Bayesian phylogenetics with BEAUti and the BEAST 1.7. *Molecular Biology and Evolution* 29:1969–1973. DOI: 10.1093/molbev/mss075.

Dufresnes C, Bonato L, Novarini N, Betto-Colliard C, Perrin N, Stöck M. 2014. Inferring the degree of incipient speciation in secondary contact zones of closely related lineages of Palearctic green toads (*Bufo viridis* subgroup). *Heredity* 113:9. DOI: 10.1038/hdy.2014.26.

Dufresnes C, Brelsford A, Jeffries DL, Mazepa G, Suchan T, Canestrelli D, Nicieza A, Fumagalli L, Dubey S, Martínez-Solano I, Litvinchuk SN, Vences M, Perrin N, Crochet P-A. 2021. Mass of genes rather than master genes underlie the genomic architecture of amphibian speciation. *Proceedings of the National Academy of Sciences* 118:e2103963118. DOI: 10.1073/pnas.2103963118.

Dufresnes C, Dubey S, Ghali K, Canestrelli D, Perrin N. 2015. Introgressive hybridization of threatened European tree frogs (*Hyla arborea*) by introduced *H. intermedia* in Western Switzerland. *Conservation Genetics* 16:1507–1513. DOI: 10.1007/s10592-015-0745-x.

Dufresnes C, Litvinchuk SN. 2021. Diversity, distribution and molecular species delimitation in frogs and toads from the Eastern Palaearctic. *Zoological Journal of the Linnean Society* XX:1–66. DOI: 10.1093/zoolinnean/zlab083.

Dufresnes C, Litvinchuk SN, Borzée A, Jang Y, Li J-T, Miura I, Perrin N, Stöck M. 2016. Phylogeography reveals an ancient cryptic radiation in East-Asian tree frogs (*Hyla japonica* group) and complex relationships between continental and island lineages. *BMC Evolutionary Biology* 16:253. DOI: 10.1186/s12862-016-0814-x.

Dufresnes C, Litvinchuk SN, Rozenblut-Kościsty B, Rodrigues N, Perrin N, Crochet P, Jeffries DL. 2020a. Hybridization and introgression between toads with different sex chromosome systems. *Evolution Letters* 4:444–456. DOI: 10.1002/evl3.191.

Dufresnes C, Nicieza AG, Litvinchuk SN, Rodrigues N, Jeffries DL, Vences M, Perrin N, Martínez-Solano Í. 2020b. Are glacial refugia hotspots of speciation and cytonuclear discordances? Answers from the genomic phylogeography of Spanish common frogs. *Molecular Ecology* 29:986–1000. DOI: 10.1111/mec.15368.

Eto K, Matsui M, Sugahara T. 2022. Description of a new subterranean breeding brown frog (Ranidae: Rana) from Japan. *Zootaxa* 5209:401–425. DOI: 10.11646/zootaxa.5209.4.1.

Evanno G, Regnaut S, Goudet J. 2005. Detecting the number of clusters of individuals using the software structure: a simulation study. *Molecular Ecology* 14:2611–2620. DOI: 10.1111/j.1365-294x.2005.02553.x.

Excoffier L. 2004. Patterns of DNA sequence diversity and genetic structure after a range expansion: lessons from the infinite-island model. *Molecular Ecology* 13:853–864. DOI: 10.1046/j.1365-294x.2003.02004.x.

Excoffier L, Foll M, Petit RJ. 2009. Genetic consequences of range expansions. *Annual Review of Ecology, Evolution, and Systematics* 40:481–501. DOI: 10.1146/annurev.ecolsys.39.110707.173414.

Excoffier L, Lischer HEL. 2010. Arlequin suite ver 3.5: a new series of programs to perform population genetics analyses under Linux and Windows. *Molecular Ecology Resources* 10:564–567. DOI: 10.1111/j.1755-0998.2010.02847.x.

Ficetola GF, Maiorano L. 2016. Contrasting effects of temperature and precipitation change on amphibian phenology, abundance and performance. *Oecologia* 181:683–693. DOI: 10.1007/s00442-016-3610-9.

Fick SE, Hijmans RJ. 2017. WorldClim 2: new 1-km spatial resolution climate surfaces for global land areas. *International Journal of Climatology* 37:4302–4315. DOI: 10.1002/joc.5086.

Fonseca RR da, Johnson WE, O'Brien SJ, Ramos MJ, Antunes A. 2008. The adaptive evolution of the mammalian mitochondrial genome. *BMC Genomics* 9:119. DOI: 10.1186/1471-2164-9-119.

Fouquet A, Vences M, Salducci M-D, Meyer A, Marty C, Blanc M, Gilles A. 2007. Revealing cryptic diversity using molecular phylogenetics and phylogeography in frogs of the Scinax ruber and Rhinella margaritifera species groups. *Molecular Phylogenetics and Evolution* 43:567–582. DOI: 10.1016/j.ympev.2006.12.006.

Frost, DR. 2023. Amphibian Species of the World: an online reference. Version 6.2 (Accessed in January, 2023). Electronic Database accessible at https://amphibiansoftheworld.amnh.org/index.php. *American Museum of Natural History*, New York, USA.

Fu Y-X. 1997. Statistical tests of neutrality of mutations against population growth, hitchhiking and background selection. *Genetics* 147:915–925. DOI: 10.1093/genetics/147.2.915.

Fukutani K, Matsui M, Tran DV, Nishikawa K. 2022. Genetic diversity and demography of *Bufo japonicus* and *B. torrenticola* (Amphibia: Anura: Bufonidae) influenced by the Quaternary climate. *PeerJ* 10:e13452. DOI: 10.7717/peerj.13452.

Funk DJ, Omland KE. 2003. Species-level paraphyly and polyphyly: frequency, causes, and consequences, with insights from animal mitochondrial DNA. *Ecology, Evolution, and Systematics* 34:397–423. DOI: 10.1146/annurev.ecolsys.34.011802.132421.

Garcia-Porta J, Litvinchuk SN, Crochet PA, Romano A, Geniez PH, Lo-Valvo M, Lymberakis P, Carranza S. 2012. Molecular phylogenetics and historical biogeography of the west-palearctic common toads (*Bufo bufo* species complex). *Molecular Phylogenetics and Evolution* 63:113–130. DOI: 10.1016/j.ympev.2011.12.019.

Gargiulo R, Kull T, Fay MF. 2021. Effective double-digest RAD sequencing and genotyping despite large genome size. *Molecular Ecology Resources* 21:1037–1055. DOI: 10.1111/1755-0998.13314.

Gent PR, Danabasoglu G, Donner LJ, Holland MM, Hunke EC, Jayne SR, Lawrence DM, Neale RB, Rasch PJ, Vertenstein M, Worley PH, Yang Z-L, Zhang M. 2011. The community climate system model version 4. *Journal of Climate* 24:4973–4991. DOI: 10.1175/2011jcli4083.1.

Gompert Z, Buerkle CA. 2010. INTROGRESS: a software package for mapping components of isolation in hybrids. *Molecular Ecology Resources* 10:378–384. DOI: 10.1111/j.1755-0998.2009.02733.x.

Grant WS. 2015. Problems and cautions with sequence mismatch analysis and Bayesian skyline plots to infer historical demography. *Journal of Heredity* 106:333–346. DOI: 10.1093/jhered/esv020.

Grant W, Bowen B. 1998. Shallow population histories in deep evolutionary lineages of marine fishes: insights from sardines and anchovies and lessons for conservation. *Journal of Heredity* 89:415–426. DOI: 10.1093/jhered/89.5.415.

Guindon S, Gascuel O. 2003. A simple, fast, and accurate algorithm to estimate large phylogenies by maximum likelihood. *Systematic Biology* 52:696–704. DOI: 10.1080/10635150390235520.

Gvoždík V, Canestrelli D, García-París M, Moravec J, Nascetti G, Recuero E, Teixeira J, Kotlík P. 2015. Speciation history and widespread introgression in the European short-call tree frogs (*Hyla arborea* sensu lato, *H. intermedia* and *H. sarda*). *Molecular Phylogenetics and Evolution* 83:143–155. DOI: 10.1016/j.ympev.2014.11.012.

Haldane JBS. 1922. Sex ratio and unisexual sterility in hybrid animals. *Journal of Genetics* 12:101–109. DOI: 10.1007/bf02983075.

Harpending HC. 1994. Signature of ancient population growth in a low-resolution mitochondrial DNA mismatch distribution. *Human biology* 66:591–600.

Harrison RG, Larson EL. 2014. Hybridization, introgression, and the nature of species boundaries. *Journal of Heredity* 105:795–809. DOI: 10.1093/jhered/esu033.

Hase K, Nikoh N, Shimada M. 2013. Population admixture and high larval viability among urban toads. *Ecology and Evolution* 3:1677–1691. DOI: 10.1002/ece3.578.

Hase K, Shimada M, Nikoh N. 2012. High degree of mitochondrial haplotype diversity in the Japanese common toad *Bufo japonicus* in urban Tokyo. *Zoological Science* 31:702–708. DOI: 10.2108/zsj.29.702.

Hase K, Takayanagi M, Hashimoto H, Ogawa H, Furuhashi Y. 2022. The introduction of the Japanese common toad in Tokyo and the current state of their breeding behavior. *Bulletin of the Herpetological Society of Japan* 2:215–223.

Hastings WK. 1970. Monte Carlo sampling methods using Markov chains and their applications. *Biometrika* 57:97. DOI: 10.2307/2334940.

Hatano N, Yoshida K. 2017. Sedimentary environment and paleosols of middle Miocene fluvial and lacustrine sediments in central Japan: implications for paleoclimate interpretations. *Sedimentary Geology* 347:117–129. DOI: 10.1016/j.sedgeo.2016.11.004.

Hayes KA, Joshi RC, Thiengo SC, Cowie RH. 2008. Out of South America: multiple origins of non-native apple snails in Asia. *Diversity and Distributions* 14:701–712. DOI: 10.1111/j.1472-4642.2008.00483.x.

Herbert TD, Lawrence KT, Tzanova A, Peterson LC, Caballero-Gill R, Kelly CS. 2016. Late Miocene global cooling and the rise of modern ecosystems. *Nature Geoscience* 9:843–847. DOI: 10.1038/ngeo2813.

Hewitt GM. 1988. Hybrid zones-natural laboratories for evolutionary studies. *Trends in Ecology & Evolution* 3:158–167. DOI: 10.1016/0169-5347(88)90033-x.

Hewitt GM. 2004. Genetic consequences of climatic oscillations in the Quaternary. *Philosophical Transactions of the Royal Society of London. Series B: Biological Sciences* 359:183–195. DOI: 10.1098/rstb.2003.1388.

Hickerson MJ, Carstens BC, Cavender-Bares J, Crandall KA, Graham CH, Johnson JB, Rissler L, Victoriano PF, Yoder AD. 2010. Phylogeography's past, present, and future: 10 years after Avise, 2000. *Molecular Phylogenetics and Evolution* 54:291–301. DOI: 10.1016/j.ympev.2009.09.016.

Hickerson MJ, Meyer CP, Moritz C. 2006. DNA barcoding will often fail to discover new animal species over broad parameter space. *Systematic Biology* 55:729–739. DOI: 10.1080/10635150600969898.

Hillis DM. 2019. Species Delimitation in Herpetology. *Journal of Herpetology* 53:3–12. DOI: 10.1670/18-123.

Hinneberg H, Bamann T, Geue JC, Foerster K, Thomassen HA, Kupfer A. 2022. Truly invasive or simply non-native? Insights from an artificial crested newt hybrid zone. *Conservation Science and Practice* 4. DOI: 10.1111/csp2.12752.

Ho SYW, Larson G. 2006. Molecular clocks: when times are a-changin'. *Trends in Genetics* 22:79–83. DOI: 10.1016/j.tig.2005.11.006.

Ho SYW, Phillips MJ, Cooper A, Drummond AJ. 2005. Time dependency of molecular rate estimates and systematic overestimation of recent divergence times. *Molecular Biology and Evolution* 22:1561–1568. DOI: 10.1093/molbev/msi145.

Ho SYW, Saarma U, Barnett R, Haile J, Shapiro B. 2008. The effect of inappropriate calibration: three case studies in molecular ecology. *PLoS ONE* 3:e1615. DOI: 10.1371/journal.pone.0001615.

Hoareau TB. 2016. Late glacial demographic expansion motivates a clock overhaul for population genetics. *Systematic Biology* 65:449–464. DOI: 10.1093/sysbio/syv120.

Hohenlohe PA, Amish SJ, Catchen JM, Allendorf FW, Luikart G. 2011. Next-generation RAD sequencing identifies thousands of SNPs for assessing hybridization between rainbow and westslope cutthroat trout. *Molecular Ecology Resources* 11:117–122. DOI: 10.1111/j.1755-0998.2010.02967.x.

Igawa T, Kurabayashi A, Nishioka M, Sumida M. 2006. Molecular phylogenetic relationship of toads distributed in the Far East and Europe inferred from the nucleotide sequences of mitochondrial DNA genes. *Molecular Phylogenetics and Evolution* 38:250–260. DOI: 10.1016/j.ympev.2005.09.003.

Ikehara K. 1992. Formation of duned sand bodies in the Osumi Strait, south of Kyushu, Japan. *Journal of the Sedimentological Society of Japan* 36:37–45. DOI: 10.14860/jssj1972.36.37.

Iwaoka Y, Watanabe T, Satoh SS, Nambu H, Yamazaki Y. 2021. Hybridization of two species of Japanese toads, *Bufo torrenticola* and *Bufo japonicus formosus*, in the central part of Japan. *Zoological Science* 38:506–512. DOI: 10.2108/zs210023.

Jombart T. 2008. *adegenet*: a R package for the multivariate analysis of genetic markers. *Bioinformatics* 24:1403–1405. DOI: 10.1093/bioinformatics/btn129.

Jombart T, Ahmed I. 2011. *adegenet 1.3-1*: new tools for the analysis of genome-wide SNP data. *Bioinformatics* 27:3070–3071. DOI: 10.1093/bioinformatics/btr521.

Jombart T, Devillard S, Balloux F. 2010. Discriminant analysis of principal components: a new method for the analysis of genetically structured populations. *BMC Genetics* 11:94–94. DOI: 10.1186/1471-2156-11-94.

Katoh K, Standley DM. 2013. MAFFT multiple sequence alignment software version 7: improvements in performance and usability. *Molecular Biology and Evolution* 30:772–780. DOI: 10.1093/molbev/mst010.

Kawamura T, Nishioka M, Sumida M, Ryuzaki M. 1990. An electrophoretic study of genetic differentiation in 40 populations of *Bufo japonicus* distributed in Japan. *Scientific report of the Laboratory for Amphibian Biology, Hiroshima University* 10:1–51. DOI: 10.15027/291.

Kawamura T, Nishioka M, Ueda H. 1980. Inter- and Intraspecific Hybrids among Japanese, European and American Toads. *Scientific report of the Laboratory for Amphibian Biology, Hiroshima University* 4:1–125. DOI: 10.15027/333.

Key KHL. 1968. The concept of stasipatric speciation. *Systematic Biology* 17:14–22. DOI: 10.1093/sysbio/17.1.14.

Komaki S, Igawa T, Lin S, Tojo K, Min M, Sumida M. 2015. Robust molecular phylogeny and palaeodistribution modelling resolve a complex evolutionary history: glacial cycling drove recurrent mtDNA introgression among *Pelophylax* frogs in East Asia. *Journal of Biogeography* 42:2159–2171. DOI: 10.1111/jbi.12584.

Kopelman NM, Mayzel J, Jakobsson M, Rosenberg NA, Mayrose I. 2015. Clumpak: a program for identifying clustering modes and packaging population structure inferences across K. *Molecular Ecology Resources* 15:1179–1191. DOI: 10.1111/1755-0998.12387.

Kubota Y, Kusumoto B, Shiono T, Tanaka T. 2017. Phylogenetic properties of Tertiary relict flora in the east Asian continental islands: imprint of climatic niche conservatism and in situ diversification. *Ecography* 40:436–447. DOI: 10.1111/ecog.02033.

Kubota Y, Shiono T, Kusumoto B. 2015. Role of climate and geohistorical factors in driving plant richness patterns and endemicity on the east Asian continental islands. *Ecography* 38:639–648. DOI: 10.1111/ecog.00981.

Kusano T, Maruyama K, Kaneko S. 1995. Post-breeding dispersal of the Japanese toad, *Bufo japonicus formosus*. *Journal of Herpetology* 29:633. DOI: 10.2307/1564755.

Leaché AD, Fujita MK, Minin VN, Bouckaert RR. 2014. Species delimitation using genome-wide SNP data. *Systematic Biology* 63:534–542. DOI: 10.1093/sysbio/syu018.

Lehtomäki J, Kusumoto B, Shiono T, Tanaka T, Kubota Y, Moilanen A. 2018. Spatial conservation prioritization for the East Asian islands: a balanced representation of multitaxon biogeography in a protected area network. *Diversity and Distributions* 25:414–429. DOI: 10.1111/ddi.12869.

Leliaert F, Verbruggen H, Vanormelingen P, Steen F, López-Bautista JM, Zuccarello GC, Clerck OD. 2014. DNA-based species delimitation in algae. *European Journal of Phycology* 49:179–196. DOI: 10.1080/09670262.2014.904524.

Letunic I, Bork P. 2021. Interactive Tree Of Life (iTOL) v5: an online tool for phylogenetic tree display and annotation. *Nucleic Acids Research* 49:W293–W296. DOI: 10.1093/nar/gkab301.

Li H, Handsaker B, Wysoker A, Fennell T, Ruan J, Homer N, Marth G, Abecasis G, Durbin R, Subgroup 1000 Genome Project Data Processing. 2009. The sequence alignment/map format and SAMtools. *Bioinformatics* 25:2078–2079. DOI: 10.1093/bioinformatics/btp352.

Li Y, Liu J. 2018. StructureSelector: A web-based software to select and visualize the optimal number of clusters using multiple methods. *Molecular Ecology Resources* 18:176–177. DOI: 10.1111/1755-0998.12719.

Lisiecki LE, Raymo ME. 2005. A Pliocene-Pleistocene stack of 57 globally distributed benthic $\delta^{18}O$ records. *Paleoceanography* 20:PA1003. DOI: 10.1029/2004pa001071.

Maddison WP. 1997. Gene trees in species trees. *Systematic Biology* 46:523–536. DOI: 10.1093/sysbio/46.3.523.

Mahony SH, Wallace LM, Miyoshi M, Villamor P, Sparks RSJ, Hasenaka T. 2011. Volcano-tectonic interactions during rapid plate-boundary evolution in the Kyushu region, SW Japan. *Geological Society of America bulletin* 123:2201–2223. DOI: 10.1130/b30408.1.

Mallet J, Barton N, Lamas G, Santisteban J, Muedas M, Eeley H. 1990. Estimates of selection and gene flow from measures of cline width and linkage disequilibrium in heliconius hybrid zones. *Genetics* 124:921–936. DOI: 10.1093/genetics/124.4.921.

Marcaida AJB, Nakao M, Fukutani K, Nishikawa K, Urabe M. 2022. Phylogeography of *Rhabdias* spp. (Nematoda: Rhabdiasidae) collected from *Bufo* species in Honshu, Shikoku, and Kyushu, Japan including possible cryptic species. *Parasitology International* 90:102612. DOI: 10.1016/j.parint.2022.102612.

Marcus J, Ha W, Barber RF, Novembre J. 2021. Fast and flexible estimation of effective migration surfaces. *eLife* 10:e61927. DOI: 10.7554/elife.61927.

Martínez-Monzón A, Cuenca-Bescós G, Bisbal-Chinesta J, Blain H. 2021. One million years of diversity shifts in amphibians and reptiles in a Mediterranean landscape: resilience rules the Quaternary. *Palaeontology* 64:673–686. DOI: 10.1111/pala.12547.

Mastrantonio V, Porretta D, Urbanelli S, Crasta G, Nascetti G. 2016. Dynamics of mtDNA introgression during species range expansion: insights from an experimental longitudinal study. *Scientific Reports* 6:30355. DOI: 10.1038/srep30355.

Matsui M. 1976. A new toad from Japan. *Contributions from the Biological Laboratory, Kyoto University* 25:1–9.

Matsui M. 1977. Genetic relationships within Eurasian toads of *Bufo bufo* species group. *Zoological magazine* 86:535.

Matsui M. 1984. Morphometric variation analyses and revision of the Japanese toads (Genus *Bufo*, Bufonidae). *Contributions from the Biological Laboratory, Kyoto University* 26:209–428.

Matsui M. 1986. Geographic variation in toads of the *Bufo bufo* complex from the far east, with a description of a new subspecies. *Copeia* 1986:561–579. DOI: 10.2307/1444939.

Matsui M, Kawahara Y, Nishikawa K, Ikeda S, Eto K, Mizuno Y. 2019a. Molecular phylogeny and evolution of two *Rhacophorus* species endemic to mainland Japan. *Asian Herpetological Research* 10:86–104. DOI: 10.16373/j.cnki.ahr.190015.

Matsui M, Maeda N. 2018. *Encyclopedia of Japanese frogs*. Tokyo: Bun-ichi Sogo Shuppan.

Matsui M, Okawa H, Nishikawa K, Aoki G, Eto K, Yoshikawa N, Tanabe S, Misawa Y, Tominaga A. 2019b. Systematics of the widely distributed Japanese clouded salamander, *Hynobius nebulosus* (Amphibia: Caudata: Hynobiidae), and its closest relatives. *Current Herpetology* 38:32–90. DOI: 10.5358/hsj.38.32.

Matsui M, Yoshikawa N, Aoki G, Sasamori K, Matsui M, Tanabe S, Misawa Y, Nishikawa K. 2020. Wide distribution but low differentiation: phylogenetic relationships and phylogeography of *Hynobius nigrescens* (Amphibia: Caudata). *Zoological Science* 37:529–537. DOI: 10.2108/zs200099.

Matsuzaki KM, Suzuki N, Tada R. 2020. An intensified East Asian winter monsoon in the Japan Sea between 7.9 and 6.6 Ma. *Geology* 48:919–923. DOI: 10.1130/g47393.1.

Mayr E. 1942. *Systematics and the origin of species, from the viewpoint of a zoologist.* Harvard University Press.

Mayr E. 1968. The role of systematics in biology. *Science* 159:595–599. DOI: 10.1126/science.159.3815.595.

McKay BD, Zink RM. 2010. The causes of mitochondrial DNA gene tree paraphyly in birds. *Molecular Phylogenetics and Evolution* 54:647–650. DOI: 10.1016/j.ympev.2009.08.024.

Metropolis N, Rosenbluth AW, Rosenbluth MN, Teller AH, Teller E. 1953. Equation of state calculations by fast computing machines. *The Journal of Chemical Physics* 21:1087–1092. DOI: 10.1063/1.1699114.

Miller MP. 2005. Allele In Space (AIS): computer software for the joint analysis of interindividual spatial and genetic information. *Journal of Heredity* 96:722–724. DOI: 10.1093/jhered/esi119.

Miller MP, Bellinger MR, Forsman ED, Haig SM. 2006. Effects of historical climate change, habitat connectivity, and vicariance on genetic structure and diversity across the range of

the red tree vole (*Phenacomys longicaudus*) in the Pacific Northwestern United States. *Molecular Ecology* 15:145–159. DOI: 10.1111/j.1365-294x.2005.02765.x.

Milne RI, Abbott RJ. 2008. Reproductive isolation among two interfertile *Rhododendron* species: low frequency of post-F1 hybrid genotypes in alpine hybrid zones. *Molecular Ecology* 17:1108–1121. DOI: 10.1111/j.1365-294x.2007.03643.x.

Miura I. 1995. Two differentiated groups of the Japanese toad, *Bufo japonicus japonicus*, demonstrated by C-banding analysis of chromosomes. *Caryologia* 48:123–136. DOI: 10.1080/00087114.1995.10797322.

Miyabuchi Y, Sugiyama S. 2020. Vegetation history after the late period of the Last Glacial Age based on phytolith records in Nangodani Valley basin, southern part of the Aso caldera, Japan. *Journal of Quaternary Science* 35:304–315. DOI: 10.1002/jqs.3153.

Miyabuchi Y, Sugiyama S, Nagaoka Y. 2012. Vegetation and fire history during the last 30,000 years based on phytolith and macroscopic charcoal records in the eastern and western areas of Aso Volcano, Japan. *Quaternary International* 254:28–35. DOI: 10.1016/j.quaint.2010.11.019.

Momohara A. 2016. Stages of major floral change in Japan based on macrofossil evidence and their connection to climate and geomorphological changes since the Pliocene. *Quaternary International* 397:93–105. DOI: 10.1016/j.quaint.2015.03.008.

Moritz C, Dowling TE, Brown WM. 1987. Evolution of animal mitochondrial DNA: relevance for population biology and systematics. *Annual Review of Ecology and Systematics* 18:269–292. DOI: 10.1146/annurev.es.18.110187.001413.

Muller HJ. 1942. Isolating mechanisms, evolution, and temperature. *Biological Symposia*:71–125.

Mussmann SM, Douglas MR, Chafin TK, Douglas ME. 2019. BA3-SNPs: Contemporary migration reconfigured in BayesAss for next-generation sequence data. *Methods in Ecology and Evolution* 10:1808–1813. DOI: 10.1111/2041-210x.13252.

Nakazato T, Warren DL, Moyle LC. 2010. Ecological and geographic modes of species divergence in wild tomatoes. *American Journal of Botany* 97:680–693. DOI: 10.3732/ajb.0900216.

Nishikawa K. 2017. Species diversity of Japanese amphibians: recent progress and future prospects of systematic studies. In: Motokawa M, Kajihara H eds. *Species Diversity of Animals in Japan. Diversity and Commonality in Animals.* Tokyo: Springer, 165–181. DOI: 10.1007/978-4-431-56432-4_6.

Nishioka M, Sumida M, Ueda H, Wu Z. 1990. Genetic relationships among 13 *Bufo* species and subspecies elucidated by the method of electrophoretic analyses. *Scientific report of the Laboratory for Amphibian Biology, Hiroshima University* 10:53–91. DOI: 10.15027/292.

Nishizawa T, Kurabayashi A, Kunihara T, Sano N, Fujii T, Sumida M. 2011. Mitochondrial DNA diversification, molecular phylogeny, and biogeography of the primitive rhacophorid genus *Buergeria* in East Asia. *Molecular Phylogenetics and Evolution* 59:139–147. DOI: 10.1016/j.ympev.2011.01.015.

Noll D, Leon F, Brandt D, Pistorius P, Bohec CL, Bonadonna F, Trathan PN, Barbosa A, Rey AR, Dantas GPM, Bowie RCK, Poulin E, Vianna JA. 2022. Positive selection over the mitochondrial genome and its role in the diversification of gentoo penguins in response to adaptation in isolation. *Scientific Reports* 12:3767. DOI: 10.1038/s41598-022-07562-0.

Nunome M, Torii H, Matsuki R, Kinoshita G, Suzuki H. 2010. The Influence of Pleistocene refugia on the evolutionary history of the Japanese hare, *Lepus brachyurus*. *Zoological Science* 27:746–754. DOI: 10.2108/zsj.27.746.

Okada Y. 1928. Notes on Japanese frogs. *Annotationes Zoologicae Japonenses* 11:269–277.

Okamiya H, Sugawara H, Nagano M, Poyarkov NA. 2018. An integrative taxonomic analysis reveals a new species of lotic Hynobius salamander from Japan. *PeerJ* 6:e5084. DOI: 10.7717/peerj.5084.

Ono Y, Aoki T, Hasegawa H, Dali L. 2005. Mountain glaciation in Japan and Taiwan at the global Last Glacial Maximum. *Quaternary International* 138–139:79–92. DOI: 10.1016/j.quaint.2005.02.007.

Orr HA. 1997. Haldane's rule. *Annual Review of Ecology and Systematics* 28:195–218. DOI: 10.1146/annurev.ecolsys.28.1.195.

Othman SN, Litvinchuk SN, Maslova I, Dahn H, Messenger KR, Andersen D, Jowers MJ, Kojima Y, Skorinov DV, Yasumiba K, Chuang M-F, Chen Y-H, Bae Y, Hoti J, Jang Y, Borzee A. 2022. From Gondwana to the Yellow Sea, evolutionary diversifications of true toads *Bufo* sp. in the Eastern Palearctic and a revisit of species boundaries for Asian lineages. *eLife* 11:e70494. DOI: 10.7554/elife.70494.

Özdemir N, Dursun C, Üzüm N, Kutrup B, Gül S. 2020. Taxonomic assessment and distribution of common toads (*Bufo bufo* and *B. verrucosissimus*) in Turkey based on morphological and molecular data. *Amphibia-Reptilia* 41:399–411. DOI: 10.1163/15685381-bja10009.

Peterson AT. 2011. Ecological niche conservatism: a time-structured review of evidence. *Journal of Biogeography* 38:817–827. DOI: 10.1111/j.1365-2699.2010.02456.x.

Petkova D, Novembre J, Stephens M. 2016. Visualizing spatial population structure with estimated effective migration surfaces. *Nature Genetics* 48:94–100. DOI: 10.1038/ng.3464.

Phillips SJ, Anderson RP, Schapire RE. 2006. Maximum entropy modeling of species geographic distributions. *Ecological Modelling* 190:231–259. DOI: 10.1016/j.ecolmodel.2005.03.026.

Pritchard JK, Stephens M, Donnelly P. 2000. Inference of population structure using multilocus genotype data. *Genetics* 155:945–959. DOI: 10.1093/genetics/155.2.945.

Provan J, Bennett KD. 2008. Phylogeographic insights into cryptic glacial refugia. *Trends in Ecology & Evolution* 23:564–571. DOI: 10.1016/j.tree.2008.06.010.

Puechmaille SJ. 2016. The program structure does not reliably recover the correct population structure when sampling is uneven: subsampling and new estimators alleviate the problem. *Molecular Ecology Resources* 16:608–627. DOI: 10.1111/1755-0998.12512.

Queiroz KD. 2007. Species concepts and species delimitation. *Systematic Biology* 56:879–886. DOI: 10.1080/10635150701701083.

Queiroz KD. 2020. An updated concept of subspecies resolves a dispute about the taxonomy of incompletely separated lineages. *Herpetological Review* 51:459–461.

Rambaut A, Drummond AJ, Xie D, Baele G, Suchard MA. 2018. Posterior summarization in Bayesian phylogenetics using Tracer 1.7. *Systematic Biology* 67:901–904. DOI: 10.1093/sysbio/syy032.

Ray N, Currat M, Excoffier L. 2003. Intra-deme molecular diversity in spatially expanding populations. *Molecular Biology and Evolution* 20:76–86. DOI: 10.1093/molbev/msg009.

Recuero E, Canestrelli D, Vörös J, Szabó K, Poyarkov NA, Arntzen JW, Crnobrnja-Isailovic J, Kidov AA, Cogălniceanu D, Caputo FP, Nascetti G, Martínez-Solano I. 2012. Multilocus species tree analyses resolve the radiation of the widespread *Bufo bufo* species group (Anura, Bufonidae). *Molecular Phylogenetics and Evolution* 62:71–86. DOI: 10.1016/j.ympev.2011.09.008.

Riemsdijk I van, Arntzen JW, Bucciarelli GM, McCartney-Melstad E, Rafajlović M, Scott PA, Toffelmier E, Shaffer HB, Wielstra B. 2023. Two transects reveal remarkable variation in gene flow on opposite ends of a European toad hybrid zone. *Heredity* 131:15–24. DOI: 10.1038/s41437-023-00617-6.

Rochette NC, Rivera-Colón AG, Catchen JM. 2019. Stacks 2: Analytical methods for paired-end sequencing improve RADseq-based population genomics. *Molecular Ecology* 28:4737–4754. DOI: 10.1111/mec.15253.

Rogers AR, Harpending H. 1992. Population growth makes waves in the distribution of pairwise genetic differences. *Molecular Biology and Evolution* 9:552–69. DOI: 10.1093/oxfordjournals.molbev.a040727.

Ronquist F, Teslenko M, Mark P van der, Ayres DL, Darling A, Höhna S, Larget B, Liu L, Suchard MA, Huelsenbeck JP. 2012. MrBayes 3.2: efficient Bayesian phylogenetic inference and model choice across a large model space. *Systematic Biology* 61:539–542. DOI: 10.1093/sysbio/sys029.

Rozas J, Ferrer-Mata A, Sánchez-DelBarrio JC, Guirao-Rico S, Librado P, Ramos-Onsins SE, Sánchez-Gracia A. 2017. DnaSP 6: DNA sequence polymorphism analysis of large data sets. *Molecular biology and evolution* 34:3299–3302. DOI: 10.1093/molbev/msx248.

Sakaguchi S, Asaoka Y, Takahashi D, Isagi Y, Imai R, Nagano AJ, Qiu Y-X, Li P, Lu R, Setoguchi H. 2021. Inferring historical survivals of climate relicts: the effects of climate changes, geography, and population-specific factors on herbaceous hydrangeas. *Heredity* 126:615–629. DOI: 10.1038/s41437-020-00396-4.

Sandel B, Arge L, Dalsgaard B, Davies RG, Gaston KJ, Sutherland WJ, Svenning J-C. 2011. The influence of Late Quaternary climate-change velocity on species endemism. *Science* 334:660–664. DOI: 10.1126/science.1210173.

Schluter D. 2009. Evidence for ecological speciation and its alternative. *Science* 323:737–741. DOI: 10.1126/science.1160006.

Schoener TW. 1968. The Anolis Lizards of Bimini: resource partitioning in a complex fauna. *Ecology* 49:704–726. DOI: 10.2307/1935534.

Schwarz G. 1978. Estimating the dimension of a model. *The Annals of Statistics* 6:461–464. DOI: 10.1214/aos/1176344136.

Scordato ESC, Wilkins MR, Semenov G, Rubtsov AS, Kane NC, Safran RJ. 2017. Genomic variation across two barn swallow hybrid zones reveals traits associated with divergence in sympatry and allopatry. *Molecular Ecology* 26:5676–5691. DOI: 10.1111/mec.14276.

Sequeira F, Bessa-Silva A, Tarroso P, Sousa-Neves T, Vallinoto M, Gonçalves H, Martínez-Solano I. 2020. Discordant patterns of introgression across a narrow hybrid zone between two cryptic lineages of an Iberian endemic newt. *Journal of Evolutionary Biology* 33:202–216. DOI: 10.1111/jeb.13562.

Servedio MR, Hermisson J. 2020. The evolution of partial reproductive isolation as an adaptive optimum. *Evolution* 74:4–14. DOI: 10.1111/evo.13880.

Shapiro B, Drummond AJ, Rambaut A, Wilson MC, Matheus PE, Sher AV, Pybus OG, Gilbert MTP, Barnes I, Binladen J, Willerslev E, Hansen AJ, Baryshnikov GF, Burns JA, Davydov S, Driver JC, Froese DG, Harington CR, Keddie G, Kosintsev P, Kunz ML, Martin LD, Stephenson RO, Storer J, Tedford R, Zimov S, Cooper A. 2004. Rise and fall of the Beringian steppe bison. *Science* 306:1561–1565. DOI: 10.1126/science.1101074.

Shiba M. 2021. Characteristics of crustal uplift since the Pliocene in central Honshu, Japan, and sea level rise. *Earth Science (Chikyu Kagaku)* 75:37–55. DOI: 10.15080/agcjchikyukagaku.75.1_37.

Slager DL, Epperly KL, Ha RR, Rohwer S, Wood C, Hemert C, Klicka J. 2020. Cryptic and extensive hybridization between ancient lineages of American crows. *Molecular Ecology* 29:956–969. DOI: 10.1111/mec.15377.

Smith SA, Donoghue MJ. 2010. Combining historical biogeography with niche modeling in the *Caprifolium* clade of *Lonicera* (Caprifoliaceae, Dipsacales). *Systematic Biology* 59:322–341. DOI: 10.1093/sysbio/syq011.

Stamatakis A. 2014. RAxML version 8: a tool for phylogenetic analysis and post-analysis of large phylogenies. *Bioinformatics* 30:1312–1313. DOI: 10.1093/bioinformatics/btu033.

Stankowski S, Ravinet M. 2021. Defining the speciation continuum. *Evolution* 75:1256–1273. DOI: 10.1111/evo.14215.

Stöck M, Moritz C, Hickerson M, Frynta D, Dujsebayeva T, Eremchenko V, Macey JR, Papenfuss TJ, Wake DB. 2006. Evolution of mitochondrial relationships and biogeography of Palearctic green toads (*Bufo viridis* subgroup) with insights in their genomic plasticity. *Molecular Phylogenetics and Evolution* 41:663–689. DOI: 10.1016/j.ympev.2006.05.026.

Sumida M, Ogata M. 1998. Intraspecific differentiation in the Japanese brown frog *Rana japonica* inferred from mitochondrial DNA sequences of the cytochrome *b* gene. *Zoological Science* 15:989–1000. DOI: 10.2108/zsj.15.989.

Suyama Y, Hirota SK, Matsuo A, Tsunamoto Y, Mitsuyuki C, Shimura A, Okano K. 2022. Complementary combination of multiplex high-throughput DNA sequencing for molecular phylogeny. *Ecological Research* 37:171–181. DOI: 10.1111/1440-1703.12270.

Suyama Y, Matsuki Y. 2015. MIG-seq: an effective PCR-based method for genome-wide single-nucleotide polymorphism genotyping using the next-generation sequencing platform. *Scientific Reports* 5:srep16963. DOI: 10.1038/srep16963.

Suzuki D, Kawase T, Hoshina T, Tokuda T. 2020. Origins of nonnative populations of *Bufo japonicus formosus* (Amphibia: Bufonidae) in Hokkaido, Japan, as inferred by a molecular approach. *Current Herpetology* 39:47–54. DOI: 10.5358/hsj.39.47.

Suzuki Y, Tomozawa M, Koizumi Y, Tsuchiya K, Suzuki H. 2015. Estimating the molecular evolutionary rates of mitochondrial genes referring to Quaternary ice age events with inferred population expansions and dispersals in Japanese Apodemus. *BMC Evolutionary Biology* 15:187. DOI: 10.1186/s12862-015-0463-5.

Szymura JM, Barton NH. 1986. Genetic analysis of a hybrid zone between the fire-bellied toads *Bombina bombina* and *B. variegata*, near Cracow in Southern Poland. *Evolution* 40:1141–1159. DOI: 10.1111/j.1558-5646.1986.tb05740.x.

Szymura JM, Barton NH. 1991. The genetic structure of the hybrid zone between the fire-bellied toads *Bombina bombina* and *B. variegata*: comparisons between transects and between loci. *Evolution* 45:237–261. DOI: 10.1111/j.1558-5646.1991.tb04400.x.

Taberlet P, Fumagalli L, Wust-Saucy A-G, Cosson J-F. 1998. Comparative phylogeography and postglacial colonization routes in Europe. *Molecular Ecology* 7:453–464. DOI: 10.1046/j.1365-294x.1998.00289.x.

Takata K, Iwase F, Iguchi A, Yuasa H, Taninaka H, Iwasaki N, Uda K, Suzuki T, Nonaka M, Kikuchi T, Yasuda N. 2021. Genome-wide SNP data revealed notable spatial genetic structure in the deep-sea precious coral *Corallium japonicum*. *Frontiers in Marine Science* 8:667481. DOI: 10.3389/fmars.2021.667481.

Tanabe AS. 2011. Kakusan4 and Aminosan: two programs for comparing nonpartitioned, proportional and separate models for combined molecular phylogenetic analyses of multilocus sequence data. *Molecular Ecology Resources* 11:914–921. DOI: 10.1111/j.1755-0998.2011.03021.x.

Tieleman BI, Versteegh MA, Fries A, Helm B, Dingemanse NJ, Gibbs HL, Williams JB. 2009. Genetic modulation of energy metabolism in birds through mitochondrial function. *Proceedings of the Royal Society B: Biological Sciences* 276:1685–1693. DOI: 10.1098/rspb.2008.1946.

Tobias JA, Seddon N, Spottiswoode CN, Pilgrim JD, Fishpool LDC, Collar NJ. 2010. Quantitative criteria for species delimitation. *Ibis* 152:724–746. DOI: 10.1111/j.1474-919x.2010.01051.x.

Toews DPL, Brelsford A. 2012. The biogeography of mitochondrial and nuclear discordance in animals. *Molecular Ecology* 21:3907–3930. DOI: 10.1111/j.1365-294x.2012.05664.x.

Tomaru N, Takahashi M, Tsumura Y, Takahashi M, Ohba K. 1998. Intraspecific variation and phylogeographic patterns of *Fagus crenata* (Fagaceae) mitochondrial DNA. *American Journal of Botany* 85:629–636. DOI: 10.2307/2446531.

Tominaga A, Matsui M, Nishikawa K, Tanabe S. 2006. Phylogenetic relationships of *Hynobius naevius* (Amphibia: Caudata) as revealed by mitochondrial 12S and 16S rRNA genes. *Molecular Phylogenetics and Evolution* 38:677–684. DOI: 10.1016/j.ympev.2005.10.014.

Tominaga A, Matsui M, Yoshikawa N, Eto K, Nishikawa K. 2018. Genomic displacement and shift of the hybrid zone in the Japanese fire-bellied newt. *Journal of Heredity* 109:232–242. DOI: 10.1093/jhered/esx085.

Tominaga A, Matsui M, Yoshikawa N, Nishikawa K, Hayashi T, Misawa Y, Tanabe S, Ota H. 2013. Phylogeny and historical demography of *Cynops pyrrhogaster* (Amphibia: Urodela): taxonomic relationships and distributional changes associated with climatic oscillations. *Molecular Phylogenetics and Evolution* 66:654–667. DOI: 10.1016/j.ympev.2012.10.015.

Toyama KS, Crochet P, Leblois R. 2020. Sampling schemes and drift can bias admixture proportions inferred by structure. *Molecular Ecology Resources* 20:1769–1785. DOI: 10.1111/1755-0998.13234.

Vähä J-P, Primmer CR. 2006. Efficiency of model-based Bayesian methods for detecting hybrid individuals under different hybridization scenarios and with different numbers of loci. *Molecular Ecology* 15:63–72. DOI: 10.1111/j.1365-294x.2005.02773.x.

Vasimuddin M, Misra S, Li H, Aluru S. 2019. Efficient architecture-aware acceleration of BWA-MEM for multicore systems. In: 2019 IEEE International Parallel and Distributed Processing Symposium (IPDPS). Rio de Janeiro, Brazil, 314–324. DOI: 10.1109/ipdps.2019.00041.

Via S. 2001. Sympatric speciation in animals: the ugly duckling grows up. *Trends in Ecology & Evolution* 16:381–390. DOI: 10.1016/s0169-5347(01)02188-7.

Waltari E, Hijmans RJ, Peterson AT, Nyári ÁS, Perkins SL, Guralnick RP. 2007. Locating Pleistocene refugia: comparing phylogeographic and ecological niche model predictions. *PLoS ONE* 2:e563. DOI: 10.1371/journal.pone.0000563.

Warren DL, Glor RE, Turelli M. 2008. Environmental niche equivalency versus conservatism: quantitative approaches to niche evolution. *Evolution* 62:2868–2883. DOI: 10.1111/j.1558-5646.2008.00482.x.

Warren DL, Glor RE, Turelli M. 2010. ENMTools: a toolbox for comparative studies of environmental niche models. *Ecography* 33:607–611. DOI: 10.1111/j.1600-0587.2009.06142.x.

Watanabe S, Hajima T, Sudo K, Nagashima T, Takemura T, Okajima H, Nozawa T, Kawase H, Abe M, Yokohata T, Ise T, Sato H, Kato E, Takata K, Emori S, Kawamiya M. 2011. MIROC-ESM 2010: model description and basic results of CMIP5-20c3m experiments. *Geoscientific Model Development* 4:845–872. DOI: 10.5194/gmd-4-845-2011.

Watanabe K, Tabata R, Nakajima J, Kobayakawa M, Matsuda M, Takaku K, Hosoya K, Ohara K, Takagi M, Jang-Liaw N-H. 2020. Large-scale hybridization of Japanese populations of Hinamoroko, *Aphyocypris chinensis*, with *A. kikuchii* introduced from Taiwan. *Ichthyological Research* 67:361–374. DOI: 10.1007/s10228-019-00730-9.

Wielstra B, Arntzen JW. 2011. Unraveling the rapid radiation of crested newts (*Triturus cristatus* superspecies) using complete mitogenomic sequences. *BMC Evolutionary Biology* 11:162. DOI: 10.1186/1471-2148-11-162.

Wielstra B, Burke T, Butlin RK, Schaap O, Shaffer HB, Vrieling K, Arntzen JW. 2016. Efficient screening for 'genetic pollution' in an anthropogenic crested newt hybrid zone. *Conservation Genetics Resources* 8:553–560. DOI: 10.1007/s12686-016-0582-3.

Wiens JJ, Graham CH. 2005. Niche conservatism: integrating evolution, ecology, and conservation biology. *Annual Review of Ecology, Evolution, and Systematics* 36:519–539. DOI: 10.1146/annurev.ecolsys.36.102803.095431.

Wiens JJ, Penkrot TA. 2002. Delimiting species using DNA and morphological variation and discordant species limits in spiny lizards (*Sceloporus*). *Systematic Biology* 51:69–91. DOI: 10.1080/106351502753475880.

Willis SC, Hollenbeck CM, Puritz JB, Gold JR, Portnoy DS. 2017. Haplotyping RAD loci: an efficient method to filter paralogs and account for physical linkage. *Molecular Ecology Resources* 17:955–965. DOI: 10.1111/1755-0998.12647.

Wilson AC, Cann RL, Carr SM, George M, Gyllensten UB, Helm-Bychowski KM, Higuchi RG, Palumbi SR, Prager EM, Sage RD, Stoneking M. 1985. Mitochondrial DNA and two perspectives on evolutionary genetics. *Biological Journal of the Linnean Society* 26:375–400. DOI: 10.1111/j.1095-8312.1985.tb02048.x.

Wilson GA, Rannala B. 2003. Bayesian inference of recent migration rates using multilocus genotypes. *Genetics* 163:1177–1191. DOI: 10.1093/genetics/163.3.1177.

Wu C. 2001. The genic view of the process of speciation. *Journal of Evolutionary Biology* 14:851–865. DOI: 10.1046/j.1420-9101.2001.00335.x.

Yamazaki Y, Kouketsu S, Fukuda T, Araki Y, Nambu H. 2008. Natural hybridization and directional introgression of two species of Japanese toads *Bufo japonicus formosus* and *Bufo torrenticola* (Anura: Bufonidae) resulting from changes in their spawning habitat. *Journal of Herpetology* 48:427–436. DOI: 10.1670/07-186.1.

Yanchukov A, Hofman S, Szymura JM, Mezhzherin SV, Morozov-Leonov SY, Barton NH, Nrnberger B. 2006. Hybridization of *Bombina bombina* and *B. variegata* (Anura, Discoglossidae) at a sharp ecotone in western Ukraine: comparisons across transects and over time. *Evolution* 60:583–600. DOI: 10.1554/04-739.1.

Yashima K. 1994. A geomorphological study of the caldrons in the Seto inland sea. *Report of Hydrographic Researches*:237–327.

Yoshida F. 1992. Geologic development of the Setouchi geologic province since early Miocene with special reference to the first and second Setouchi Inland Sea times. *Bulletin of the Geological Survey of Japan* 43:43–67.

Yoshikawa N, Matsui M. 2014. Two new Salamanders of the genus *Onychodactylus* from Eastern Honshu, Japan (Amphibia, Caudata, Hynobiidae). *Zootaxa* 3866:53–78. DOI: 10.11646/zootaxa.3866.1.3.

Yoshikawa N, Matsui M, Nishikawa K, Kim J-B, Kryukov A. 2008. Phylogenetic relationships and biogeography of the Japanese clawed salamander, *Onychodactylus japonicus* (Amphibia: Caudata: Hynobiidae), and its congener inferred from the mitochondrial cytochrome *b* gene. *Molecular Phylogenetics and Evolution* 49:249–259. DOI: 10.1016/j.ympev.2008.07.016.

Yu T-L, Lin H-D, Weng CF. 2014. A new phylogeographic pattern of endemic *Bufo bankorensis* in Taiwan Island is attributed to the genetic variation of populations. *PLoS ONE* 9:e98029. DOI: 10.1371/journal.pone.0098029.

Zeisset I, Beebee TJC. 2008. Amphibian phylogeography: a model for understanding historical aspects of species distributions. *Heredity* 101:109–19. DOI: 10.1038/hdy.2008.30.

Zhao H, Beck B, Fuller A, Peatman E. 2020. EasyParallel: A GUI platform for parallelization of STRUCTURE and NEWHYBRIDS analyses. *Plos One* 15:e0232110. DOI: 10.1371/journal.pone.0232110.

※著作権等

Fukutani K, Matsui M, Tran DV, Nishikawa K. 2022. Genetic diversity and demography of *Bufo japonicus* and *B. torrenticola* (Amphibia: Anura: Bufonidae) influenced by the Quaternary climate. *PeerJ* 10:e13452. DOI: 10.7717/peerj.13452.

Fukutani K, Matsui M, Nishikawa K. 2023. Population genetic structure and hybrid zone analyses for species delimitation in the Japanese toad (*Bufo japonicus*). *PeerJ* 11:e16302. DOI: https://doi.org/10.7717/peerj.16302.